UNIVERSITY OF
BIRMINGHAM

MODIFIED COLLOIDAL LITHOGRAPHY:

A FLEXIBLE TOOL FOR FABRICATION OF

PERIODIC NANOSTRUCTURES

By

Ali Mohammadkhani

A thesis submitted to

The University of Birmingham

for the degree of

DOCTOR OF PHILOSOPHY

School of Mechanical Engineering

College of Engineering and Physical Sciences

The University of Birmingham

April 2013

ABSTRACT

This PhD project sets out to investigate the potential of colloidal lithography and explore its application for the creation of highly accurate periodic nanostructures. Furthermore the author plans to show it is possible to achieve high-throughput and novel nanostructures by developing facile and precise fabrication techniques suitable for mass production. In the current research, a group of new fabrication approaches have been proposed and the results have been characterised. This research can be classified into three main sections based on the materials used in fabrication.

In the first section, fabrication of high precision nanopatterns on a photoresist surface was studied using the inherent potential of polystyrene spheres as lenses. Computer simulation was carried out to study the behaviour of electromagnetic waves on the inside and near-outside of the microspheres. In particular, much attention was paid to investigate the role of monolayer and bilayer polystyrene microspheres while light was transmitted through them. The experiments were conducted to obtain uniform arrays of single and dual nanoholes on a surface of AZ 5214-E photoresist via monolayer and bilayer colloidal lithography, respectively. The proposed bilayer colloidal lithography was furthermore extended to reverse the patterns' shape through a precise controllable approach.

In the second section, the research intention was to produce uniform arrays of nanostructures by using colloidal lithography, soft lithography and metal deposition. In this section, two different strategies were proposed. The first strategy was mainly devoted to fabricated ordered arrays of periodic nanostructures on the basis of PDMS/PDMS replica moulding. A comparison study was conducted to fully investigate the best film thickness for gold and platinum as a releasing layer for developing the PDMS/PDMS nano-replication process. The second strategy was focused on creating periodic metallic nanopatterns over a replica PDMS mould. Surface treatment was performed using oxygen plasma to optimise the hydrophobic nature of the PDMS mould.

In the third section, nickel electroforming was developed to produce periodic nanostructures through a highly accurate approach. The aforementioned nanostructures were subjected to an electroforming process. The influence of using a wetting agent and applying a vacuum on the quality of the electroformed nanostructures were studied in detail. The proposed nanofabrication methods within this research facilitate production of multi-material periodic nanostructures with a high precision and tuneable size.

DEDICATED

TO

MY WIFE

ACKNOWLEDGEMENTS

I would like to take this opportunity to acknowledge some wonderful and helpful people that I came across in the past four years of my education. First and foremost, I would like to send my greatest gratitude to my lead supervisor, Prof. Kyle Jiang, whose assistance, encouragement and unlimited support helped me to progress my PhD research at the best level. He has challenged me to push beyond what I thought was possible in my research. My special thanks go to my second supervisor, Dr Carl Anthony, for his continuous guidance and feedback throughout the period of my study. I would also like to thank Prof. Philip Prewett, Prof. Shuang Zhang, Dr Michael Ward, Dr Xianzhong Chen, Dr Xueyong Wei, Dr Ming Lee, Dr James Bowen and Dr Andrew Murray. This research project would not have been successful without their knowledge and assistance. I am also grateful to the all current and previous members of Microengineering and Nanotechnology group for being kind and supportive, and especially those who share their knowledge and expertise with me.

Finally, I would like to take this opportunity to express my profound gratitude to my beloved wife, my parents and my sister for their moral support and patience during my PhD research at the University of Birmingham.

TABLE OF CONTENTS

ABSTRACT.....I
ACKNOWLEDGEMENTS.....IV
TABLE OF CONTENTS.....V
LIST OF FIGURES.....IX
LIST OF TABLES.....XIV
ABBREVIATIONS.....XV
LIST OF PUBLICATIONS DURING THE PHD STUDY.....XVII
1 INTRODUCTION.....1
1.1 Introduction.....1
1.2 Aims and Objectives.....3
1.3 Thesis Outline.....5
2 LITERATURE REVIEW.....8
2.1 Introduction.....8
2.2 Fabrication Techniques of Periodic Nanostructures.....8
2.2.1 Traditional Lithography Techniques.....9
2.2.1.1 Nanofabrication using Photolithography.....9
2.2.1.2 Nanofabrication using Electron and Ion Beam Lithography.....10
2.2.1.3 Nanofabrication using Soft Lithography.....12
2.2.1.4 Nanofabrication using Scanning Probe Lithography.....14
2.2.2 Modern Lithography Techniques.....15
2.2.2.1 Nanofabrication using Nano-Imprint Lithography.....15
2.2.2.2 Nanofabrication using Colloidal Lithography.....17
2.3 Comparison of Nanofabrication Techniques.....18
2.4 Review of the State-of-the-Art in Colloidal Lithography.....20
2.4.1 Preparation of Lithographic Mask.....22
2.4.1.1 Self Assembly using Drain Coating.....23
2.4.1.2 Self Assembly using Drop Coating.....24
2.4.1.3 Self Assembly using Spin Coating.....25

2.4.1.4 Self Assembly using Electric Field....26
2.4.2 Dynamics of Self Assembly Formation....27
2.4.3 Colloidal Lithography as a Patterning Tool....30
2.4.3.1 Shadow Colloidal Lithography....31
2.4.3.2 Mould Colloidal Lithography....38
2.4.3.3 Complex Colloidal Lithography....41
2.5 Classifications and Applications of Periodic Nanostructures Assisted by Colloidal Lithography....44
2.6 Summary....51
3 PS SPHERES AS MICRO-LENSES....53
3.1 Introduction....53
3.2 General Overview of Fabrication Process....54
3.3 Modelling and Simulation....55
3.3.1 Modelling of Monolayer Spheres....56
3.3.1.1 Definition Phase....56
3.3.1.2 Post-Processing Phase....58
3.3.2 Modelling of Bilayer Spheres....62
3.3.2.1 Definition Phase....62
3.3.2.2 Post-Processing Phase....64
3.4 Materials Used in Experiments....66
3.4.1 Mono-Dispersed Spheres....66
3.4.2 AZ Photoresist....67
3.5 Fabrication of Single Arrays of Nanoholes using MCL....68
3.5.1 Photoresist Coating....69
3.5.2 Self Assembly of Single Layer PS Spheres....70
3.5.2.1 Effect of Surface Treatment....72
3.5.2.2 Effect of Evaporation Rate....73
3.5.3 Results of Monolayer Colloidal Lithography....75
3.6 Fabrication of Dual Arrays of Nanoholes using BCL....79
3.6.1 Photoresist Coating....80
3.6.2 Self Assembly of Double Layer PS Spheres....80
3.6.2.1 Tilting Method....81
3.6.2.2 Spin-Coating Method....82
3.6.3 Results of Bilayer Colloidal Lithography....84

3.7 Summary 90
4 PS SPHERES AS A TEMPLATE 92
4.1 Introduction 92
4.2 General Overview of Fabrication Processes 92
4.3 Materials Used in Experiments 95
4.3.1 Polydimethylsiloxane (PDMS) 95
4.3.2 Mono-Dispersed Spheres 96
4.4 Preparation of a PDMS Soft Mould 97
4.4.1 PS Pattern Template 98
4.4.2 PDMS Experiments 100
4.4.3 Structural Characterisation 102
4.4.3.1 Three-Dimensional Reconstruction through SEM Stereoscopic Imaging 102
4.4.3.2 Cross-Section Characterisation through FIB Milling 104
4.4.3.3 Characterisation Results 104
4.5 Fabrication of 2D Periodic Nanostructure 106
4.5.1 PDMS/PDMS Replication Process 108
4.5.2 Surface Characterisation 109
4.5.3 Results of Patterning 2D Nanostructure 110
4.6 Fabrication of 3D Periodic Nanostructure 120
4.6.1 PS Spheres Reassembly Process 121
4.6.2 Surface Treatment of the PDMS Template 122
4.6.3 Results of Patterning the 3D Nanostructure 123
4.7 Summary 128
5 NANOSTRUCTURE FABRICATION BY NICKEL ELECTROFORMING 130
5.1 Introduction 130
5.2 Electroforming Background 131
5.2.1 Theory of Electroforming 131
5.2.2 Thickness Control through Electroforming 132
5.3 General Overview of Fabrication Process 135
5.4 Electroforming Setup 136
5.4.1 Nickel Electrolyte Solution 138
5.5 Experimental Details for Production of a Metallic Nanostructure 138

5.6 Challenges of Nickel Electroforming at Nanoscale 141
5.6.1 Defects in the Master Nanotemplate 141
5.6.2 Defects in the Electroformed Nanostructure 143
5.7 Experimental Results and Discussion 147
5.8 Summary 153
6 CONCLUSIONS AND FUTURE WORK 154
6.1 Conclusions 154
6.2 Suggestions for Future Work 159
7 REFERENCES 161

LIST OF FIGURES

Figure 2-1 Methods of exposure in photolithography.....10
Figure 2-2 Comparison between electrons and ions particles scattering through resist film. As can be seen when electrons penetrate through resist, spread over large area which is not suitable for either sub 100 nm patterns or high aspect ratio structures with vertical side wall [10].....11
Figure 2-3 Schematic procedures describing soft lithographic techniques: a) principal of replica moulding, b) principal of nano-contact printing and c) principal of solvent assisted nano-moulding.....13
Figure 2-4 Schematic diagrams of scanning probe lithography methods: a) when tip is used as a mechanical or thermo-mechanical tool, b) when tip is used as electrons emitter for resist exposure.....14
Figure 2-5 Schematic view of nano-imprint lithography: a) using a transparent mould for imprinting, b) using an opaque mould for imprinting.....16
Figure 2-6 Schematic view of colloidal lithography in etching and deposition process.....18
Figure 2-7 Schematically illustrates the various MSA processes: a) using the drain mechanism, b) using the drop coating mechanism, c) using the spin coating mechanism and d) using the electrophoretic deposition.....23
Figure 2-8 The diagram shows two spheres that are partially immersed in the wetting film over a substrate.....29
Figure 2-9 The diagram shows the convective flow towards the ordered region because of evaporation.....30
Figure 2-10 The ordered arrays of triangular-shape silver nanopatterns derived from colloidal shadow mask [51].....32
Figure 2-11 The treatment effect; a) the interstitial spaces between spheres have been changed due to temperature treatment, b) the in-plane shape of patterns has been changed due to electrochemical treatment[52, 53].....33
Figure 2-12 The schematic and SEM images of two different approaches in AR NSL: a) showing top and side views of colloidal mask (left) and nanoparticle arrays (right), b) showing the modified evaporation system (left) and resulting nanopatterns (right) [54, 55].....34
Figure 2-13 The schematic view of different steps in fabrication of nanopillars using colloidal mask (top) and their SEM images respectively (bottom) [58].....35
Figure 2-14 The schematic processes of two different approaches: a) using metallic mask instead of colloidal mask, b) using an alternative material beneath the shadow mask [60, 61].....36
Figure 2-15 The fabrication process of high-aspect-ratio nanopore arrays using double layer PS spheres [62].....37
Figure 2-16 The SEM images of patterned polymer film using colloidal stamp: a) nanowells structure when a pre-patterned template used as stamp [63], b) arrays of nanowells when a PDMS colloidal stamp is applied [64].....39

Figure 2-17 Honeycomb structures based on mould colloidal lithography: a) the Cu nanostructure fabricated by electroless plating [66], b) shows the Ni nanostructure fabricated by electrochemical deposition [67]. 40
Figure 2-18 The fabrication steps for creating arrays of micro-lenses over glass substrate [69]. 42
Figure 2-19 Top and side view of nanopillar arrays in negative photoresist with the period of 1µm [72, 73]. 43
Figure 2-20 All of the fabrication steps for creation of colloidal particles with patterned nanopores [75]. 44
Figure 2-21 (a, b) the top view SEM images of nanodisk and nanoring, (c) the experimental and theoretical extinction spectra of nanostructure arrays (r1: 14 nm, r2:10 nm, r3:8 nm) [81] 46
Figure 2-22 The schematic design and the experimental results: a) transmission UV-Vis spectroscopy is used to measure the optical properties of LSPR-based nanoparticles, b) LSPR spectra for aging human CSF sample, c) LSPR spectra for AD human CSF sample [83]. (The black, blue and pink curves represent the specific spectra for samples with antibodies, antibodies-CSF and antibodies-CSF-antibodies, respectively.) 47
Figure 2-23 The super-hydrophobicity effect: a) a water drop profile onto a silicon patterned substrate, b) a water drop profile onto a glass patterned substrate, c) rate of changes in water CA by increasing etching time [87]. 49
Figure 3-1 Schematic diagram of fabrication: a) casting of photoresist, b & b') self assembly of single and double layer spheres, c & c') UV light exposure, d & d') developed mould after spheres removal. 55
Figure 3-2 Constructed model of single layer spheres in CST Microwave Studio. 57
Figure 3-3 The carpet plot shows the intensity of modelled UV light on the photoresist surface when a single layer of spheres are considered. 59
Figure 3-4 The calculated field distribution for sphere with radiuses of 275 nm, 550 nm and 1.1 µm at wavelength of 365 nm. (From left to right the sphere's radius is increased) 60
Figure 3-5 The normalised intensity of hot spot versus the lateral position for different wavelengths. 61
Figure 3-6 Constructed model of double layer spheres in CST Microwave Studio. .63
Figure 3-7 The carpet plot shows the intensity of modelled UV light on the photoresist surface when double layer of spheres are considered. 64
Figure 3-8 Simulation result: a) Propagated waves are focused after passing through the top layer of microspheres (bottom view), b) Propagated waves are focused into three hot spots at the shadow side of the bottom layer microspheres (bottom view), c) Direction of propagated waves starts from the top layer to the bottom layer (side view). 65
Figure 3-9 A schematic diagram of fabrication steps using MCL technique. 68
Figure 3-10 Non-uniform arrays of self assembled microspheres over the resist surface. 71
Figure 3-11 SEM image of obtained template after treatment in AZ developer for 30 seconds. 73
Figure 3-12 Self assembled PS microspheres over photoresist by controlling the evaporation rate. 75
Figure 3-13 Uniform arrays of nanoholes over photoresist. 77

Figure 3-14 Ordered arrays of nanopatterns with different sizes are shown using different exposure doses: a) nanoholes with mean diameter of 450±5 nm (75.6 mJ/cm^2), b) nanoholes with mean diameter of 750±8 nm (126 mJ/cm^2).....78
Figure 3-15 A schematic diagram of fabrication steps using BCL technique. 79
Figure 3-16 The coverage area of assembled bilayer of PS spheres as a function of base's tilting angle.....82
Figure 3-17 The coverage area of assembled bilayer of PS spheres as a function of spin speed. 83
Figure 3-18 The SEM image of double layer PS microspheres over photoresist coated substrate. 84
Figure 3-19 Top view SEM images: a) single arrays of uniform nanoholes, b) magnified image of uniform nanoholes' arrays. 85
Figure 3-20 Top view SEM images: a) arrays of binary uniform nanoholes, b) magnified image of uniform nanoholes arrays.....86
Figure 3-21 Tilted SEM images: a) finer features at the bottom of nanoholes, b) arrays of binary nanoholes in the presence of bottom layer spheres.....87
Figure 3-22 Ordered arrays of dual featured nanopatterns with different sizes are shown using different exposure doses: a) appearance of small nanoholes in between big nanoholes at exposure dose of 50 mJ/cm^2, b) arrays of small nanoholes with mean diameter of 220±5 nm in between arrays of big nanoholes, c) arrays of small nanoholes with mean diameter of 380±5 nm in between arrays of big nanoholes. 88
Figure 3-23 Shows the switching moment in which: a) arrays of binary nanoholes turn to b) arrays of triangular-shaped nanopillars. 89
Figure 3-24 Tilted SEM images of experimental result; a) arrays of uniform binary nanoholes, b) magnified image of arrays of binary nanoholes, c) ordered array of triangular-shaped nanopillars, d) magnified image of triangular-shaped nanopillars. 90
Figure 4-1 A schematic diagram shows the preparation steps of a PDMS soft mould. 93
Figure 4-2 Schematic diagrams of both proposed nanofabrication strategies: 1) nano-replication process (top), 2) nanopatterning process (bottom).....94
Figure 4-3 The diagram shows the preparation steps for producing a PDMS mould. 97
Figure 4-4 Self assembled arrays of PS microspheres over treated silicon substrate: a) top view SEM image, b) magnified tilted SEM image. 100
Figure 4-5 Obtained PDMS soft mould after demoulding process: a) top view of order arrays of hybrid nanostructure, b) side view is specified microbowls and nanopillars. 101
Figure 4-6 Stereo images of an object before (black) and after (red) tilting. Tilting about O transforms A_1 to A_2. 103
Figure 4-7 Pair of SEM stereo images of a microbowl PDMS surface taken with tilt angle of 10º and its 3D reconstruction model: a) left image, b) right image, and c) the digital elevation model of PDMS microbowl structure (Green, red and blue colour dimensions correspond to 7.2 µm × 5.4 µm × 0.5 µm respectively). 105
Figure 4-8 A PDMS microbowl structure after FIB milling. The dashed line shows the bottom of the microbowls. 106
Figure 4-9 The diagram shows the proposed fabrication process using PDMS/PDMS replica moulding.....107

Figure 4-10 Surface topography of PDMS master template as a function of the deposited layer. 111
Figure 4-11 The SEM images of PDMS template which are coated with different gold film thicknesses: a) layer of 20 nm, b) layer of 120 nm, c) layer of 550 nm, and d) layer of 1250 nm. 112
Figure 4-12 The contact angle images for different sets: a) group A, b) group B, c) group C, d) group D, e) group E, f) group F, g) group G, and h) group H. 113
Figure 4-13 The SEM images of PDMS nanopatterned after peeling off for set E coated with a 20 nm platinum film: a) PDMS master template, b) magnified image of PDMS template shows damaged bowls, c) PDMS replica, and d) magnified image of PDMS replica shows damaged bumps and pillars. 115
Figure 4-14 The SEM images of PDMS nanopatterned after peeling off for set F coated with a 20 nm gold film: a) PDMS master template, b) magnified image of PDMS template shows perfect bowls and pillars, c) PDMS replica, and d) magnified image of PDMS replica shows perfect bumps and voids. 116
Figure 4-15 SEM images of PDMS nanopatterned after peeling off for set G: a) PDMS master template, b) PDMS replica. 117
Figure 4-16 SEM images of PDMS nanopatterned after peeling off for set H: a) PDMS master template, b) PDMS replica. 117
Figure 4-17 A schematic explanation of demoulding mechanism of platinum coated samples. 118
Figure 4-18 A Schematic explanation of demoulding mechanism of gold coated samples. 119
Figure 4-19 Diagram shows the proposed fabrication process using microspheres reassembly process. 120
Figure 4-20 The SEM image shows arrays of curvilinear triangular pillars slightly above the microbowl structures. 124
Figure 4-21 SEM image shows assembled PS spheres over a PDMS template without treatment. 125
Figure 4-22 SEM images of self-assembled PS microspheres: a) over treated silicon substrate, b) over treated PDMS master template. 126
Figure 4-23 Effect of the sphere's size on the curvilinear triangular profile. 126
Figure 4-24 The SEM image of the gold nanopatterns above curvilinear triangular pillars. 127
Figure 5-1 A schematic diagram showing the electrodeposition process. 132
Figure 5-2 A schematic illustrates different local current densities and electroformed thicknesses for: a) a uniform nanopatterned structure, b) a non-uniform nanopatterned structure. 134
Figure 5-3 A schematic picture shows the nano electroforming process. 135
Figure 5-4 Digital image of electroforming setup along with its components details. 137
Figure 5-5 A schematic diagram illustrates the three steps for gold sputtering process. 139
Figure 5-6 Digital images show two imperfect samples: a) some areas of gold coated resist are swollen and other areas are removed, b) right corner of the electroformed structure is totally missing. 142
Figure 5-7 SEM image shows an imperfect nickel electroformed nanostructure. 144
Figure 5-8 Changes of the surface tension of the nickel electrolyte by increasing SDS amount [135]. 145

Figure 5-9 The contact angle measurements for different sets: a) wetter-free nickel solution, b) nickel solution containing SDS.....146
Figure 5-10 SEM image of a nickel electroformed structure using SDS surfactant in its process. The diameter of achieved nickel nanopillars is 390±5 nm which is in agreement with the size of nanoholes structure used as the master template. .146
Figure 5-11 Tilted SEM image shows uniform arrays of nickel nanopillars with 100±5 nm height. 147
Figure 5-12 SEM images show milled arrays of nanoholes created by MCL method. 148
Figure 5-13 SEM images illustrate milled arrays of dual nanoholes created by BCL method.....149
Figure 5-14 Comparison of the obtained height between single and dual patterned nanostructure. 150
Figure 5-15 SEM images show the nickel nanopillars fabricated by electroforming process: a) single patterned metallic nanostructure, b) double patterned metallic nanostructure. 151
Figure 5-16 Tilted SEM image of a nickel nanostructure with periodic nanopillars arrays. 152

LIST OF TABLES

Table 2-1 Comparison of different strategies for fabrication of periodic nanostructures. 19
Table 3-1 Parameter list for defining components dimensions..... 57
Table 3-2 Material properties of photoresist and colloidal particles..... 57
Table 3-3 Values of focal length associated with classical calculation and simulation results. 61
Table 3-4 Selected properties of polystyrene spheres type 4011 suspension in water [107]. 66
Table 3-5 Experimental parameters for surface treatment of AZ 5214-E. 72
Table 3-6 Effect of evaporation rate on quality of template formation. 74
Table 3-7 The experimental parameters for investigation of exposure doses effects. 78
Table 3-8 The experimental parameters for investigation of exposure doses effects. 87
Table 4-1 Effect of the volume of sealed area on the quality of spheres template formation. 99
Table 4-2 The contact angle and peeling off ability of the replication process. 113
Table 4-3 The experimental results provide the effects of different plasma-treatment times. 122
Table 5-1 Required specifications for thickness control in nickel electroforming. . 133
Table 5-2 The information on ingredients of the nickel electrolyte bath used in the electroforming process. 148

ABBREVIATIONS

AD	Alzheimer's disease
ADDL	Amyloid-derived diffusible ligand
AFM	Atomic force microscope
AR NSL	Angle-resolved nanosphere lithography
BCL	Bilayer colloidal lithography
CCL	Complex colloidal lithography
CL	Colloidal lithography
CSF	Cerebrospinal fluid
CST	Computer simulation technology
DEM	Digital elevation model
DRIE	Deep reactive ion etching
ECD	Electro chemical deposition
ESEM	Environmental scanning electron
FIB	Focused ion beam
FIT	Finite Integration Technique
FWHM	Full width at half maximum
HCP	Hexagonal close packing
HSQ	Hydrogen silsesquioxane
IPA	Isopropanol
ITO	Indium tin oxide
LSPR	Localised surface plasmon resonance
MCL	Monolayer colloidal lithography
MSA	Monolayer self assembly
PBA	Perfect boundary approximation
PBG	Photonic band gap

PDMS	Polydimethylsiloxane
PS	Polystyrene
RCA Co	Radio Corporation of America
RF	Radio frequency
RIE	Reactive ion etching
SEM	Scanning electron microscope
SDS	Sodium dodecyl sulphate
SPL	Scanning probe lithography
STM	Scanning tunnelling microscope
TEM	Transmission electron microscopy
UV	Ultraviolet
UV-Vis	Ultraviolet–visible

LIST OF PUBLICATIONS DURING THE PHD STUDY

Conference Papers:

1. A. Mohammadkhani, H. Ostadi, and K. Jiang, "Morphological Characterisation of Submicron PDMS Bowl Structures," in Nanotechnology (IEEE-NANO), 12th IEEE Conference, Oral, WeA2T5.3, Birmingham, 2012.

2. H. Hassanin, A. Mohammadkhani, and K. Jiang, "Ceramic Nanocomposite by Electrodeposition of Nickel into Porous Alumina Matrix," in Nanotechnology (IEEE-NANO), 12th IEEE Conference, Poster, P.076, Birmingham, 2012.

3. A. Mohammadkhani, H. Hassanin, C. Anthony, and K. Jiang, "Formation of Three Dimensional Nanopattern via Nanosphere Lithography and Soft Lithography," in Nanotechnology (MNE), 37th International Micro & Nano Engineering Conference, Oral, O-LITH-20, Berlin, 2011.

4. A. Mohammadkhani and K. Jiang, "Fabrication of Dual Patterned Nano-Cavities using Double Layer Nanosphere Lithography," in Nanotechnology (IEEE-NANO), 11th IEEE Conference, Oral, TuA2T1.3, Portland, 2011, pp. 9-12.

5. A. Mohammadkhani, M. Malboubi, C. Anthony, and K. Jiang, "Surface Property Characterization of Ordered Nanostructure sing SEM Stereoscopic Technique," in Nanotechnology (MNE), 36th International Micro & Nano Engineering Conference, Poster, P-NANO-09, Genoa, 2010.

Journal Papers:

6. A. Mohammadkhani, X. Chen, S. Zhang, and K. Jiang, "Uniform Arrays of Binary Nano-apertures Derived from Bilayer Colloidal Lithography," SMALL, Submitted.

7. A. Mohammadkhani, H. Hassanin, C. Anthony, and K. Jiang, "Nanopatterning of Metallic Features over Uniformed Arrays of Microbowl Structures," Microelectronic Engineering, vol. 98, pp. 266-269, 2012.

8. H. Hassanin, A. Mohammadkhani, and K. Jiang, "Fabrication of Hybrid Nanostructured Arrays using a PDMS/PDMS Replication Process," Lab on a Chip, vol. 12, pp. 4160-4167, 2012.

9. A. Mohammadkhani, M. Malboubi, C. Anthony, and K. Jiang, "Characterization of Surface Properties of Ordered Nanostructures using SEM Stereoscopic Technique," Microelectronic Engineering, vol. 88, pp. 2687-2690, 2011.

CHAPTER 1: INTRODUCTION

1.1 Introduction

This thesis presents an investigation into fabrication and characterisation of periodic nanostructures using colloidal lithography. The project was driven by the need to achieve higher densities and novel nanopatterns in order to meet the design requirements of nanoscience developments. Formation and utilization of materials, devices, and systems through the control of matter on the nanometre scale can be defined as nanotechnology. Since the properties of material at the nano range are unpredictable compared with those at larger dimensions, nanotechnology can continuously exhibit new phenomena. For instance, the melting point of gold nanoparticles drops when the particle size is less than 10 nm [1]; a particular colour is emitted from semiconductor nanoparticles for a specific size while they are exposed by light [2]. Hence, design and controlled fabrication as well as integration of materials and devices in the nanoworld can be named as the science and technology revolution.

Bottom-up and top-down are known as two distinct concepts to create structures and devices at nanoscale. The bottom-up approaches begin from the basic building blocks such as atoms and molecules to construct nanosized features, while in the top-

down approaches nanoscale patterns are sculpted by etching and milling through bulk materials. In general, extremely complex and advanced techniques are needed to create a periodic nanostructure with a regular size and shape. However, inescapably, high precision always consumes more cost and time, particularly when the desired feature size reaches to several hundred nanometres. Fortunately, nature has already offered a good quality approach to overcome this challenge.

Colloidal lithography (CL) as a versatile and conceptually facile technique for the fabrication of both two-dimensional (2D) and three-dimensional (3D) nanostructures was first coined by Van Duyne and his co-workers in 1995 [3]. In the CL process, a sophisticated mask to produce highly symmetric surface nanopatterns is generated through the self assembly of polymer colloids [4]. The first decade of the true advent of colloidal lithography witnessed an enormous increase in the combination of colloidal lithography with other standard processes, such as metal deposition and reactive ion etching (RIE), to create a periodic nanostructure with uniform features. A variety of CL techniques have been developed in recent years, but the potential to develop more processes for new patterns has been widely recognized.

The proposed approaches employ colloidal lithography as a main core to present novel structures in this research. The first approach uses a single and double layer of polystyrene (PS) microspheres as the super-lenses to create uniform arrays of nanoholes over the photoresist surface. The second approach combines colloidal lithography, soft lithography and metal deposition in order to produce either truncated tetrahedron gold nanopatterns over uniform arrays of microbowl structures

or offers a PDMS/PDMS replication process. Characterizations of structures were alternatively performed through focused ion beam (FIB) milling and surface 3D reconstruction. Extensive electroforming experiments were successfully conducted based on master structures to create metallic nanostructures.

1.2 **Aims and Objectives**

The aim of this PhD project is to investigate the potential of colloidal lithography and explore its application for the creation of highly accurate periodic nanostructures. The project is furthermore aimed to achieve high-throughput and novel nanostructures by developing facile and precise fabrication approaches suitable for mass production.

The project will start based on the existing nanofabrication techniques proposed by other research groups and progress further to develop new nanopattern processes. It is planned to tackle the challenges by introducing the latest nanotechnology into the fabrication of periodic nanostructures. Self assembly of colloidal spheres, the readily engineered foundation of colloidal lithography, was found as a gorge which has direct influence upon the subsequent structures. Hence, more attention is required to choose the right self assembly method based on the substrate properties to achieve a good quality hexagonal close packing (HCP) arrays of PS spheres. Apart from assembly problems, the major challenges in the project originate from the complexity of the required structures and they fall into three categories. First,

presentation of simultaneous and parallel fabrication techniques to produce ordered arrays of nanopatterns under precisely controlled conditions. Second, recognize a proper method for either removal or reassembly of PS spheres with minimum damage to fabricated structures. Finally, find a productive standard process which is compatible with the fabricated structures and consequently yields the desired patterns with high resolution at low cost.

In order to achieve the aforementioned research aims, the project objectives are set out as follows:

1. Review of the state-of-the-art of colloidal lithography. This includes reviewing colloidal lithography and recently developed combined techniques to reveal its limitations and overcome them by appropriate approaches.
2. Find out the influence of surface hydrophilicity of different substrates upon uniformity of HCP spheres' arrays, and develop an experimental method based on specifications of each substrate.
3. Investigate the role of monolayer and bilayer dielectric spheres while light is transmitted through them.
4. Develop conventional colloidal lithography to present a novel technique in the fabrication of uniform arrays of binary nanoholes through the inherent potential of PS spheres as lenses. Extend the proposed fabrication technique to achieve uniform arrays of nanopillars via precision dimension control.
5. Develop the PDMS/PDMS replication process in nanoscale to present a novel fabrication technique. The proposed process involves monolayer

colloidal spheres, PDMS nano replication, thin film coating, and PDMS to PDMS replication.

6. Combine colloidal lithography and soft lithography techniques to develop a new nanostructure: first, create highly ordered arrays of microbowl structures via polydimethylsiloxane (PDMS), second, reassembly of PS spheres onto the prepared structure and finally, produce gold nanopatterns over the PDMS microbowl structure.
7. Morphological inspection of fabricated PDMS template using FIB milling and a scanning electron microscope (SEM) stereoscopy technique to reconstruct the 3D digital model.
8. Develop nickel electroforming as a compatible and precise method for production of nanoimprint stamps from the aforementioned structures.

1.3 **Thesis Outline**

The main text of this dissertation is organized into six chapters. Chapter 1 introduces the project research topic covered by this thesis. It includes the project aims, objectives and thesis outline.

Chapter 2 reviews the current research progress on nanofabrication development. It starts with the current nanofabrication techniques in the patterning of periodic structures, and is followed by a comparison between the advantages and drawbacks of each method. Afterwards, a literature surveys the full review of the state-of-the-art

in colloidal lithography (CL) as the candidate method. Finally, classifications and potential applications of CL assisted periodic nanostructures are reviewed to exhibit the interest of scientists for further development in this field.

Chapter 3 introduces fabrication of two dimensional periodic nanostructures. Since usage of microspheres as super-lenses is the foundation to this proposed technique, the investigation was carried out, via computer simulation technology (CST) microwave studio software, to understand the behaviour of electromagnetic waves at the inside and near-outside of spheres. Then the processing route for fabrication is introduced and the experimental steps including photoresist processing and assembly of colloidal spheres into order arrays are discussed. The results from the experiments are compared.

Chapter 4 introduces two strategies for fabrication using colloidal lithography, soft lithography and metal deposition. Both strategies require a high precision PDMS soft mould as the master template in their fabrication approaches. Structural characterisation of the soft mould is accomplished using SEM stereo imaging technique and FIB milling method.

In the first case a high precision soft mould is the basis to produce a 2D nanostructure. A self-assembled monolayer of PS spheres is used as the first template. Second, a PDMS soft mould is achieved by replica moulding. Third, the PDMS soft mould is coated with a platinum or gold layer. Finally, a PDMS

nanostructured array is developed by casting PDMS slurry on top of the coated PDMS.

In the second case a high precision soft mould is the basis to produce a 3D nanostructure. Therefore, the required soft mould was similarly prepared using PDMS material. Reassembly of colloidal spheres over a PDMS microbowl structure is the most demanding part, which is implemented with the help of a treatment method. A thermal evaporation system is then used to cover a desired gold film over the entire surface of the structure.

Chapter 5 explains the detail of a nickel electroforming process to achieve metallic structures. It begins with an introduction of electroforming in micro/nanotechnology. Both of the fabricated structures in the above chapter are used as the master moulds in this method. The challenges of this process are discussed and solutions are subsequently provided. The experimental results are then compared.

The study of colloidal lithography in nanofabrication is finally concluded in Chapter 6. The major findings obtained from the study are summarised and possible future research topics are subsequently suggested.

CHAPTER 2: LITERATURE REVIEW

2.1 Introduction

This chapter presents a literature review of research on periodic nanostructures including the current nanofabrication techniques, classifications and potential applications of these sorts of nanopatterns. The current nanofabrication techniques in the patterning of periodic structures are discussed in Section 2.2. The comparison between these techniques is made to highlight the advantages and drawbacks of each method in Section 2.3. In Section 2.4, a review of the state-of-the-art in colloidal lithography (CL) as the candidate method is presented. Classifications and potential applications of CL assisted periodic nanostructures are explained in Section 2.5. Finally, the literature review is summarised in Section 2.6.

2.2 Fabrication Techniques of Periodic Nanostructures

There are different approaches for the categorisation of nanopatterning techniques. In some cases these techniques are separated based on the fabrication tools, whereas in other cases they are classified based on the resolution of achievable patterns. It is worth noting that the desired structure is sometimes created by the implementation of several processes (i.e. not only one method). In this research these techniques are

categorized as either traditional lithography or modern lithography. The traditional lithography techniques include photolithography, electron/ion beam lithography, soft lithography and scanning probe lithography; whereas the modern lithography techniques consist of imprint lithography and colloidal lithography. In this section, these nanofabrication techniques are reviewed to determine their feasibility as potential candidates for the fabrication of periodic nanostructures.

2.2.1 Traditional Lithography Techniques

2.2.1.1 Nanofabrication using Photolithography

In the photolithography process light is applied to define desired patterns from a mask in a photoresist layer. **Figure 2-1** illustrates two approaches in photolithography: (i) contact-mode and (ii) projection-mode [5]. In the contact-mode a mask and a photoresist film are normally in physical or proximity contact together, while in the projection-mode an optical system is also placed between a mask and a photoresist film to produce demagnified projection of the mask onto photoresist film. The reported resolution which is achievable through contact-mode is about 500 to 800 nm with UV light at 360 to 460 nm in wavelength, while a higher resolution of 150 nm is possible using projection-mode with light at 200 nm [6, 7]. Light diffraction, which is caused due to the existence of the gap between mask and resist, is the main barrier to the achievement of a high resolution feature through contact-mode photolithography. However, most nano photolithography processes are carried out using projection-mode techniques, i.e. extreme UV and X-ray photolithography.

These methods are also limited because of the requirement of expensive equipment for their implementation.

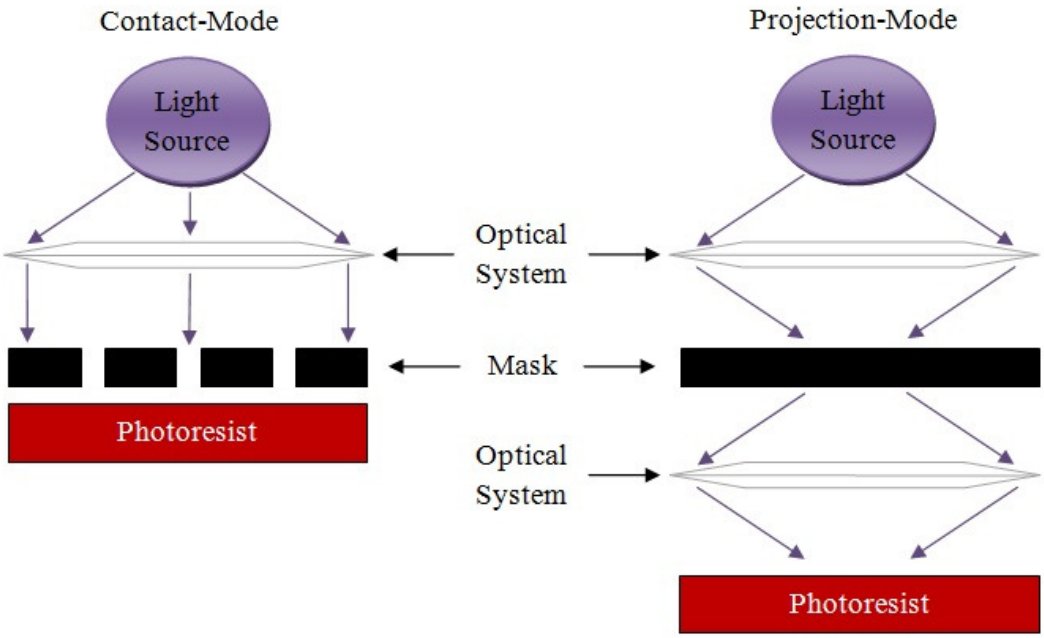

Figure 2-1 Methods of exposure in photolithography.

2.2.1.2 Nanofabrication using Electron and Ion Beam Lithography

Energetic particles such as electrons and ions are the other alternatives for the patterning of features at nanometre scale [7]. Focused beams of electrons or ions, beyond observing and inspecting a sample surface, can be employed as a tool for the pattering of nano features over appropriate resist films. For instance, fabrication of high resolution nanopatterns with a feature size of about 10 nm and 8 nm have been reported through electron and ion beam lithography more than 20 years ago [8, 9]. Although, conventional lithography with focused beams of electrons and ions can provide higher resolution, the limited throughput, slow process and high cost are the

major drawbacks of these fabrication techniques. A focused beam of ions typically has advantage over an electrons beam, due to its negligible scattering and penetration in the resist film as is shown in **Figure 2-2** [10]. However, the damage to the sample caused by high-energy ions is a main problem for this type of lithography.

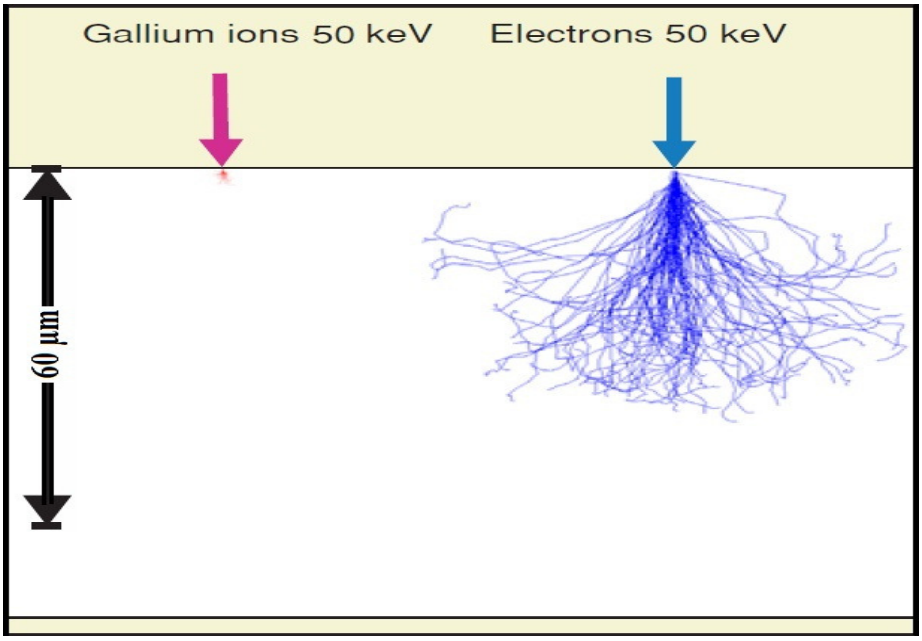

Figure 2-2 Comparison between electrons and ions particles scattering through resist film. As can be seen when electrons penetrate through resist, spread over large area which is not suitable for either sub 100 nm patterns or high aspect ratio structures with vertical side wall [10].

Apart from the above mentioned issues, machining with FIB is the other concept that is widely used as a versatile maskless lithography technique to directly pattern or shape materials at micron and nano levels. FIB systems normally use a finely focused beam of gallium (Ga) ions with a spot size as small as 7 nm in diameter and accelerated up to 50 keV energies [11]. Energetic focused ions are incident on a solid surface with constituent atoms and remove material from the solid surface. However FIB machining offers a unique opportunity to fabricate arrays of complex

nanopatterns with higher resolution, but still high cost and long processing time are such barriers for implementation of this technique.

2.2.1.3 Nanofabrication using Soft Lithography

Soft lithography is another lithographic technique for the fabrication of micro and nanostructures, which uses a patterned relief elastomer as a soft mould or stamp to create or transfer structures with micro and nanopatterns. In soft lithography the patterned relief elastomer is typically fabricated through casting a liquid polymer against a rigid master, followed by curing to induce cross-linking, and finally peeling off from the master [12, 13]. Soft lithography, as an increasingly popular technique, offers immediate advantages over other fabrication methods especially when large area patterning and low cost are the first priorities. Different polymers can be applied to prepare a soft mould, but polydimethylsiloxane (PDMS) is the most common elastomer in soft lithography due to its low surface energy which helps in the demoulding process and its biological compatibility [14, 15]. There is a group of lithographic techniques based on using a soft mould in fabrication which are all known as soft lithography. These techniques include replica moulding, nano-contact printing, and solvent assisted nano-moulding. When a soft mould is filled with a liquid precursor and then the prepolymer is cross-linked and is peeled off from the soft mould, this method is considered as replica moulding [16]. When a soft mould is used to transfer a solution (ink) from its protruding areas to a substrate surface through direct contacting, the technique is called nano-contact printing [17]. When a soft mould is wetted by an appropriate solvent and is then placed over a polymer

coated substrate, the solvent can locally dissolve and deform the polymer to copy the mould patterns onto the polymer surface. This method is called solvent assisted nano-moulding [18]. The fabrication processes related to the aforementioned methods are schematically shown in **Figure 2-3**. The resolution of created nanopatterns through soft lithography is mainly dependent on the filling ability of master capillaries, for example features with sub-15 nm resolution were generated using replica moulding [19]. However, soft lithography is still challenging because of using high cost fabrication methods to prepare a rigid master as the first step.

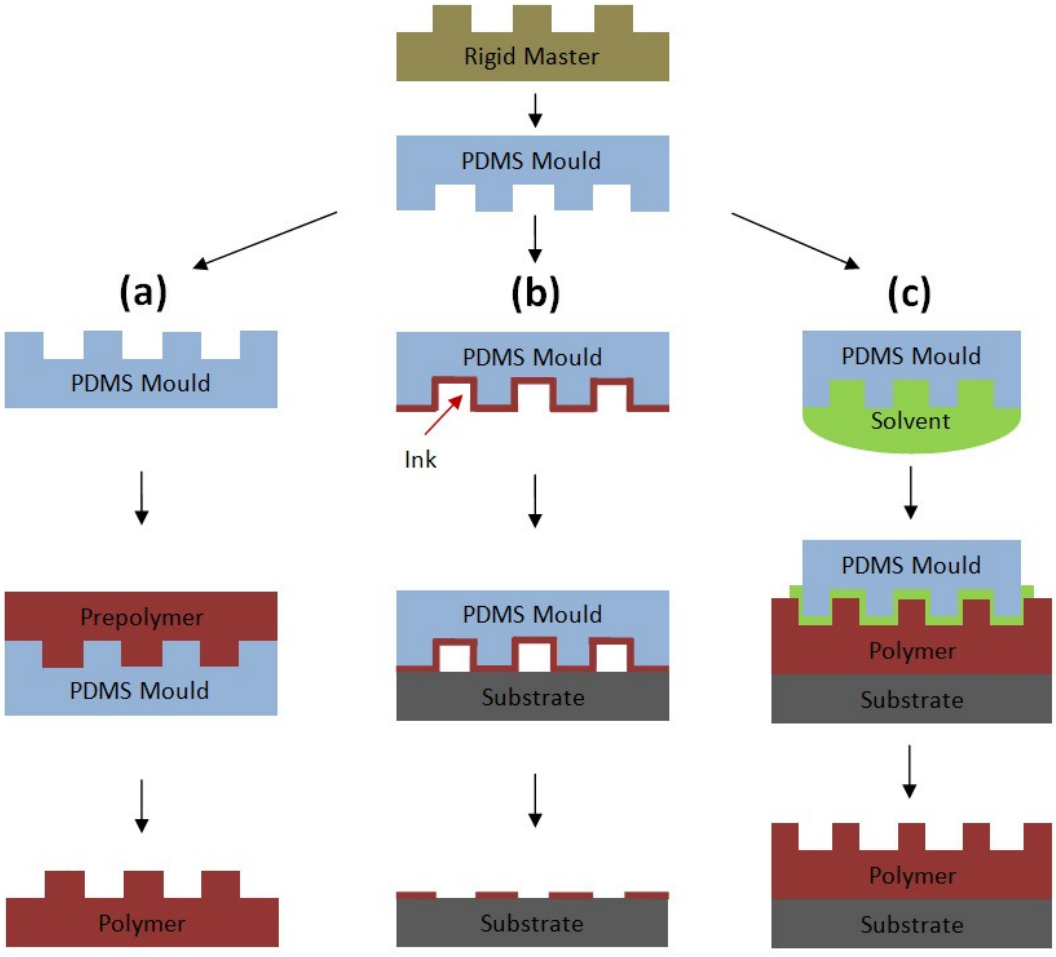

Figure 2-3 Schematic procedures describing soft lithographic techniques: a) principal of replica moulding, b) principal of nano-contact printing and c) principal of solvent assisted nano-moulding.

2.2.1.4 Nanofabrication using Scanning Probe Lithography

Although scanning probes, such as a scanning tunnelling microscope (STM) and an atomic force microscope (AFM), are principally designed to inspect surfaces by providing high-resolution images, their capability as a fabrication tool have been discovered only a couple of years after their first usage in recording images [20]. In scanning probe lithography (SPL) a sharp tip of an STM or AFM is used to generate nanometre patterns when it is close enough to the sample surface [21]. The major advantage of SPL is the achievement of high resolution nanopatterns with notable accuracy. The patterning process using scanning probes can be divided into different categories such as mechanical writing, thermo-mechanical modification and electron exposure of resist as their schematic diagrams are shown in **Figure 2-4**.

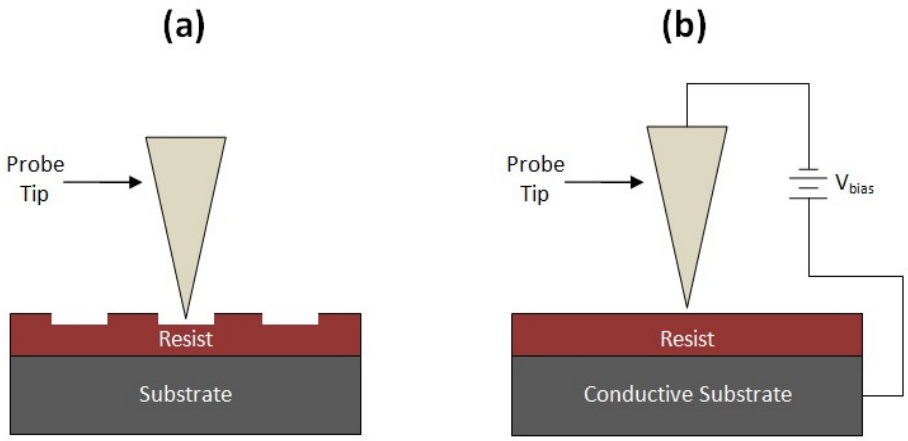

Figure 2-4 Schematic diagrams of scanning probe lithography methods: a) when tip is used as a mechanical or thermo-mechanical tool, b) when tip is used as electrons emitter for resist exposure.

The application of the probe tip is varied for each method. For instance, in the resist exposure method a pattern is fabricated by the emission of electrons from the tip

through a resist layer, whereas in the mechanical and thermo-mechanical method a pattern is created by ploughing a tip over a soft material and by heating a tip to melt a material, respectively [22]. Like electron and ion beam lithography, scanning probe lithography is limited because of its low throughput, serial processes and small area patterning.

2.2.2 Modern Lithography Techniques

2.2.2.1 Nanofabrication using Nano-Imprint Lithography

Nano-imprint lithography is known as a simple and high throughput lithographic technique to fabricate nanostructures at low cost. Unlike soft lithography, nano-imprint lithography relies on a hard master for production of nanopatterns[23]. Nano-imprint lithography consists of two sections. In the first section, an imprint stamp is placed and pressed over a resist casted substrate to copy the stamp features onto the resist and is followed by releasing it from the resist. In the second section, one of the pattern transfer processes (e.g. reactive ion etching) can be applied to clean the substrate from the residual resist and provide a conclusive structure. Photo nano-imprinting and thermal nano-imprinting are two recognized approaches for this standard process [24]. As is shown in **Figure 2-5**, the stamp material and the curing procedure of a resist are two differences that distinguish these two types of nano-imprinting from each other.

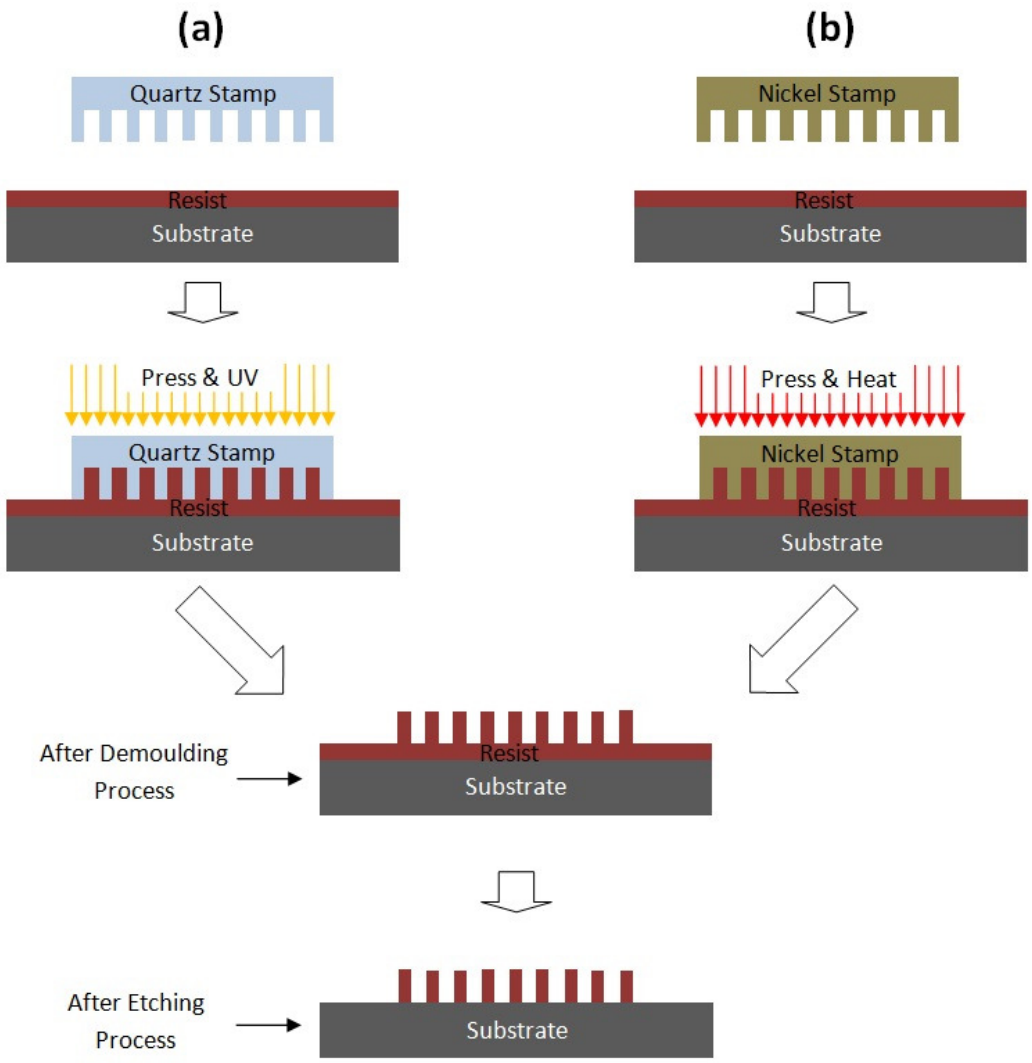

Figure 2-5 Schematic view of nano-imprint lithography: a) using a transparent mould for imprinting, b) using an opaque mould for imprinting.

In the photo imprinting category the stamp is normally made of a transparent material (e.g. quartz) and UV light is used to cure a resist; while in the thermal imprinting category the stamp is typically created from opaque material (e.g. nickel) and heat is applied to cure a resist. High resolution patterns with size of 25 nm have been reported through the use of the nano-imprinting method, by Chou and his co-workers [25]. This technique, like other lithographic methods, includes some

disadvantages such as damage to the stamp patterns because of pressure and damage to the resist patterns at the demoulding moment.

2.2.2.2 Nanofabrication using Colloidal Lithography

Colloidal lithography offers an extremely convenient procedure in the fabrication of features at nanoscale over relatively large areas. In colloidal lithography a self-assembled layer(s) of micro or nanospheres is normally used as a mask to generate nanostructures [26]. In contrast to other nanofabrication methods, colloidal lithography does not employ a highly expensive and sophisticated tool for the creation of nano features [27]. However, the resolution of the final pattern is totally dependent on the precision of the self-assembled layer. A self-assembled layer of spheres is typically created through the following steps: (i) dispersion of spheres in a colloidal solution, (ii) placing a droplet of the solution onto a substrate surface, (iii) leaving the droplet to dry. The quality of the self-assembled layer mainly relies on the environmental assembly condition and the substrate properties. When the self-assembling process is prepared in a proper manner, uniformed hexagonal close packed arrays of spheres would cover the entire surface of the substrate. These uniformed arrays of spheres are then considered as a mask that can be followed by a standard process such as deposition or etching as schematically illustrated in **Figure 2-6**. Colloidal lithography has now evolved into an advanced technique that allows production of arbitrary features including 3D nanopatterns. Fabrication of high resolution nanopatterns with a feature size of about 50 nm has been reported using a colloidal lithography technique [28].

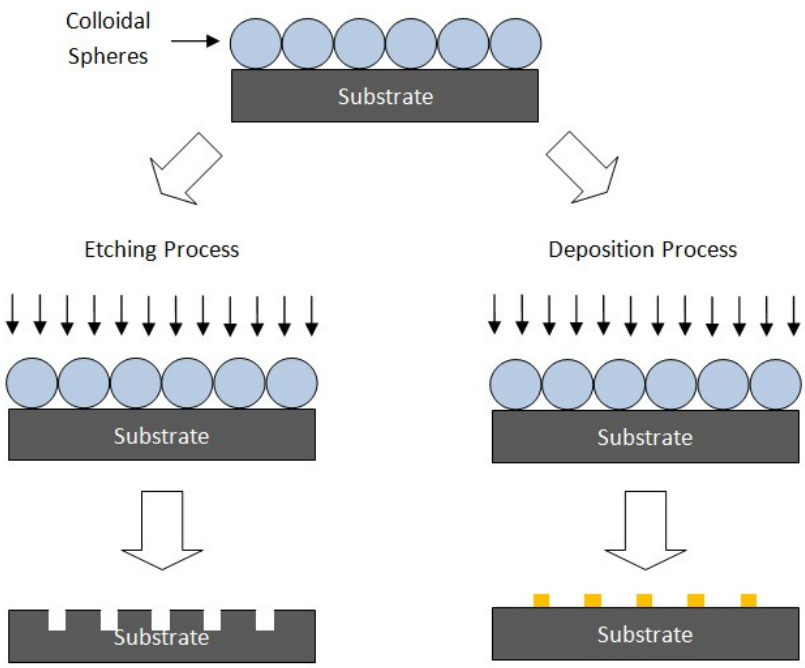

Figure 2-6 Schematic view of colloidal lithography in etching and deposition process.

2.3 **Comparison of Nanofabrication Techniques**

A fabrication method would be normally proposed as a volume nano patterning technique, if the following protocols are satisfied [7]. The technique should be able to create high resolution features and its throughput should be practically high. The uniformity of the patterns should be provided in a simple manner over a large area and it should potentially produce a structure with desired features. The defect density of the achieved structure through this method should be reasonably low and also it should enable mass production. The last protocol, but not the least: cost effectiveness should be guaranteed by the proposed technique. In this section a comparison is made between the aforementioned fabrication techniques based on the above protocols and it is presented in **Table 2-1**.

Table 2-1 Comparison of different strategies for fabrication of periodic nanostructures.

Fabrication Methods	Patterning Procedures	Resolutions	Operational Conditions	Advantages	Drawbacks
Photolithography	Exposure of resist coated substrate by light	~ 150 nm	Ambient or Vacuum	➢ Low cost ➢ Large area patterning	➢ Light diffraction ➢ Multiple steps ➢ High resolution mask ➢ Low productivity
Electron and Ion Beam Lithography	Interaction between electrons or ions with substrate	~ 10 nm	Vacuum	➢ Well developed ➢ High precision	➢ High cost ➢ Slow process ➢ Small area patterning ➢ Low throughput
Soft Lithography	Replication of features using soft mould	~ 15 nm	Vacuum	➢ Low cost ➢ High throughput ➢ Large area patterning	➢ Filling capillaries issue ➢ High resolution master needed
Nano Imprinting	Deformation of resist using rigid stamp	~ 25 nm	Ambient or Vacuum	➢ Low cost ➢ High throughput ➢ Large area patterning	➢ Damage to rigid stamp due to pressure ➢ Damage to resist patterns due to demoulding ➢ Precision issue
Scanning Probe Lithography	Interaction between probe tip and substrate	~ 5 nm	Vacuum	➢ High precision ➢ Applicable to wide range of materials	➢ High cost ➢ Serial process ➢ Small area patterning ➢ Slow process
Colloidal Lithography	Assembling of colloidal particles	~ 50 nm	Ambient or Vacuum	➢ Low cost ➢ Applicable to wide range of materials ➢ Parallel fabrication ➢ Easy process ➢ Large area patterning	➢ Patterning single arrays ➢ Defected area in self-assembly process

As can be understood from the table, scanning probe lithography has better pattern resolution while photolithography has lower resolution in production of patterns. Nanoimprint lithography and colloidal lithography methods have revolutionized the lithographic technique due to their capability for implementation in either ambient or vacuum conditions. Although all of the aforementioned techniques overcome some of the fabrication difficulties and do not cover all protocols, it is colloidal lithography that has become the gold standard for fabrication of periodic nanostructures. The low throughput and slow process are the main barriers of scanning probe lithography and electron/ion beam lithography methods, which prevent them from performing as an alternative to colloidal lithography. In the next section a review of the state-of-the-art in colloidal lithography as the candidate method is discussed and the important issues for development of this method are introduced.

2.4 **Review of the State-of-the-Art in Colloidal Lithography**

The history of colloidal lithography goes back to its early stages in the 1980s, when Deckman and his co-worker proposed a new fabrication approach for the creation of nanopatterns' arrays, which is called natural lithography [29]. In their proposed technique, they used either random or ordered arrays of polymer spheres as a lithographic mask. This lithographic mask is then followed by a suitable transferring process such as deposition or etching for generating patterns. This technique drew more attention soon after it was revealed due to its cost efficiency and versatility. Natural lithography was then extended by the Van Duyne group in 1995 because of

the use of multiple layers of micro/nano spheres in the fabrication process [3]. Since then natural lithography is also known by variant names such as colloidal lithography or nanosphere lithography.

The flexibility of colloidal lithography was explored through wide-ranging research on the choice of different pattern transferring methods and different substrate materials. The colloidal lithography method can offer fabrication of 2D uniformed arrays of various nanopatterns like triangles, posts, and holes. It can also offer fabrication of 3D ordered arrays of complex nanopatterns such as bumps and bowls [30].

There are two major trends that can be observed by screening through the recent registered patents and published papers in the field of colloidal lithography. The first trend is focused on finding out the best method for the assembling of micro/nano spheres over a relativity large area with minimum defects. The most common defects that occur after the assembling process are line and point defects. The second trend is totally devoted to explore either a novel fabrication approach or a new nanostructure with various patterns based on colloidal lithography. In the next subsections the following topics will be discussed on the basis of the above trends. Firstly, a brief review on the preparation of spheres mask will be given since this is a critical step in the colloidal lithography method. Finally, the application of colloidal lithography in production of uniformed arrays of nanopatterns will fully be reviewed.

2.4.1 Preparation of Lithographic Mask

The most critical step in colloidal lithography involves a uniformed hexagonal close packed array of spheres which is required as the lithographic mask. This stage is generally known as the monolayer self assembly (MSA), in which a single layer of micro/nano spheres can be formed onto a substrate in an excellent order [31]. This mask is normally prepared on a desired substrate through various strategies. One of the issues that may influence the quality of the assembly process is the physical and chemical properties of the materials in use. This issue consists of two factors, which are the particles and the substrate. Each of them can individually affect the uniformity of the self assembly process. Regarding the particles material, silica and polystyrene spheres are the common materials that normally are preferred, due to their better performance in the self assembly process [32].

As mentioned above, the other factor for achievement of a good quality MSA is related to the substrate properties. On the basis of the substrate materials, different techniques have been developed to perform the right surface treatment and consequently result in high performance self assembly. Apart from the influence of particle and substrate materials in the quality of the MSA, formation of uniformed arrays of micro/nano spheres depends on the assembly strategies. Different strategies have been proposed to provide a simple and rapid process with high performance and minimum defects. All of the proposed techniques for the self assembly process can be classified into four categories. These categories include drain coating, drop coating, spin coating and electrophoretic deposition; their assembly processes are

schematically shown in **Figure 2-7**. It is worth noting that the largest ordered area of micro/nano spheres through the various methods of assembly can reach up to 5 cm^2 [33, 34].

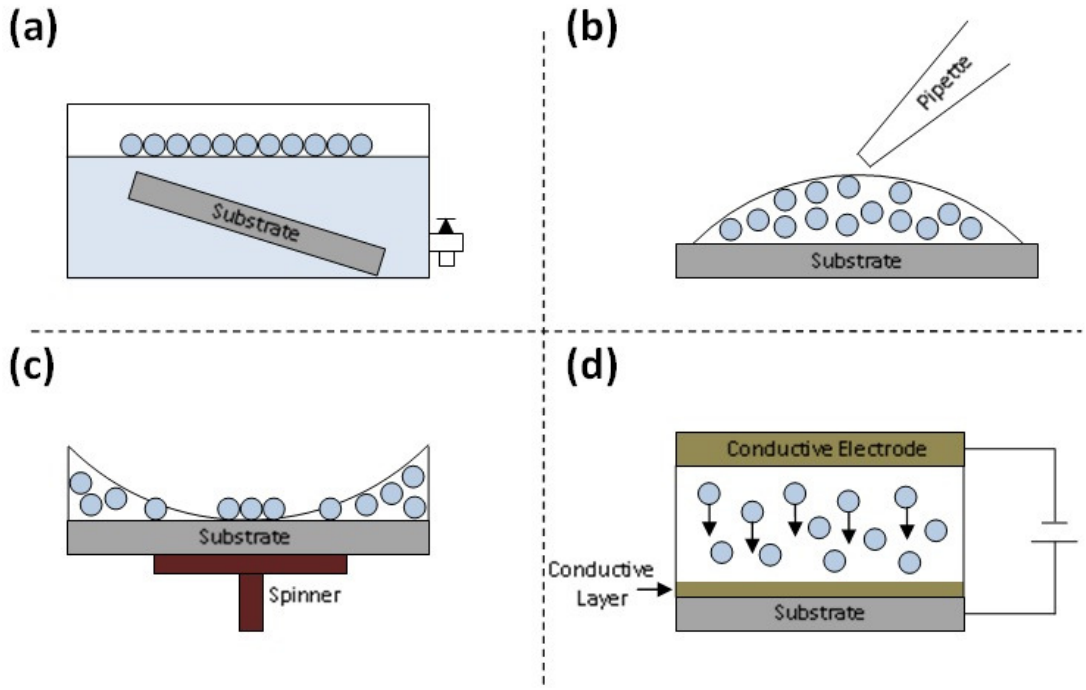

Figure 2-7 Schematically illustrates the various MSA processes: a) using the drain mechanism, b) using the drop coating mechanism, c) using the spin coating mechanism and d) using the electrophoretic deposition.

2.4.1.1 Self Assembly using Drain Coating

One of the interesting methods for preparation of ordered arrays of colloidal particles on the desired substrate is using the liquid-gas interface [35]. In this case, the surfaces of colloidal spheres are firstly modified to enhance their hydrophobicity and floatability. The spheres are next spread over a liquid surface utilizing a spreading solvent. The colloidal spheres are then self-assembled on the liquid surface after the evaporation of the solvent. The ordering and close-packing of the self assembled

layer is typically performed using a Teflon barrier. Finally, as the liquid gently drains or evaporates, the 2D arrays of colloidal spheres are transferred to the submerged substrate with a slight slope. The major barrier of this approach is the necessity of the substrate appearance at a reasonable level below the liquid surface, which may not be applicable for some of the pre-coated substrate [36]. For example, surfaces of silica spheres were modified by the addition of chloroform solvent under severe stirring to enhance the hydrophobicity of the silica particles and then self assembled at the water-air interface to form 2D particle arrays [37]. In comparison to the drop coating and spin coating assembly processes, the colloidal spheres at the liquid-gas interface only formed a monolayer of ordered arrays.

2.4.1.2 Self Assembly using Drop Coating

The drop coating method is a really simple and compatible technique for the formation of ordered particles' arrays. In this strategy a droplet of prepared dilution, which is normally a mixture of particles and water, is placed onto the flat substrate [38]. The drop is then spread depending on the substrate hydrophilicity and particles' wettability, to cover the substrate surface. Well-ordered arrays of closely packed spheres would be achieved after evaporation of the solvent. The key element for improvement of the self-assembled arrays through this strategy is the slow and homogeneous evaporation of the solvent. As is mentioned above the drop coating method is generally applied on a flat substrate, while the Ohtsu group proposed a similar assembly process over a slightly tilted substrate [39]. Their observation showed that the evaporation begins from the upper edge of the sample towards the

lower edge, instead of starting from the middle of the sample as in the flat substrate case. More recently, Kim and his co-workers developed a new process for assembly based on the drop coating [40]. They placed two glass substrates with a 100 μm gap from each other, and they filled the gap between the substrates with the colloidal dilution. Both substrates were attached to a dipping machine for controlling their lift up rate. The ordered arrays of spheres were successfully assembled on the main substrate, while the substrate was being raised up by the machine and simultaneously blown by hot air.

2.4.1.3 Self Assembly using Spin Coating

The other strategy for formation of the hexagonal arrays of colloidal particles is the spin coating method [41]. In this method the 2D colloidal mask is organized through centrifugal spreading of the prepared dilution onto the substrate. In comparison to the drain and drop coating methods, spin coating is considered as a rapid and handy technique. In the course of spinning, the suspension spreads rapidly across the wettable substrate, while the colloidal particles are densely seated to make the closely packed structure. The quality of the self assembled mask and the thickness of the prepared mask (i.e. numbers of layers) are highly affected by the parameters such as the particles/solvent proportion, spin speed and wettability of the substrate. For example, in the spin coating method, a mixture of Triton X-100 and methanol was diluted with colloidal solutions to assist the solutions in wetting the substrate[3]. Complex forms of self assembled colloidal mask like multiple layers or non-close packed arrays are also obtainable using spin coating methods [42]. Recently, the

McLellan group reported a new approach that forms the colloidal particles into the desired shape and order by assisting with a pre-patterned substrate. Their proposed approach can be implemented by either drop coating or spin coating methods [43]. In this approach, the covered area and the ordering sequence of the colloidal spheres can be manipulated by either varying the feature size of the pattern on the substrate or by changing the spheres size.

2.4.1.4 Self Assembly using Electric Field

The other suggested method for assembly of colloidal particles is the electrophoretic deposition or electrochemical deposition. In this technique, the assembly of micro/nano spheres generally occurs when an electric field persuades the movement of the negative charged particles towards the positively charged electrode. In 1996, Trau and his co-workers proposed the electrophoretic method for the formation of submicron particles [44]. They successfully assembled 2D arrays of silica and polystyrene spheres on an indium tin oxide (ITO) coated glass substrate. Although the self assembly of colloidal particles using a DC or AC field has been widely studied and is known as a rapid and precisely controlled method [45, 46], this technique is limited due to the necessity of using a conductive substrate. In a typical experiment, the colloidal solution is sandwiched between two conductive electrodes in a Teflon sealed box. An electric field is then applied to transfer the spherical particles towards the surface of the working electrode. Recently, the Park group developed the electrophoretic deposition by utilizing this method onto a surface of a gold patterned electrode [47]. They first used a TEM-grid over an ITO electrode as a

mask to create the gold patterns onto the surface of this electrode via a thermal evaporation system. Their results showed that after a short term electrophoretic deposition, the ordered arrays of PS spheres are only assembled on the gold domains due to the existence of stagnant regions among the convective flows of the colloidal solution.

2.4.2 Dynamics of Self Assembly Formation

There are several models that have been suggested to describe the mechanism of self assembly. Among those suggested models, the mechanism which has been proposed by the Nagayama group is the best candidate to understand the dynamics of assembly [38]. They identified lateral capillary attraction and convective flow as the main elements in their proposed system. There are two types of lateral capillary forces associated with colloidal particles. These lateral capillary forces are principally generated because of a deformation on the liquid surface. It is worth noting that the larger deformation on the liquid surface causes the stronger capillary interaction. When the origin of these forces is the weight of the particle they are called flotation capillary forces, whereas when the origin of them is the wetting properties of the particle they are called immersion capillary forces[48, 49]. In the case of flotation forces the particles are contained in the bulk solution and float on a liquid surface. While, in the case of immersion forces the particles are immersed in a liquid layer and constrained in the vertical direction by a substrate. On the basis of similarity or dissimilarity of interacting particles, the lateral capillary forces can be either attractive or repulsive. Hence, an attractive flotation force appears when a pair

of heavy particles or a pair of light particles interacts at the water-air interface, whereas an attractive immersion force appears when a pair of hydrophobic particles or a pair of hydrophilic particles interacts in the wetting film at the water-substrate interface. The capillary forces are considered as repulsive for both floatation and immersion conditions when two dissimilar particles interact together. As mentioned earlier, the particles' weight is one of the parameters which influence the surface deformation of the wetting film. The smaller the particles used in the assembly process, the weaker the capillary forces between them. However, this theory is only applied to the particles at the water-air interface of the wetting film, and not to those which are immersed and restricted in the wetting film, because as the wetting film becomes thinner, the deformation of the film surface is enhanced. Therefore, the flotation forces arising from the particles with a mean diameter of less than 20 μm become negligible, while the immersion forces remain significant for particles with a mean diameter down to 20 nm [50].

In all cases the formation of the spheres' arrays occurs when the wetting film (water layer) thickness is approximately equal to the diameter of the spheres. This stage is named the nucleation by Denkov and his co-workers. Since the spheres are physically restricted due to the existence of the substrate, any deformation on the water surface can develop strong and long-range attractive immersion forces. The meniscus slope angle (ψ) is the key element in the determination of the spheres' interaction nature. As is shown in **Figure 2-8** the meniscus slope angle is the angle between a line tangential to the water-air interface at the three-phase contact line and the horizontal dash-line. The value of the meniscus slope angle is either positive or negative based on the hydrophilicity or hydrophobicity of particles, respectively. In

the case of $\psi = 0$, there is no interaction force. The values of the meniscus slope angle are measured at two regions for identical particles, and they are varied because of the presence of a second sphere. The outer region is illustrated by $\psi_1$and the inner region is illustrated by ψ_2. The differences between the values of meniscus slope angles at the inner and outer regions cause the perturbation at the surface of the wetting film (i.e. variation of surface tension σ), and result in a lateral capillary force towards the inner region.

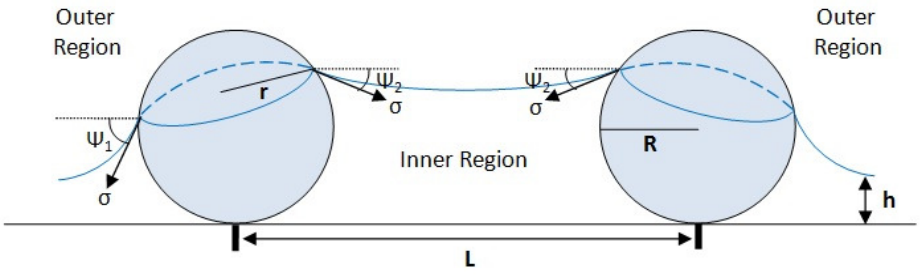

Figure 2-8 The diagram shows two spheres that are partially immersed in the wetting film over a substrate.

Once the nucleation stage is completed through the formation of an ordered nucleus, the second stage is started. In the second stage, the convective flow causes the growth of the nucleus by directing the spheres' motion towards the ordered nucleus as depicted in **Figure 2-9.** The main reason for the appearance of the convective flow can be described as the following: the evaporation ratio of the water remains uniform in the entire surface, until the thickness of the wetting film reaches several scales larger than the spheres' diameters. Once the closely-packed spheres are formed, the evaporation of water from that ordered region leads to increasing of the curvature of the meniscus. However the thinning process of the water, which is

placed in between spheres, is gentle because of the hydrophilicity of the spheres. Therefore, the water in bulk solution is sucked towards the ordered region through the channel below the spheres, and replaced with the evaporated water at that region. When the motion occurs in the bulk solution, those spheres which are completely immersed in the bulk solution are directed towards the ordered region and remain attached to the pack. It is worth noting that the convective flow will be directed towards the area of the higher evaporation rate in comparison with the bulk solution. For samples that are prepared by dropping solution onto a flat substrate without a boundary the dispersion liquid will have a higher curvature at the edge of the substrate, particularly at the corners. Therefore it is likely that lateral capillary attraction and convective flow occur simultaneously.

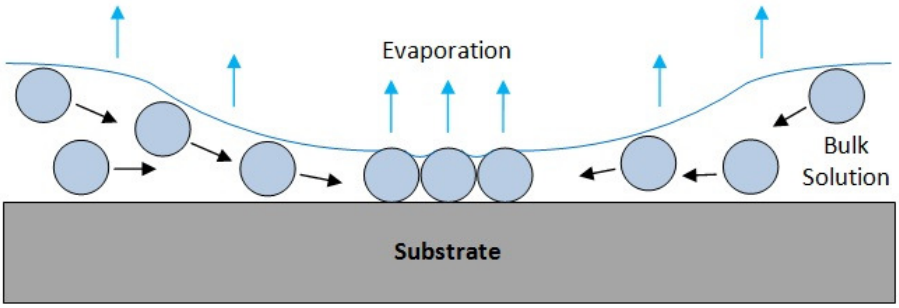

Figure 2-9 The diagram shows the convective flow towards the ordered region because of evaporation.

2.4.3 Colloidal Lithography as a Patterning Tool

Although the self assembly process remains the challenging part of colloidal lithography and new approaches are constantly suggested to develop this process, colloidal lithography is known as the best candidate for creation of ordered

nanostructures at low cost and high throughput. Regarding the fabrication of ordered nanostructure arrays via the colloidal lithography method, there are many registered patents and research achievements. To fully understand the fundamental strategies of these techniques, they are categorized into three groups on the basis of their similarity in fabrication. Besides classification and identification of these registered patents, the main goal was to find out the unstudied and missing area in the field of colloidal lithography for further development. In this section the following three groups will be discussed: the first group consists of the fabrication processes which the colloidal spheres use as a shadow mask. In these techniques the shadow mask is normally nominated for a deposition or etching process. The second group includes the fabrication processes which the colloidal spheres utilise as a mould. In these techniques the mould is generally nominated for an electroforming or soft lithography process. The third group is focused on the fabrication processes which the colloidal particles use as a template to create a complex array of nanostructure. In this category the template either consists of multiple layers of colloidal spheres or uses different standard processes in its fabrication technique.

2.4.3.1 Shadow Colloidal Lithography

The phrase of shadow mask is applied when the arrays of colloidal spheres encounter with an evaporation system or etching process. In both cases the interstitial spaces between spherical particles are chosen to generate the periodic nano/micro patterns on the surface of the substrate by either deposition of the desired materials or removal of the substrate materials. The advantage of these interstitial spaces was first

discovered by the Van Duyne group, when they deposited the silver particles through the monolayer of hexagonally close packed nanospheres to create ordered arrays of nanopatterns [51]. As the result, they successfully produced ordered arrays of triangular-shape silver nanopatterns as is shown in **Figure 2-10a**. Their investigation indicates that the in-plane shape of the silver patterns and the periodicity of these patterns can be entirely controlled by varying the deposition ratio and using different size of particles. They also introduced the bilayer colloidal mask for fabrication of differently shaped nanostructures using the material deposition method. In the bilayer colloidal mask some of the interstitial spaces of first layer spheres are covered by the second layer spheres, so the different features will be revealed after the material deposition step as is illustrated in **Figure 2-10b**.

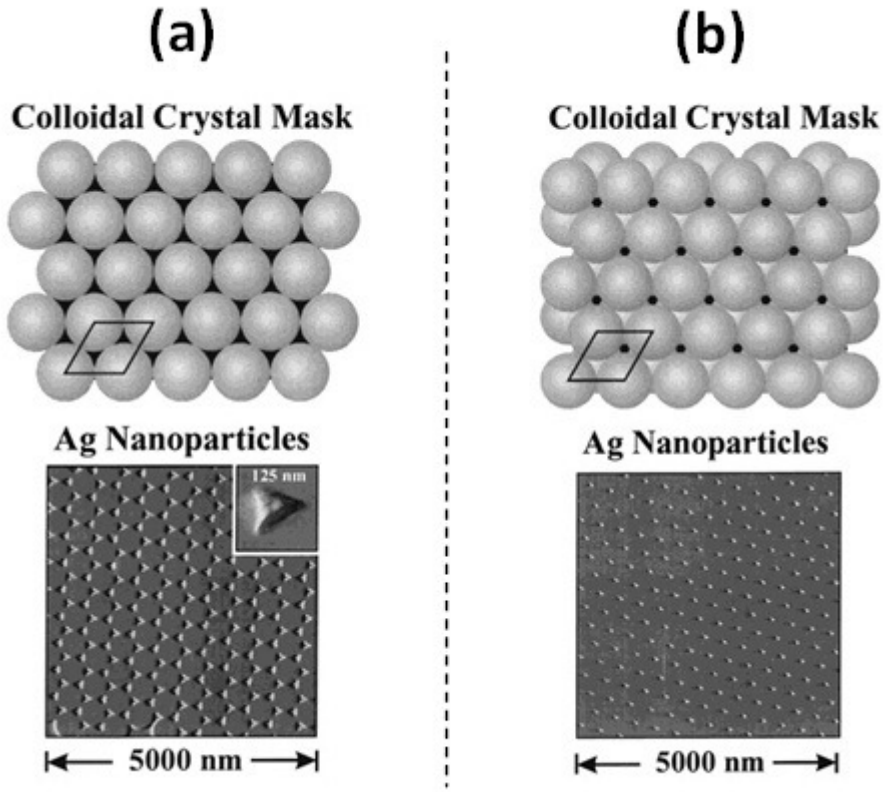

Figure 2-10 The ordered arrays of triangular-shape silver nanopatterns derived from colloidal shadow mask [51].

Furthermore, the recent achievements by other researchers show that the physical appearance of the obtained patterns is modifiable. In some cases the interstitial spaces between spheres can be controlled by temperature treatment which effectively deforms the shape of the colloidal spheres [52] as is shown in **Figure 2-11a**; whereas in other cases the shape of the obtained patterns can be tuned by electrochemical treatment which effectively changes the in-plane shape of the pattern from triangle to circle as is shown in **Figure 2-11b** [53].

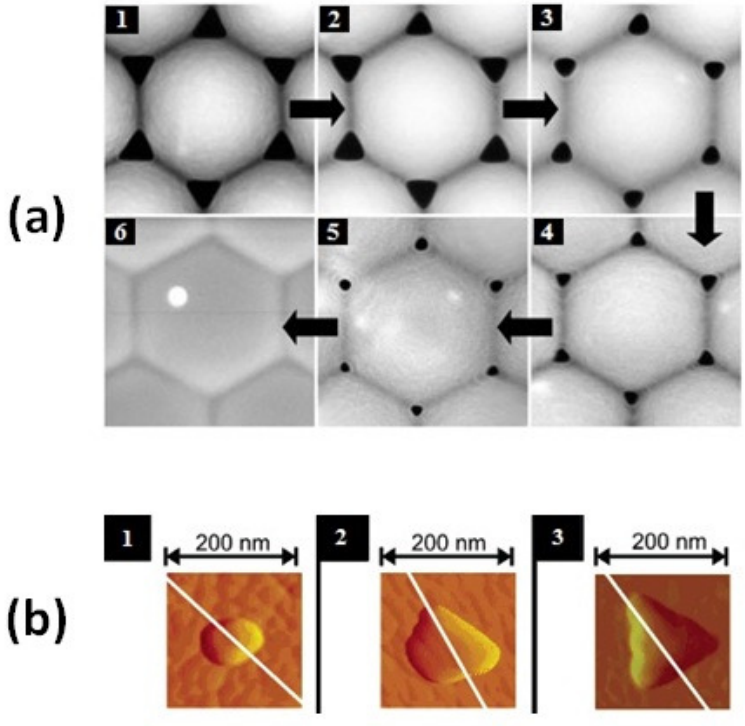

Figure 2-11 The treatment effect; a) the interstitial spaces between spheres have been changed due to temperature treatment, b) the in-plane shape of patterns has been changed due to electrochemical treatment[52, 53].

More developments have been made by Haynes and his co-workers to create ordered arrays of various shaped and sized nanostructures using colloidal spheres as the shadow mask [54]. Since their proposed method is on the basis of the angle changes, they named their technique angle-resolved nanosphere lithography (AR NSL). In this

method for producing different nanopatterns the angle between the normal surface of the assembled colloidal mask and the propagation vector of the material deposition is controlled, as is illustrated in **Figure 2-12a**. Based on this method, the material is not deposited uniformly onto the substrate, because as the angle increases, there are some areas below the colloidal spheres which are accessible for the material deposition while the other part of the interstitial area will be under the shadow side of the neighbouring spheres. Recently, the Giersig group modified this technique by applying a rotation to the sample holder at a specific tilted angle while the AR NSL was in the process [55]. Using this approach, they not only improved the AR NSL method, but also they achieved a variety of complex patterns as is shown in **Figure 2-12**.

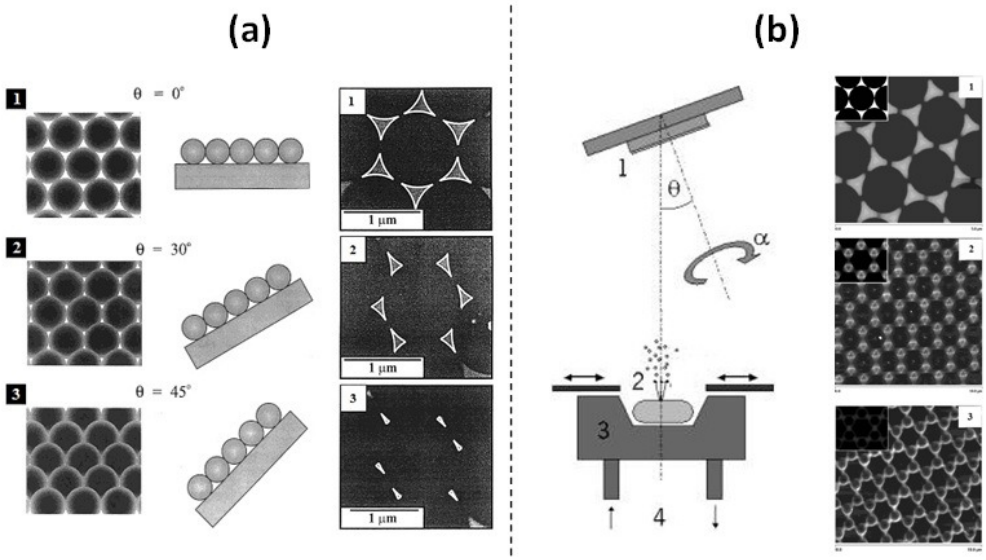

Figure 2-12 The schematic and SEM images of two different approaches in AR NSL: a) showing top and side views of colloidal mask (left) and nanoparticle arrays (right), b) showing the modified evaporation system (left) and resulting nanopatterns (right) [54, 55].

A two dimensional array of colloidal spheres can also be used as the shadow mask in the etching process to produce a variety of ordered nanostructure arrays. In early

2004 researchers combined colloidal lithography and reactive ion etching (RIE) to present a new tool for fabrication of periodic nanostructures. The Van Duyne group used this approach to fabricate triangular-shaped nanopores with an in-plane width of 404 nm and depth of 250 nm. They minimized the nanopores' dimensions through changing the sizes of the colloidal spheres and the etching conditions. They successfully reported the nanopores with 44 nm width and 25 nm depth [56]. Similar work has been performed by the Lin He group to achieve arrays of triangular-shaped nanoholes using silica spheres [57]. The aforementioned approach has been further developed for production of different nanostructures. Cheung and his colleagues used deep reactive ion etching (DRIE) to remove the substrate materials through the open windows between colloidal spheres [58]. They successfully fabricated uniformed arrays of silicon nanopillars as is illustrated in **Figure 2-13**. They used a monolayer of polystyrene spheres as the mask. They modified the sizes of the colloidal spheres utilizing the oxygen plasma treatment.

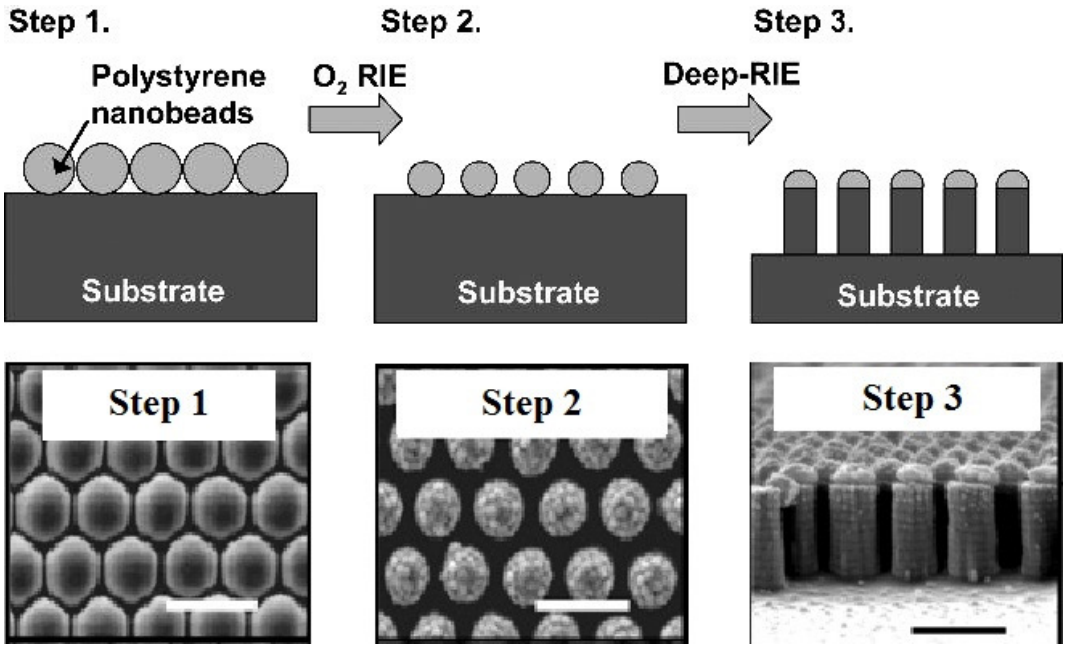

Figure 2-13 The schematic view of different steps in fabrication of nanopillars using colloidal mask (top) and their SEM images respectively (bottom) [58].

The diameter of the colloidal spheres is decreased, as the oxygen treatment time is increased. High aspect ratio arrays of silicon pillars with a diameter of 500 nm were achieved via this technique. The size and periodicity of these nanopillars can be controlled by either choosing a different spheres diameter or varying treatment time. The fabricated silicon nanopillars can be then used directly as the imprinting stamp to create polymer nanostructures [59]. As is observed from this figure the colloidal spheres degrade during the etching process, and subsequently cause dissimilarity in the nanopillars' shapes. The recent published papers in this area are concentrated on either changing the materials of the mask or using an alternative material beneath the shadow mask. For example, Kuo and his co-workers demonstrated a new method for fabrication of large-area periodic nanopillar arrays[60]. In their proposed method, they applied metal deposition over the colloidal mask and next they removed the colloidal mask. In fact they replaced the metallic mask with the colloidal spheres' mask to prevent dissimilarity of nanopillars after a long etching process. Their proposed method is schematically illustrated in **Figure 2-14a**.

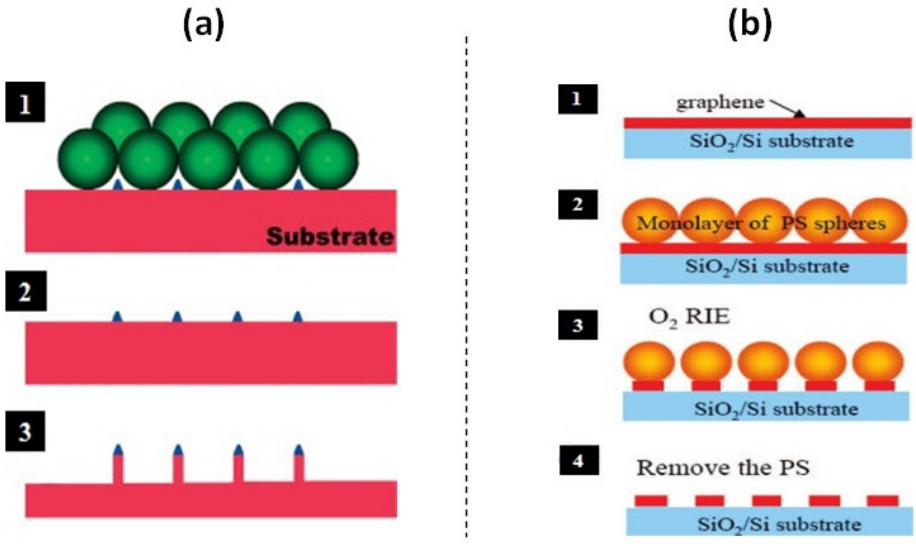

Figure 2-14 The schematic processes of two different approaches: a) using metallic mask instead of colloidal mask, b) using an alternative material beneath the shadow mask [60, 61].

Recently, the Huang group used a graphene layer in between the colloidal spheres and substrate to fabricate ordered arrays of graphene nanodisk[61]. They used the combination of colloidal lithography and etching process as is shown in **Figure 2-14b**. The oxygen RIE is then applied to resize the spheres' diameter and etch a portion of the graphene sheets that was not protected by the colloidal spheres. In 2009 Chen and his colleagues demonstrated the other aspect of this technique by employing the double layer spheres as the etching mask [62]. They first applied oxygen RIE to decrease the size of the top layer PS spheres. As the diameters of the top layer spheres decrease, the sizes of interstitial space between spheres at bottom layer increase. After the etching process the arrays of nanopores with the in-plane width ranging from 120 to 340 nm and a depth up to 2 μm have been obtained as shown in **Figure 2-15**.

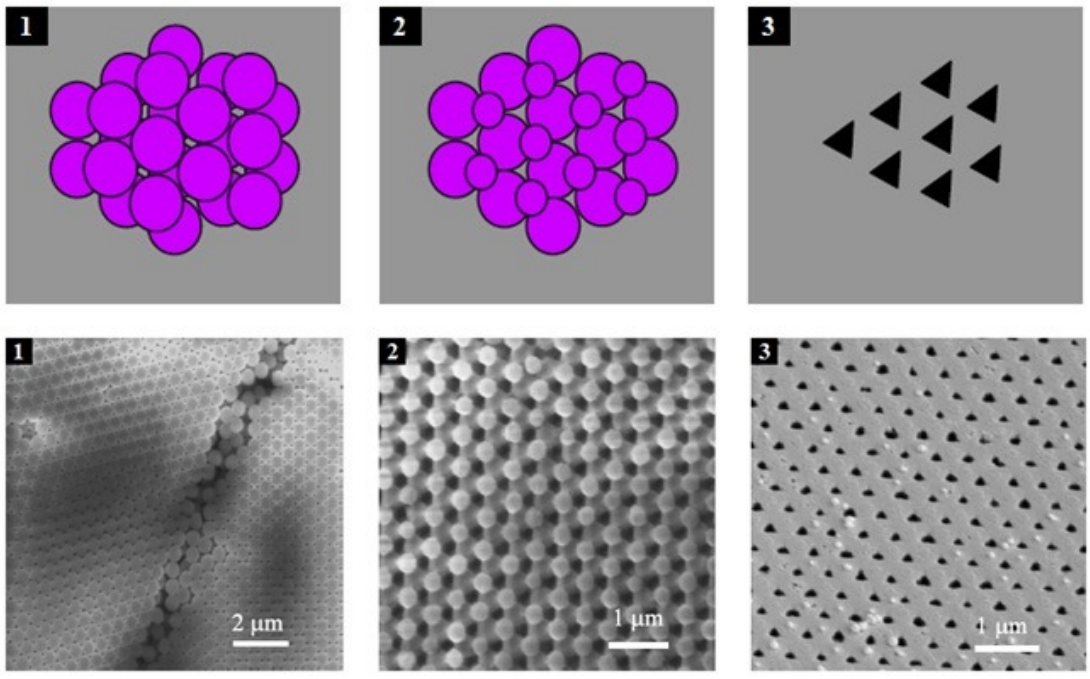

Figure 2-15 The fabrication process of high-aspect-ratio nanopore arrays using double layer PS spheres [62].

2.4.3.2 Mould Colloidal Lithography

Unlike shadow colloidal lithography, the uniformed hexagonal close packed arrays of spheres are used as a structural template in mould colloidal lithography. Different filling techniques can be processed in which the desired material is filled into the structural template. The negative replica is finally obtained after the demoulding and cleaning process. When the colloidal spheres are used as the structural template for the imprinting process, the uniformed arrays of a hemispherical shape structure will normally be achieved. In the following paragraphs some of the latest patents which used the assembled arrays of spheres as the structural template are discussed.

The earliest demonstration of this method goes back to 2004, when the Yang group fabricated a 2D nanowells polymer structure by using 2D arrays of colloidal crystals as a stamp for imprinting [63]. They first coated their entire pre-patterned template with silica spheres using the spin coating method. They used low speed coating to allow the colloidal particles to settle into the ordered structure. Next, they employed this patterned colloidal stamp to generate the arrays of nanowells over polymer. So, a liquid prepolymer was coated on a silicon substrate and followed by placing the fabricated stamp over the prepolymer. After curing the prepolymer by UV light, the 2D arrays of nanowells were obtained as a result and is shown in **Figure 2-16a**. Some similar work was also reported by the Yang group later in 2006. In this report, instead of assembly of colloidal particles into pre-patterned substrate, they used the lift-up technique to create a PDMS colloidal stamp [64]. The PDMS stamp with ordered arrays of silica spheres was first coated with Ag nanoparticles and then

brought into contact with the polymer coated substrate. A certain pressure and heat were applied to provide the right conditions to transfer the silica microspheres from the PDMS stamp to the polymer in the course of the peeling off process. After chemical etching of colloidal particles, ordered arrays of nanowells were achieved. The SEM image of the obtained structure is illustrated in **Figure 2-16b**.

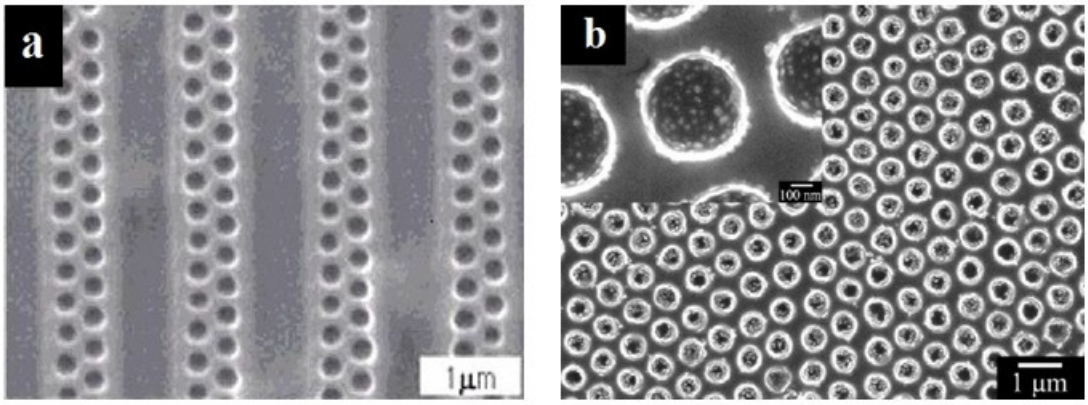

Figure 2-16 The SEM images of patterned polymer film using colloidal stamp: a) nanowells structure when a pre-patterned template used as stamp [63], b) arrays of nanowells when a PDMS colloidal stamp is applied [64].

Lu and his co-workers have similarly presented a new approach for fabrication of a nanopore structure utilizing colloidal spheres as the mould. They used the combination of sol-gel and thin film processes to create uniform arrays of nanowells in a silica membrane [65]. They first coated a thin layer of polystyrene over the surface of a glass slide. Next, they prepared the sphere-doped silica sol by mixing the aged silica solution and PS spheres suspension followed by the spin coating process. When the membrane formed over the template, the sample was placed in an appropriate solvent to dissolve the polystyrene film as well as the PS spheres. The silica membrane with ordered nanopores was then detached and floated to the solvent surface. The top and bottom diameters of the achieved nanowells were

varied, as they are functions of the sphere diameter and the sphere contact area with the underlying surface, respectively. Compared to those aforementioned patents that used colloidal particles as a stamp, a combination of colloidal lithography with either electroless plating or electrochemical deposition (ECD) is also reported as a simple and economical method in nanofabrication. In both cases, the colloidal particles perform as a mould to generate a honeycomb structure. In 2007, the Ono group fabricated an ordered copper honeycomb pattern over silicon substrate using electroless plating [66]. They first self assembled PS spheres over silicon substrate using drop coating and then heated the substrate more than the glass transition point of the PS particles to fix them to the substrate. The prepared substrate with the colloidal mould was next immersed in an aqueous solution to create a honeycomb structure. The SEM image of the fabricated structure after removal of the colloidal particles is shown in **Figure 2-17a**. A similar approach was published by Chen et al in 2008, regarding fabrication of metallic hybrid nanostructures, as illustrated in **Figure 2-17b**. They used the same principle in applying colloidal spheres as a mould, but they chose electrochemical deposition [67].

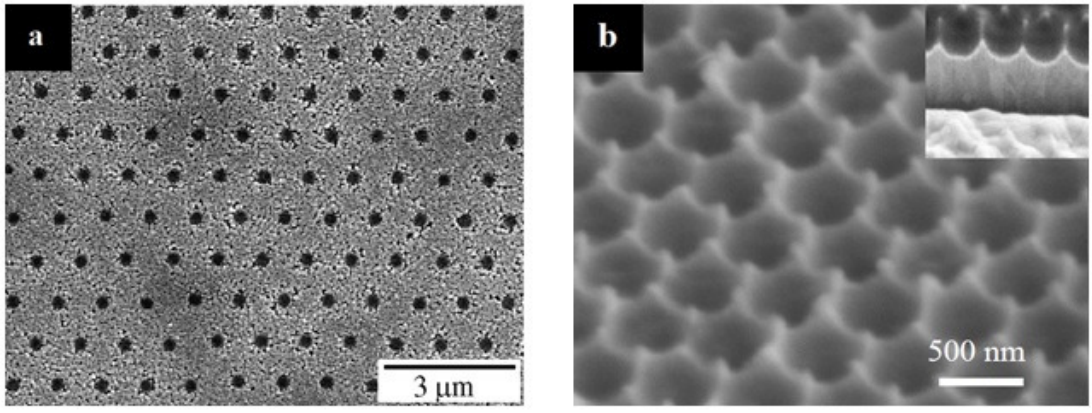

Figure 2-17 Honeycomb structures based on mould colloidal lithography: a) the Cu nanostructure fabricated by electroless plating [66], b) shows the Ni nanostructure fabricated by electrochemical deposition [67].

More recently, a double layer of PS spheres was also used as the mould for the ECD process to create 2D or 3D arrays of well ordered metallic nanodots[68]. Although this is a promising approach to generate such hybrid structures, it is crucial to keep the assembled colloidal mould steady over the substrate in the course of the electrochemical deposition process as it is affected by parameters like agitation or pH values of electrolyte.

2.4.3.3 Complex Colloidal Lithography

Apart from shadow and mould colloidal lithography as discussed above, there is another aspect that has been here named as complex colloidal lithography (CCL). As was studied earlier in this section, the arrays of colloidal spheres are normally employed as a mask or mould in nanofabrication, but, the 'complex' that here has been attached to colloidal lithography is due to the complexity of the fabrication steps, or the revealing of a new concept for fabrication. In the following paragraphs some of the latest patents and recent publications in this area will be discussed.

The first example of complex colloidal lithography is the fabrication of micro-lenses' arrays based on a modified micro-contact printing technique [69]. Their schematic fabrication process is illustrated in **Figure 2-18**. The Yang group first self assembled arrays of PS spheres over a substrate. Next, they used PDMS to replicate the self assembled structure and they used that structure as the new template for fabrication of micro-lenses' arrays. Next, a viscous UV-curable photopolymer was coated onto the PDMS template and was followed by placing a glass substrate over its surface. As the last step, they used UV light to cure the photopolymer and create a

micro-lens structure over a glass substrate by removing the PDMS. Similar work has been reported by the Yang group in 2007 and the only obvious development in their method was the creation of non-close-packed microwell arrays [70].

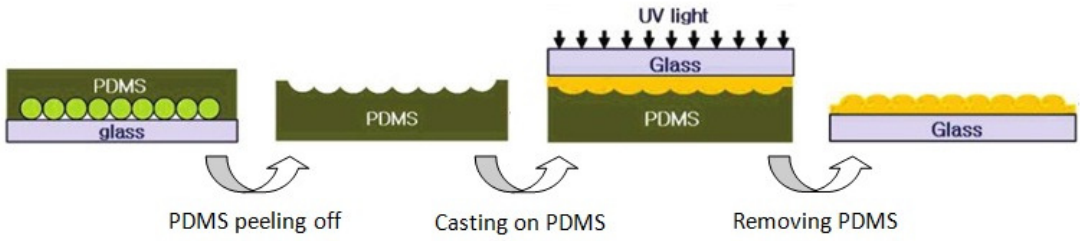

Figure 2-18 The fabrication steps for creating arrays of micro-lenses over glass substrate [69].

The other patent regarding the fabrication of ordered nanostructures using complex colloidal lithography is proposed by the Tan group [71]. Their proposed strategy is on the basis of colloidal lithography, porous anodic alumina template and electrochemical deposition. The colloidal particles' sizes are first reduced using oxygen plasma. Arrays of metallic nano-features are created on the silicon substrate through a thermal evaporation system. After removal of the PS particles, an aluminum film is coated over the prepared sample and is followed by anodization in oxalic acid to make the porous template. The final step is to use this template for the ECD process to grow nanowires only on the areas where there are underlying gold nanostructures.

However, the more interesting example of complex colloidal lithography is proposed by Wu and his co-workers [72, 73]. They revealed a new concept for colloidal lithography to be used as a fabrication tool. This group employed a single layer of silica spheres as lenses for focusing the UV light and creating nanopatterns over a photosensitive resist for the first time. They first self assembled a monolayer of

spheres over Shipley 1805 photoresist. Next, they used UV light to cure the photoresist and then removal of the spherical particles occurred. The final pattern of nanopillars was achieved after development of the photoresist; the result is shown in **Figure 2-19**.

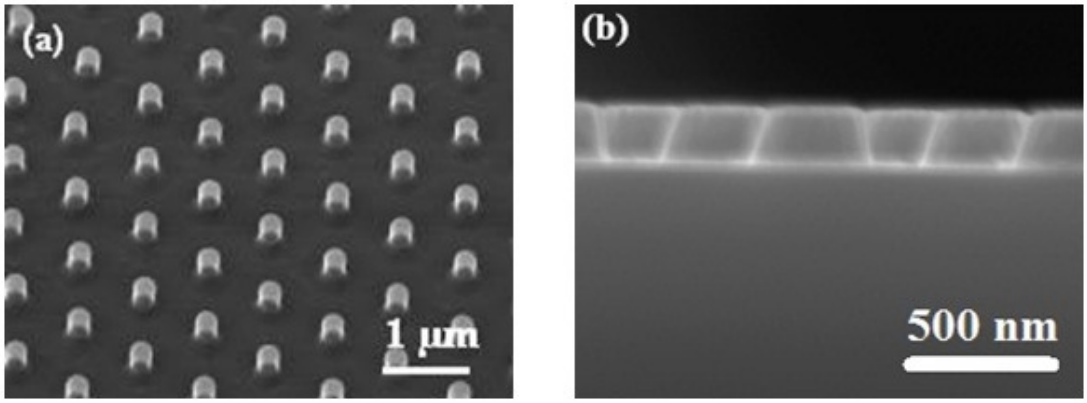

Figure 2-19 Top and side view of nanopillar arrays in negative photoresist with the period of 1µm [72, 73].

Two years after Wu's proposal, in 2011, a similar technique was applied in the Massachusetts Institute of Technology for the fabrication of nanostructures. Chang et al also used arrays of polystyrene spheres as lenses in their research [74]. The other noticeable change in their technique, which distinguished their proposal from the Wu group, was the usage of a transparent hydrogen silsesquioxane (HSQ) in between the spheres' layer and the photoresist, as a spacer layer. Through this approach, they were able to control the wave propagation distance for even a thin resist layer.

There is another CCL method in which the spherical particles are subjected to nano-machining [75]. A scheme of this strategy is illustrated in **Figure 2-20**. In this approach, an aqueous mix of PS spheres with 1 µm and silica nanoparticles with 50

nm is first prepared. This aqueous mix is then coated on a silicon substrate to form a bilayer of colloidal PS spheres with silica matrix at interstices between the PS spheres. Next, the RIE process is partially implemented to remove the top layer of PS spheres, and the continuation of this process would cause the appearance of three nanopores in each of the bottom layer PS spheres. Some similar works have been published later based on the same concept, and the slight changes were in either the assembly process or the etching process with a tilting angle [76].

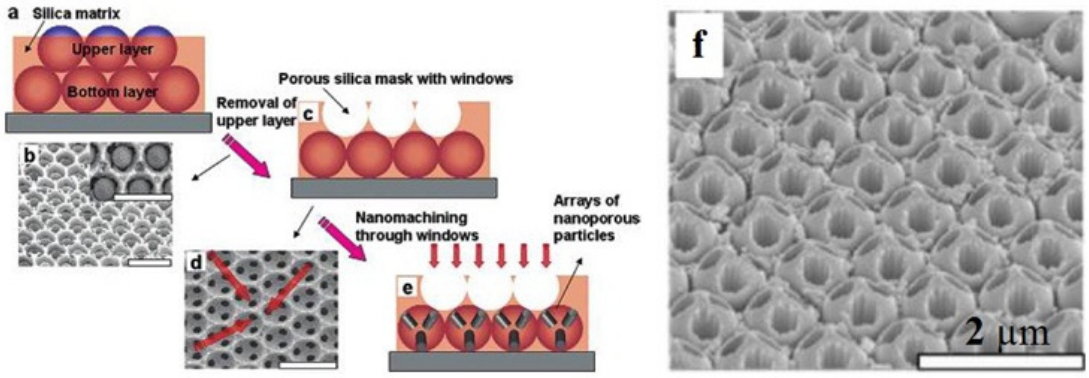

Figure 2-20 All of the fabrication steps for creation of colloidal particles with patterned nanopores [75].

2.5 Classifications and Applications of Periodic Nanostructures Assisted by Colloidal Lithography

Thus far, we have reviewed a number of the new types of nanostructures that have used colloidal lithography in their fabrication process. Although some of the created structures can be possibly generated with other lithography techniques, those methods are not able to offer cost-effectiveness, mass-production and a facile process. As was reviewed earlier in this chapter, there are different types of periodic

nanostructures; ordered arrays of nanopillars, nanoholes, nanodots, nanoposts or even complex nanopatterns are some of those structures. These patterned structures attracted much attention due to their variety of applications. In this section, some applications of CL assisted patterns will be reviewed to show the importance of focusing research in colloidal lithography.

The first example concerns ordered arrays of metallic nanopatterns. In particular, arrays of gold and silver nanoparticles have attracted the interest of scientists due to their advantages in biological and optical devices. Localised surface plasmons are charge density oscillations confined to metallic nanoparticles and metallic nanostructures [77]. Excitation of these localised surface plasmons by light at a specific wavelength where resonance occurs induces strong absorption or scattering of incident light and electromagnetic field enhancement [78, 79]. This phenomenon is known as localised surface plasmon resonance (LSPR). Factors like shape, size, periodicity of patterns and materials as well as the surrounding environment are considered as those parameters which directly influence the position of maximum excitation (λ_{max}) and the peak shape. The Van Duyne group have investigated the lattice spacing and the shape dependence of fabricated gold and silver nanostructures through LSPR measurement [80]. They observed shifts in the position of λ_{max} for different sets of cylindrical nanopatterns with various surface morphologies or with different periodicities. Aizpurua et al and Hanarp et al both used colloidal lithography to fabricate ordered arrays of nanoring and nanodisk, respectively [81, 82]. Both groups have studied the size and shape dependence of fabricated structures by varying the thickness of the nanorings or the diameter of the nanodisks. As is

illustrated in **Figure 2-21**, the position of maximum excitation was blue-shifted as the wall-thickness of the nanoring was increased.

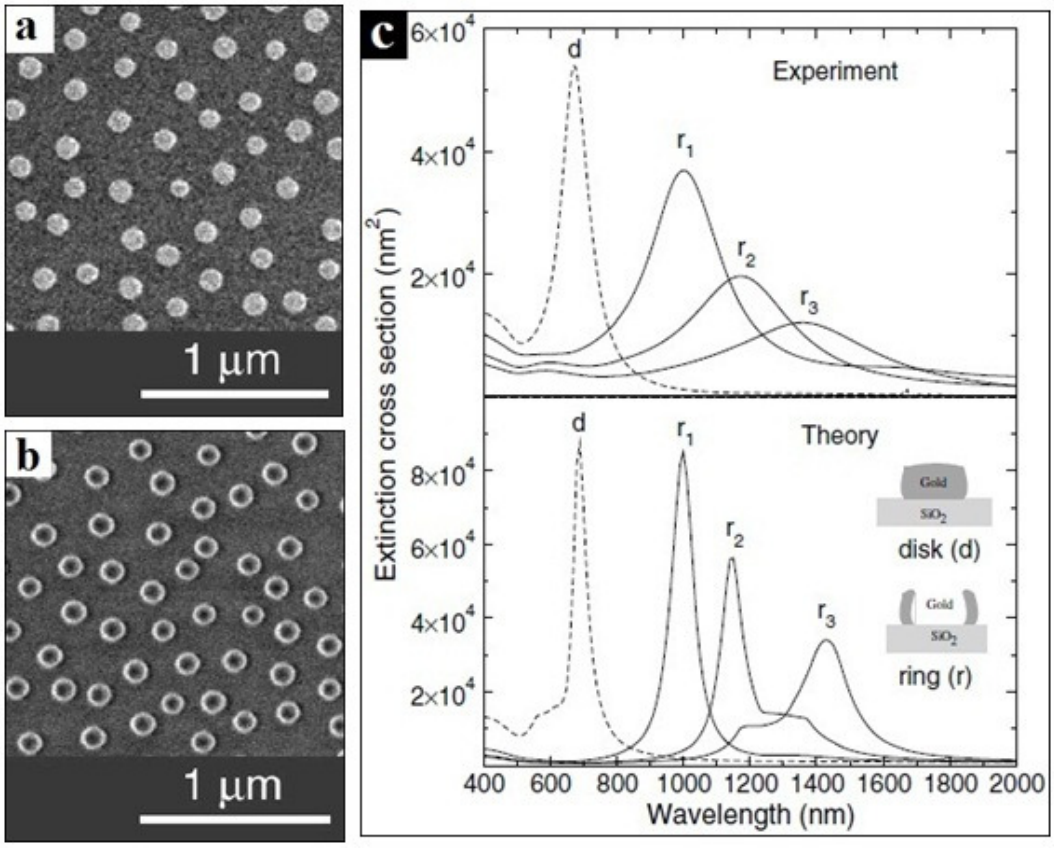

Figure 2-21 (a, b) the top view SEM images of nanodisk and nanoring, (c) the experimental and theoretical extinction spectra of nanostructure arrays (r1: 14 nm, r2:10 nm, r3:8 nm) [81].

Bio-sensing or chemical-sensing is one of the leading applications for this sort of metallic nanostructure. In the LSPR-based optical sensing method, ordered arrays of metallic nanopatterns are employed as an effective platform to detect biological or chemical targets. The signal transduction mechanism of the LSPR nanosensor is based on small changes in the refractive index near the surface of the nanostructure as stated earlier. The first appearance of a LSPR nanosensor as a detection tool was reported by Haes and his co-workers to determine if amyloid-derived diffusible ligands (ADDLs) antibodies are a potential biomarker for Alzheimer's disease [83].

In their research, they prepared arrays of triangular Ag nanoparticles with 25 nm thickness over a glass substrate using polystyrene spheres. Next, several chemical functionalisation steps were run to complete the sandwich assay (attaching antibodies to nanopatterns) over the nanostructures. Their initial experimental results confirmed that the position of maximum extinction is varied even for small changes in concentrations of ADDLs antibodies. Since their achievement of the detection of changes in the antibodies concentrations' was successful, they were encouraged to analyse cerebrospinal fluid (CSF) from an aging patient and an Alzheimer's disease patient. As is depicted in **Figure 2-22**, a significant LSPR shift is observed for the CSF sample of an Alzheimer's disease (AD) patient in respect to an aging patient.

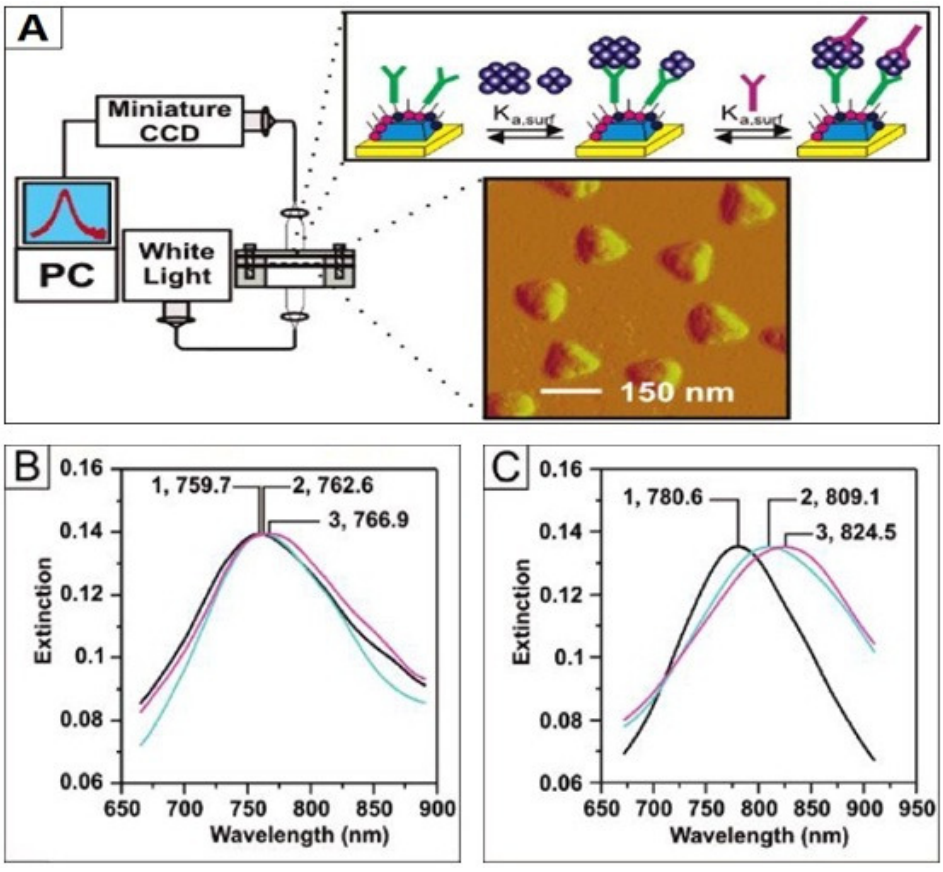

Figure 2-22 The schematic design and the experimental results: a) transmission UV-Vis spectroscopy is used to measure the optical properties of LSPR-based nanoparticles, b) LSPR spectra for aging human CSF sample, c) LSPR spectra for AD human CSF sample [83]. (The black, blue and pink curves represent the specific spectra for samples with antibodies, antibodies-CSF and antibodies-CSF-antibodies, respectively.)

In addition to the aforementioned application for the CL assisted nanostructures, ordered arrays of patterns with high aspect ratio have also attracted researchers' attention due to their surface wettability. This sort of structure is identified as a self-cleaning film for applications like eye glasses or swimming goggles. They have potential to remove dirt and contamination from their surfaces when a water droplet slides along their surfaces [84, 85]. The self-cleaning effect for structures with nanoposts and nanopillars arrays is generally focused on the super-hydrophobicity effect of a surface. Due to the low surface free energy and large contact angle of a water droplet the self-cleaning process happens. Periodic nanopatterns assisted by a colloidal template provide sufficient roughness on the surface for trapping the air and enhancing the hydrophobicity effect. Further modifications through chemical coating of low free energy materials over nanostructures may lead the formation of a super-hydrophobic surface [86]. For example, Min et al studied the effect of etching time on the surface hydrophobicity for nanopillars' structure. They used the colloidal spheres as a template to fabricate uniformed arrays of nanopillars over a glass and a silicon substrate [87].

As is shown in **Figure 2-23**, the surface hydrophobicity dramatically increased because of the enhancement in the structure aspect ratio. They could successfully achieve a super-hydrophobic structure with a water contact angle of 172º after a one hour RIE process. A similar approach has been carried out by the Yang group in 2009, which terminated in the creation of high aspect ratio silicon hollow-tip arrays[88]. This group observed that such nanostructures have the potential to trap the air in the area between tips after chemically coating them with fluorosilane. Their

results revealed the advantage of using low free energy materials over periodic structures in converting a hydrophobic platform to a super-hydrophobic platform.

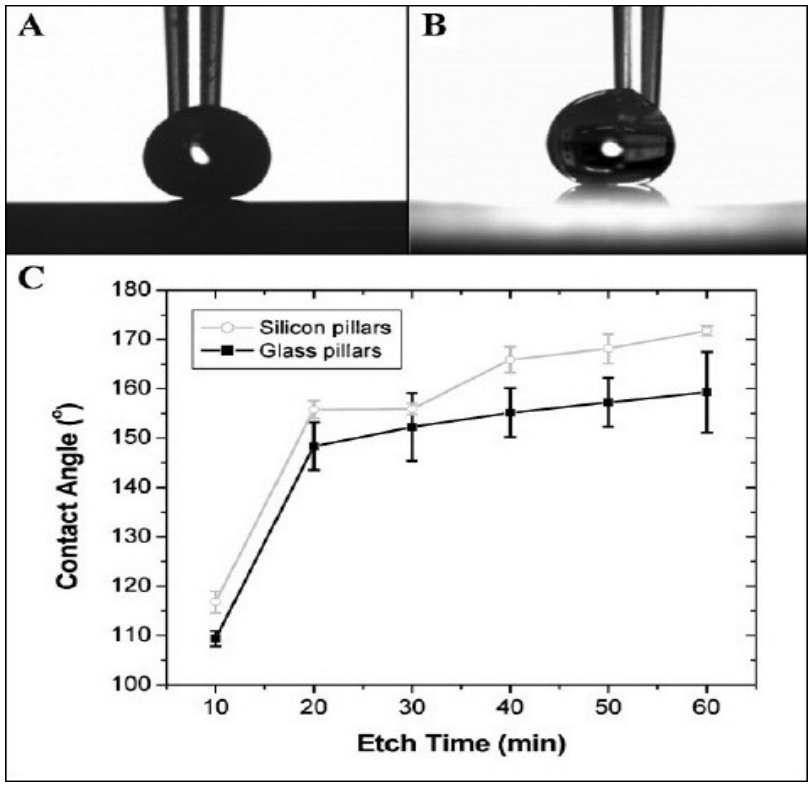

Figure 2-23 The super-hydrophobicity effect: a) a water drop profile onto a silicon patterned substrate, b) a water drop profile onto a glass patterned substrate, c) rate of changes in water CA by increasing etching time [87].

The other advantage of CL assisted structures can be discovered in photonic crystal studies. The term photonic crystals is applied to periodic micro/nanostructures which are able to control light. In a nutshell, the idea is to design periodic structures so that they can affect the motion of photons in much the similar principle that the atomic lattices in semiconductor crystals affect the motion of electrons [89]. A periodic structure could possess an absolute photonic band gap (PBG), when it contains arrays of that periodic structure with a large dielectric constant embedded in a material with a low dielectric constant [90]. Therefore, some ranges of wavelengths

do not exist at that band gap, unless there is a defect or mistake in the structure which assists the photons localization. Based on the nature of the defect, these structures can be used for different applications such as a waveguide. It is worth noting that the periodicity constant of the photonic structures must be comparable to the light wavelength [91]. Kempa et al created periodic arrays of aligned carbon nanotubes using colloidal spheres and they observed that the patterned structure appeared colourful due to the strong diffraction of visible light [92]. Additionally, they mentioned that because of the different dielectric constants of aligned structures from the environment, this structure is a good candidate to be used as a 2D PBG structure.

Apart from the above applications, there are some more reported applications for CL assisted nanostructures including nano-filtration [93], memory devices [94] and fuel cells [95] which all together determine the necessity of focusing research on colloidal lithography to develop new label-free nanostructures.

2.6 **Summary**

In this chapter the current lithographic nanofabrication methods are reviewed to identify the most reliable and high throughput nano-patterning technique. Colloidal lithography as the candidate method is fully studied to not only clarify the necessity of research in this area, but also recognise its drawbacks for further development. In Section 2.2 the major lithography techniques for creating periodic nanostructures have been discussed. These methods include photolithography, electron and ion beam lithography, soft lithography, nanoimprint lithography, scanning probe lithography and colloidal lithography. In Section 2.3 the main advantages and disadvantages of each technique as well as some other parameters such as patterning procedures, feature resolutions and operating conditions are evaluated. On the basis of the comparison between the mentioned nano-patterning methods it can be concluded that, colloidal lithography is the most promising fabrication tool when periodic structures are needed. Colloidal lithography can satisfy all those protocols which are required for volume nano patterning like time and cost efficiency.

The evaluation of major lithographic techniques is followed by a detailed review of the state-of-the-art in colloidal lithography in Section 2.4. Silica and polystyrene spheres were identified as the main candidates due to their high performance in the self assembly process. Four methods including drain coating, drop coating, spin coating and electrophoretic deposition were introduced as the proposed assembly processes. Dynamics of self assembly were studied to not only understand the mechanism of spheres arrays formation, but also to purposely identify the affective

parameters in the assembly process. The detailed review of colloidal lithography was finalized by classification and identification of registered patents in which the CL technique is applied as a patterning tool. Although, this work presents the recent achievements in the CL technique for creating periodic nanostructures, there is still plenty of room for researchers to investigate and improve colloidal lithography. Challenges such as achieving a wider defective free area of nano-features or patterning dual arrays of nano-features still remain unsolved. Some applications of CL assisted nanostructures are reported in Section 2.5 to exhibit the interest of scientists and engineers for further development in this field.

The review in this chapter has a considerable influence on the direction of this research. The possible approaches for the fabrication of periodic nanostructures with varied shape are selected. Preparation of a defects-free monolayer or bilayer colloidal template, and fabrication of well ordered nanopatterns are identified as the main challenges faced in this research. The following research opens up a new route to the fabrication of periodic nanostructures with different materials.

CHAPTER 3: PS SPHERES AS MICRO-LENSES

3.1 Introduction

This chapter describes the use of colloidal spheres as micro-lenses for the fabrication of two dimensional (2D) periodic nanostructures over a photoresist coated template. The study involves simulations of UV light through colloidal spheres as well as fabrication and characterization of periodic nanostructures using modified colloidal lithography. The chapter begins by presenting the general fabrication processes of single and dual nanoholes arrays in Section 3.2. The investigation is carried out by computer simulation to understand the behaviour of electromagnetic waves at inside and near-outside of the spheres and the work is presented in Section 3.3. The materials used in the fabrication process are presented in Section 3.4. Fabrication process details and experimental results of monolayer colloidal lithography (MCL) and bilayer colloidal lithography (BCL) are discussed in Sections 3.5 and 3.6, respectively. The assembly processes of single and double layer of spheres over photoresist are crucial parts in this modified colloidal lithography technique and affect the quality of each subsequent step in the fabrication process. This chapter is finally summarised in Section 3.7.

3.2 General Overview of Fabrication Process

The general process for the fabrication of 2D periodic nanostructures including single arrays of nanoholes and dual arrays of nanoholes consists of the following steps:

1. Preparation of thin film photoresist over substrate.
2. Self assembly of monolayer and bilayer colloidal spheres over the photoresist coated substrate.
3. Implementation of UV exposure process.
4. Removal of colloidal particles from the photoresist coated substrate.
5. Development process

The general overview of periodic nanostructures fabrication is schematically illustrated in **Figure 3-1**. AZ photoresist and polystyrene spheres are proposed as suitable materials for this fabrication process, the reasons for this will be explained in the related sections of this chapter. Apart from the proposed materials, modification and optimization are carried out for each processing step to achieve high resolution and accurate patterns over a relatively large area through a completely controlled process.

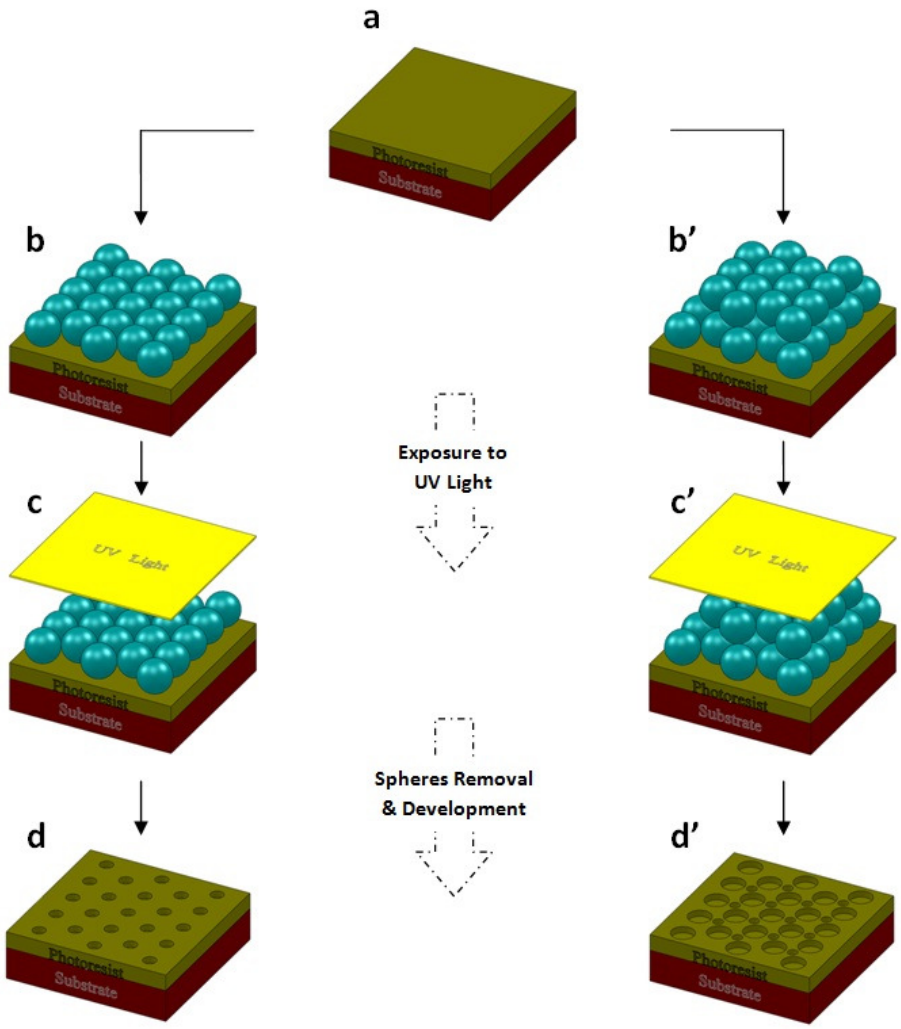

Figure 3-1 Schematic diagram of fabrication: a) casting of photoresist, b & b') self assembly of single and double layer spheres, c & c') UV light exposure, d & d') developed mould after spheres removal.

3.3 **Modelling and Simulation**

Studying the behaviour of electromagnetic waves at the inside and near-outside of cylinders or spheres through computer simulation is the best way to understand and analyse propagation of UV light in colloidal particles [96]. The modelling and simulation was carried out using Microwave Studio Software provided by Computer Simulation Technology (CST) [97]. The modelling consists of three steps. The

definition phase is the first step in which the parameters such as geometry of the structure, properties of the material and boundary conditions are defined. The second step is called the analysis phase which is performed thoroughly by nominated software based on pre-defined physics and relevant solver. The last step is the post-processing phase which is related to the numerical results and graphical outputs. Since the monolayer and bilayer of the colloidal spheres are planned to be used as a fabrication tool for the creation of periodic nanostructures, the modelling of a real profile is required. The following subsections show the aforementioned phases when a single and double layer of spheres are exposed by electromagnetic waves.

3.3.1 Modelling of Monolayer Spheres

3.3.1.1 Definition Phase

This model consists of three components as is shown in **Figure 3-2**. The first component is a thin film which represents the photoresist layer. The second component is a sphere which represents the colloidal particle. To make the model more similar to the real case which is a monolayer of self assembled colloidal spheres, seven spheres are considered as a single layer. The final component of this modelling is a big box that indicates the whole area is surrounded by a vacuum. The dimensions of the defined components are given in **Table 3-1**. Since the geometry of components is not complicated, the modelling section of the CST Microwave Studio was used to generate the 3D model. Although the modelling procedure in 3D required more time to set up and solve, this procedure was preferred to 2D modelling

to achieve more accurate results. The material properties of each component were defined after generating the model geometry. **Table 3-2** gives the material properties of the colloidal particles and photoresist which were required by the software.

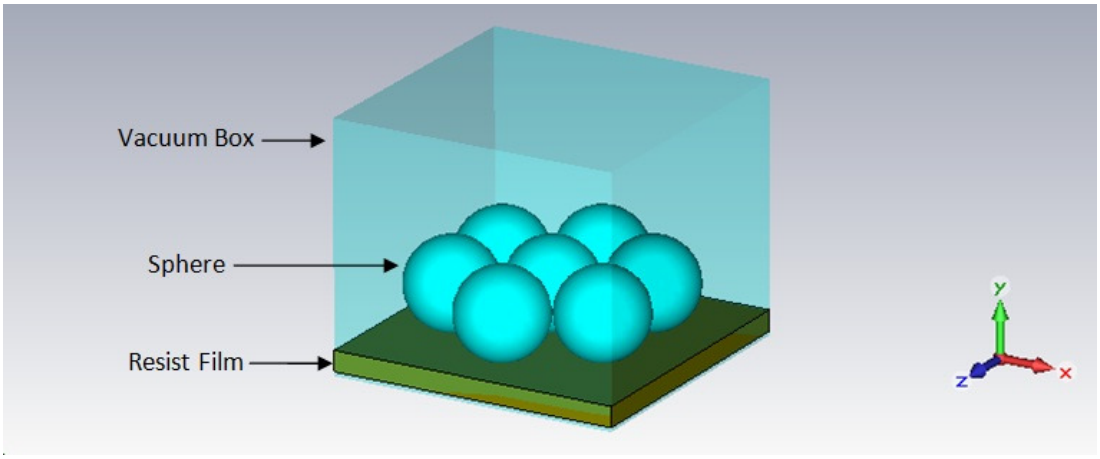

Figure 3-2 Constructed model of single layer spheres in CST Microwave Studio.

Table 3-1 Parameter list for defining components dimensions.

Name	**Value** (nm)	**Description**
a	3500	Length of vacuum box
b	3500	Width of vacuum box
c	3000	Height of vacuum box
h	300	Height of resist film
r	550	Radius of sphere

Table 3-2 Material properties of photoresist and colloidal particles.

	Density (ρ) kg/m^3	**Refractive index (n)** (at wavelength 400 nm)
Polystyrene sphere	1050 [98, 99]	1.61 [100, 101]
AZ photoresist	1000 [102]	1.68 - 1.70 [103]

To prevent any unexpected reflection or absorption of electromagnetic waves, open boundary conditions were specified for the vacuum box walls. All exterior walls of other components including spheres and resist film which had interfaces together, were defined as the fixed constraints. After constructing the model and defining the boundary conditions, the hexahedral grid which is the fully automatic meshing procedure was selected to divide the model into several thousand elements. To increase the accuracy of the simulation even more, the perfect boundary approximation (PBA) feature was applied to the aforementioned meshing procedure. The exact number of 2,789,964 mesh cells was created after running the meshing system. To simulate the UV light propagation through single arrays of spheres, a plane wave was incident from the top. In other words, the top surface of the vacuum box was considered as the light source with the wavelength of 365 nm representing the i-line in a conventional mask aligner. As the final step, Transient Solver was chosen as a remarkably efficient method to support the plane wave excitation. Transient Solver allows the simulation of a structure's behaviour for a wide frequency range in just a single computation run [104].

3.3.1.2 Post-Processing Phase

The graphical output is illustrated in **Figure 3-3**. This result confirmed that each individual sphere acts as a near field lens to focus UV light. The intensity of the achieved hot spot (focused light) at the shadow-side surface of the sphere is about five times stronger than the input light. It is worth noting that there is not any diffraction in the hot spot. Therefore, highly ordered arrays of nanopatterns would be

expected to be possible achieve in experiments. The full width at half maximum (FWHM) waist of the hot spot is about 225 nm. The radius of microspheres and the value of input wavelengths are recognized as effective parameters which can influence the simulation results. For studying the effects of these variables, the investigation was performed with one variable changed each time.

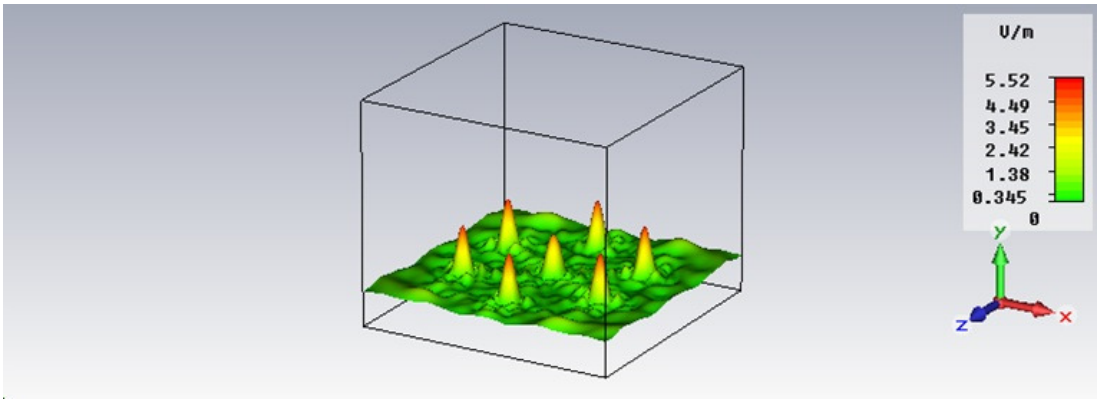

Figure 3-3 The carpet plot shows the intensity of modelled UV light on the photoresist surface when a single layer of spheres are considered.

The constructed model was simplified to a single microsphere which embedded in the vacuum. The reason for this issue was to prevent the high number of meshing and consequently a long analysis phase. The simulation was run for a sphere with different radiuses of 275 nm, 550 nm and 1.1 μm while the wavelength was kept constant at 365 nm. In **Figure 3-4**, the right cross-section view shows the calculated field distribution when the radius of the sphere is varied. As is observed from this figure, the FWHM waist of the hot spots is slightly changed despite a 4-time change which applied to the sphere radius.

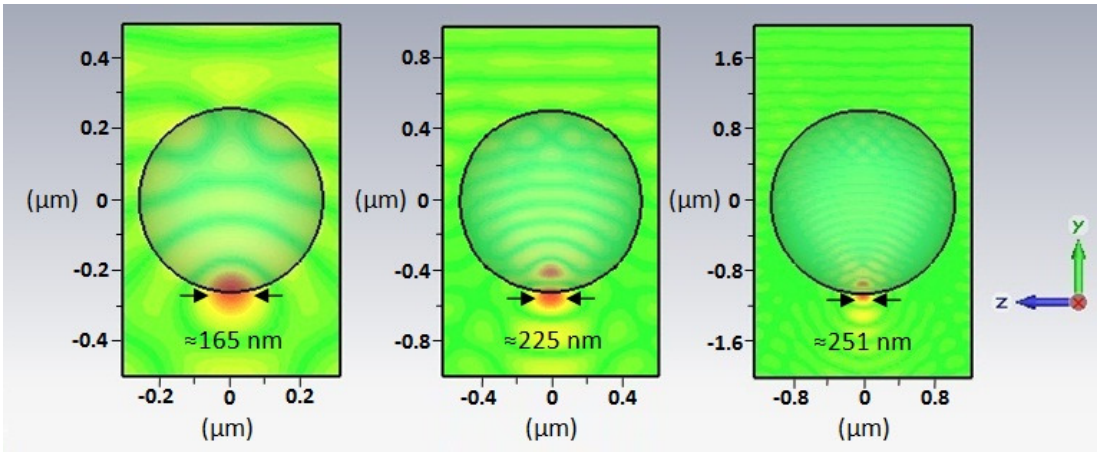

Figure 3-4 The calculated field distribution for sphere with radiuses of 275 nm, 550 nm and 1.1 µm at wavelength of 365 nm. (From left to right the sphere's radius is increased)

By applying different wavelengths to the model while the radius of the sphere was kept constant at 550 nm, it was realised that the FWHM waist of the hot spot tends to be bigger as the wavelengths get bigger. The normalised intensity cross-section for different wavelengths of 350 nm, 450 nm and 550 nm is illustrated in **Figure 3-5**. Unlike the achieved results when the sphere size was subject to change, the slight changes in wavelengths noticeably influenced the FWHM waist of the hot spot. The waist of the hot spots is reduced from about 390 nm to 220 nm, when the wavelengths decrease from 550 nm to 350 nm. The value of the FWHM waist of a hot spot is a good measure to roughly estimate the size of nanopatterns that would be created on photoresist surface. Using the linear trend-line, the relations of hot spot waist (w) with sphere radius (r) and with wavelength (λ) are found as the following **3-1** and **3-2 Equations**, respectively.

$$w = 0.0961r + 152 \qquad \textbf{Eq. 3-1}$$

$$w = 0.85\lambda - 82.5 \qquad \textbf{Eq. 3-2}$$

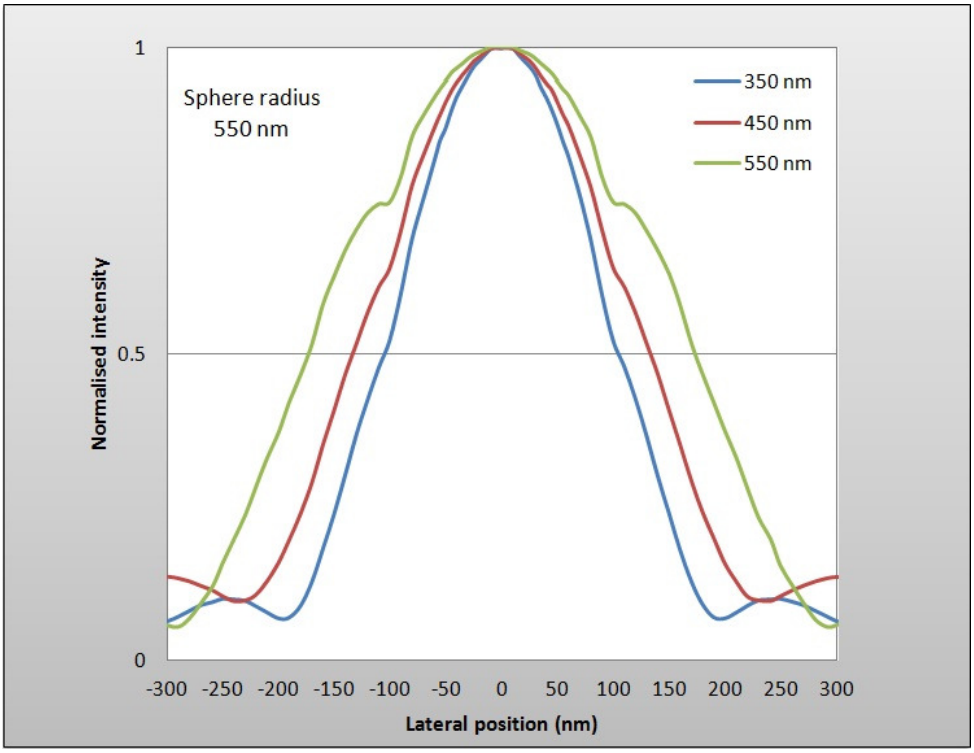

Figure 3-5 The normalised intensity of hot spot versus the lateral position for different wavelengths.

From the simulation results in **Figure 3-4**, it can be observed that the focal point of each microsphere is placed exactly at its shadow side, while the classical optical predictions for focal length demonstrate other values for a simple spherical lens. The values of focal length for classical calculation and simulation results are give in **Table 3-3**.

Table 3-3 Values of focal length associated with classical calculation and simulation results.

Sphere's diameter (μm) / **Values of focal length**	**0.55**	**1.1**	**2.2**
Classical optical predictions	230 nm	458 nm	916 nm
Simulation results	275 nm	550 nm	1100 nm

The comparison of classical optical predictions and simulation results shows a discrepancy between the values of focal length when a microsphere with same radius is used. It is worth noting that the values of material's relative permittivity and relative permeability are required by software instead of the value of refractive index. Therefore, it can be possible that the value of calculated refractive index by the software is slightly smaller than the value of proposed refractive index. Hence, a discrepancy is observed between the focal length for the classical optical predictions and the simulation results.

It should be noted that CST Microwave Studio is a general-purpose electromagnetic simulator based on the Finite Integration Technique (FIT), and the simulation results describing the interaction between electromagnetic waves and microspheres by solving Maxwell's equations.

3.3.2 Modelling of Bilayer Spheres

3.3.2.1 Definition Phase

Similarly to the single layer modelling, this model consists of three components as is shown in **Figure 3-6**. These three include a thin film, sphere and a box which represent the photoresist layer, the colloidal particle and the vacuum, respectively. To make the model more similar to the real case which is a bilayer of self assembled colloidal spheres, ten spheres are considered in total. The double layer of microspheres consists of seven spheres as the bottom layer and three spheres as the

top layer. The same parameters which were previously mentioned in **Table 3-1** and **Table 3-2** are considered to define the dimensions and the material properties of components, respectively.

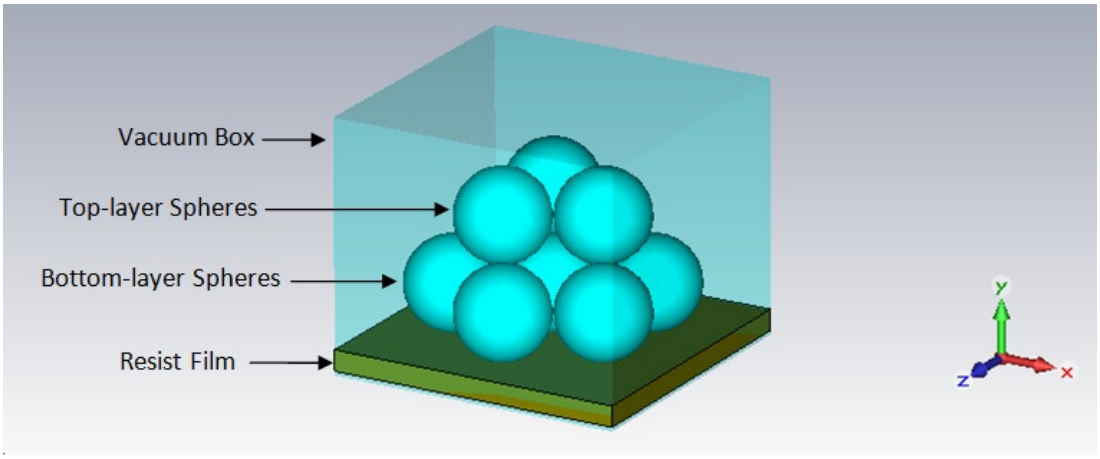

Figure 3-6 Constructed model of double layer spheres in CST Microwave Studio.

For defining the boundary conditions, again the vacuum chamber walls are considered as the open boundaries and the rest of the exterior walls including those surfaces that have interfaces together were defined as fixed constraints. After constructing the model and defining the boundary conditions, the hexahedral grid was used to mesh the geometry and the exact number of 3,286,332 mesh cells was created after running the meshing procedure. Similarly, a plane wave was incident from the top at a wavelength of 365 nm and the Transient Solver was selected for the analysis phase.

3.3.2.2 Post-Processing Phase

The graphical output of the simulation is displayed in **Figure 3-7**. The carpet plot shows a different result in comparison to the achieved result from when a single layer was used, especially for the position of the centre sphere in the bottom layer which was totally covered by the top layer spheres. As is observed, the intensity of focused light resulting from the centre sphere in the bottom layer is much lower compared to the surrounding spheres.

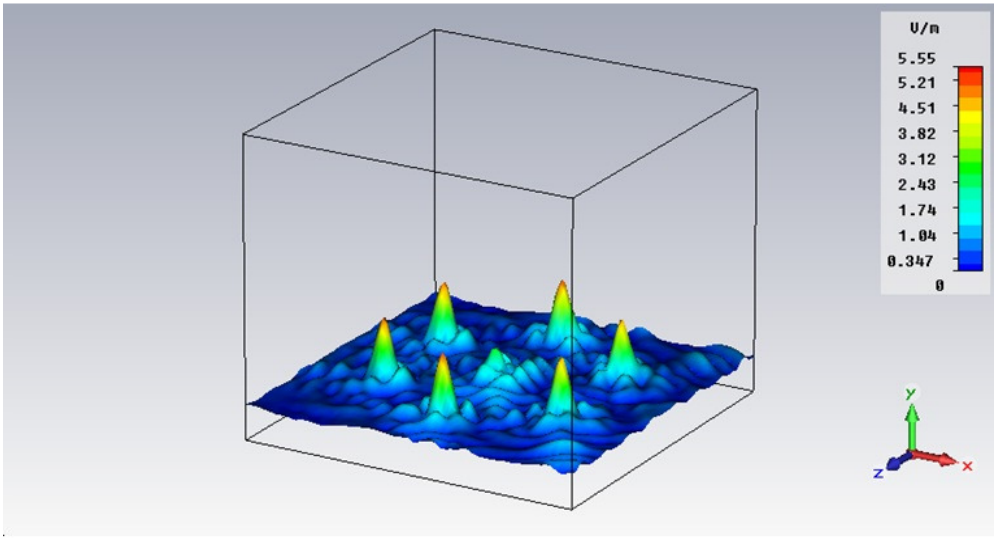

Figure 3-7 The carpet plot shows the intensity of modelled UV light on the photoresist surface when double layer of spheres are considered.

Figure 3-8a illustrates the field distribution at the bottom of the top layer spheres. As it is expected, each of the top layer spheres acts as a near field lens to focus UV light. Interestingly, the middle sphere surrounded by six other spheres in the bottom layer formed three hot spots as shown in **Figure 3-8b**. The FWHM size of each hot spot caused by the centre sphere at the bottom layer is about 110 nm. It is also observed that the intensity of the three hot spots produced by the bottom layer is less

than half of the intensity of the single spot resulting from the top layer. Despite the weak intensity of the three spots in the bottom layer, they can still expose the photoresist. The simulation indicates that the top layer of spheres not only act as lenses to focus light, but also direct the light to the bottom spheres as shown in **Figure 3-8c**. Beams are channelled into each bottom sphere from the top three spheres.

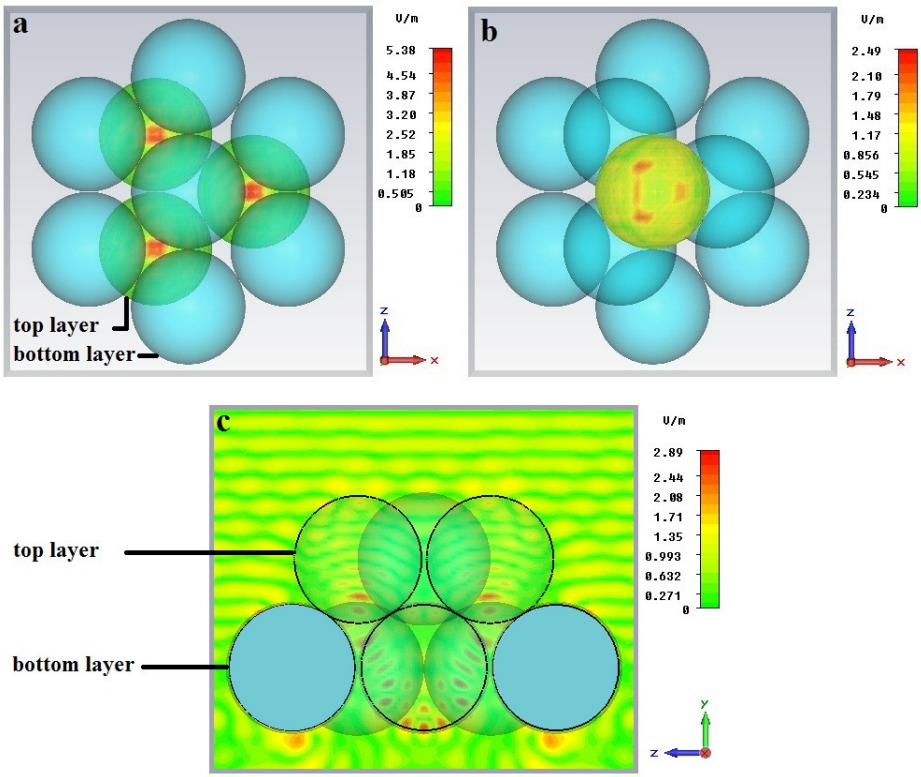

Figure 3-8 Simulation result: a) Propagated waves are focused after passing through the top layer of microspheres (bottom view), b) Propagated waves are focused into three hot spots at the shadow side of the bottom layer microspheres (bottom view), c) Direction of propagated waves starts from the top layer to the bottom layer (side view).

Simulation further shows that the size of the hot spots resulting from the bottom layer spheres is reduced from about 135 nm to 105 nm, when the wavelengths decrease from 450 nm to 350 nm; however, no obvious changes were observed in respect to varying the spheres' radius from 275 nm to 1.1 μm.

3.4 **Materials Used in Experiments**

3.4.1 Mono-Dispersed Spheres

The research for the preparation of mono-dispersed spheres or highly uniform spheres dates back to the early 1940s, when LaMer and Barnes obtained uniform particles through the Burst Nucleation process [105, 106]. Nowadays, these highly uniform spheres are commercially supplied in various forms and sizes. Highly uniform particles align themselves into systematic hexagonal arrays when delivered on a flat surface along with their liquid medium, and this is counted as the main reason for utilizing them in various nanofabrication processes. Mono-dispersed polystyrene (PS) spheres are the nominated types that were used in the following experiments because of their better performance in the assembly process and also their appropriate value of optical index. Among different groups of mono-dispersed PS spheres, the size-standard category was selected due to its high precision in terms of size. Each mono-dispersed PS sphere in the size-standard category is identified by its four digits that point to the particles' series and diameters. The selected properties of PS-4011 are presented in **Table 3-4**.

Table 3-4 Selected properties of polystyrene spheres type 4011 suspension in water [107]**.**

Properties	**Unit**
Density (g/cm^3)	1.05
Solids content (%)	1
Size distribution (%)	1
Particle size (µm)	1.1
Melting point (c°)	240
Glass transition (c°)	95

3.4.2 AZ Photoresist

AZ photoresists, polyhydroxystyrene-based polymers, comprise negative and positive tone resists for almost all lithography applications. The first AZ product was manufactured by Hoechst in 1962. In general, the AZ photoresists are divided into two major groups including standard and advanced which cover all the AZ series. Each AZ photoresist is identified by its four digits. The first two designated digits point to the resist series while the last two designated digits indicate the coating thickness at 4000 rpm in 100 nm units. The photoactive compound in AZ resist is converted to indene acid in the presence of UV light. A relatively humid of environment is required for this conversion. This acid is later dissolved in the developer. A post exposure bake is occasionally applied to some AZ products to improve their lithography performance [108].

The lithography process using AZ resist provides products with the followings advantages: striated-free coating quality, high contrast, high resolution and vertical wall profiles [109]. AZ photoresists cover a wide range of thicknesses from 0.5 to 50 micrometers, depending on the type of AZ resist and the subsequent processing steps like spin coating and soft baking. The AZ 5200 series is a developed version of AZ resist for operation at shorter wavelengths. It is worth noting that the AZ 5200 series are only sensitive near the i-line and h-line due to the existence of different photoactive compound in its formula [110]. AZ 5214-E is the nominated type that was used in the following experiments.

3.5 **Fabrication of Single Arrays of Nanoholes using MCL**

The fabrication steps are schematically illustrated in **Figure 3-9**. A clean silicon substrate is first coated with a thin layer of AZ 5214-E resist followed by soft baking. Afterwards, a monolayer of PS spheres is assembled on the photoresist coated substrate. Surface treatment is essential prior to the self assembly process to achieve uniform arrays of the mask of nanospheres. The sample is then exposed to UV light using a conventional mask aligner. In a positive photoresist such as AZ 5214-E, the unexposed area remains insoluble during the developing process. Next, the PS spheres are removed from the sample ultrasonication in deionised water. After the development step, ordered arrays of nanoholes are formed over the remaining photoresist on the substrate. As the final step, hard baking is applied to prevent any morphological changes of the prepared patterns during the subsequent processes.

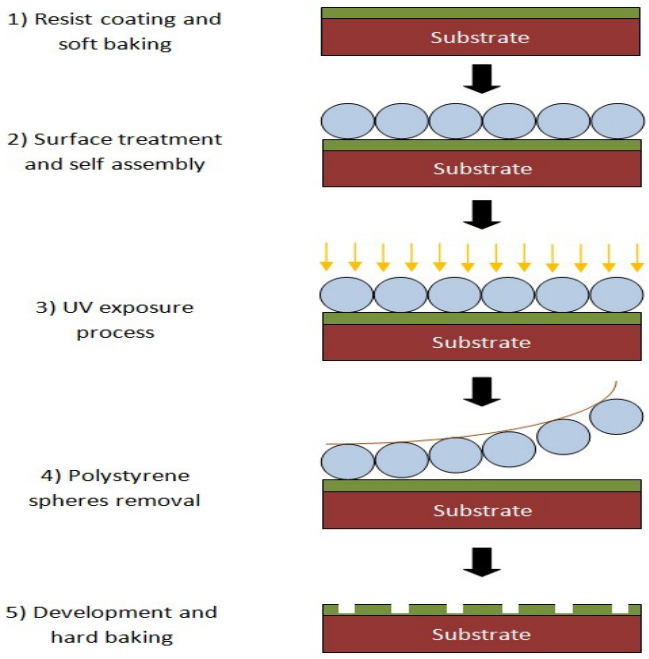

Figure 3-9 A schematic diagram of fabrication steps using MCL technique.

3.5.1 Photoresist Coating

A standard 4 inch silicon wafer with a thickness of 500 µm was selected as the substrate. The selected substrate was then cut into 1.5 cm × 1.5 cm pieces. Next, these pieces were cleaned prior to the resist coating process to ensure there were no chemicals or dust on the surface of the pieces. Weak bonding of the photoresist with the substrate or cross-linking of the photoresist before exposure, are some of the common problems which occur due to the existence of any particles over the substrate surface. The surface of each substrate was cleaned with acetone and Isopropanol (IPA) while it was being spun by a spinner at 800 rpm. Afterwards, they were immersed in deionised water and their surfaces were dried using nitrogen gas. Finally, to ensure the cleanliness of all the silicon pieces from any remaining solvents, they were placed over a hotplate at 150 ºC for 10 minutes.The spin coating technique was used to cover the substrate surface with the desired photoresist. According to the datasheet of AZ 5214-E, the thinnest film thickness of 1.14 µm is achievable when using a spinner with a spin speed of 6000 rpm [111]. The AZ 5214-E resist was dispensed to cover 40% of the silicon substrate and then spun coated to obtain a thin film with 1.14 µm thickness. One of the common problems using the spin coating method is the appearance of air bubbles on the resist surface. To minimise this issue, prior to the spin coating process, a gentle rotational movement was applied to spread the resist all over the substrate.

The rest of the air bubbles were treated by simply using a metallic needle after the spin coating process. The samples were then baked over a levelled hotplate for 50

seconds at 100 ºC. It is worth noting that any baking above 115 ºC would affect the resist formulation and consequently cause the activation of image reversal capability of the resist.

3.5.2 Self Assembly of Single Layer PS Spheres

As explained in the literature, there are several proposed techniques for monolayer self assembly. Since the self assembly process is performed over a photoresist coated substrate, the drop coating technique is chosen as the most appropriate candidate for this experimental work. As the first step, the latex/water proportion was estimated by considering that a monolayer of microspheres should cover the area of the substrate thoroughly. The amount of latex/water proportion for covering the desired surface can be calculated based on the following equations [39].

$$\alpha = \left(\frac{3\omega}{4\rho\pi r^3}\right) \times 10^{12} \qquad \textbf{Eq. 3-3}$$

$$N_p = \frac{A_d}{\pi r^2} \qquad \textbf{Eq. 3-4}$$

$$\beta = \frac{N_p}{C} \qquad \textbf{Eq. 3-5}$$

The original concentration of spheres in the purchased product is determined using **Equation 3-3**, in which ω is the solid content of product, ρ is the density, and r is the sphere radius. After obtaining the original concentration of particles per micro-litre, it is necessary to calculate the required latex/water proportion for the desired surface.

For this issue, the number of microspheres which occupied the desired area is determined using **Equation 3-4**. A droplet of C = 10 µl was supposed to cover the desired area of A_d = 2.25 cm^2. The required latex/water proportion can be found through **Equation 3-5**.

Preparation of a single layer of microspheres over photoresist coated substrate begins with resuspension of particles in the bottle. Since particles settle at the bottom of the bottle, a gentle rolling is required prior to usage. Then, a micropipette was used to place a droplet of diluted aqueous suspensions of polystyrene spheres with a mean diameter of 1.1 microns onto the substrate. PS spheres evenly spread out across the surface of the substrate due to the lateral capillary attraction and convective flow in between the particles. The droplet was spread evenly and a monolayer of spheres was formed after about 40 minutes. **Figure 3-10** shows the initial result of the experiment.

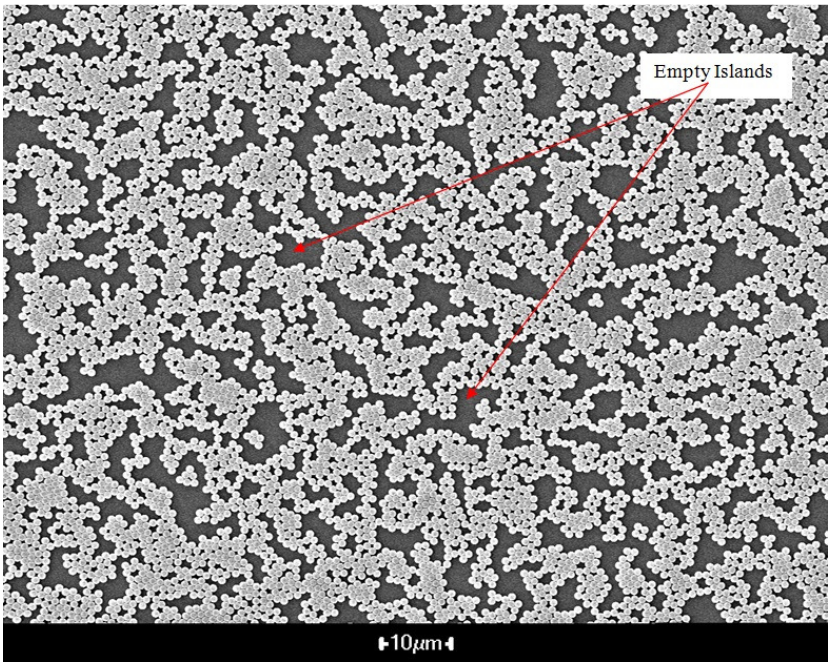

Figure 3-10 Non-uniform arrays of self assembled microspheres over the resist surface.

3.5.2.1 Effect of Surface Treatment

As observed from **Figure 3-10**, the perfect hexagonal close pack of PS spheres was not achieved over the substrate due to the hydrophobicity of the resist surface. To overcome the surface hydrophobicity of the resist and optimise the uniformity of the PS sphere arrays, several experiments were performed. **Table 3-5** presents some of these experiments from the investigation of different treatment times. The samples were categorised into three groups on the basis of the treatment time. In these experiments, each time, a group of samples were dipped into the AZ developer followed by rinsing with deionised water for a certain amount of time. The treatment time for the group A was 10 seconds, the treatment time for the group B was 20 seconds, and the treatment time for the group C was 30 seconds. The resulting template confirmed the improvement in the assembly process over the resist coated substrate. The best experimental result was obtained when the resist was immersed into the developer for 30 seconds as is illustrated in **Figure 3-11**.

Table 3-5 Experimental parameters for surface treatment of AZ 5214-E.

Groups	**Treatment time in developer (seconds)**	**Rinsing time in water (seconds)**	**Drying on hotplate**
A	10	5	60ºC/2 minutes
B	20	5	60ºC/2 minutes
C	30	5	60ºC/2 minutes

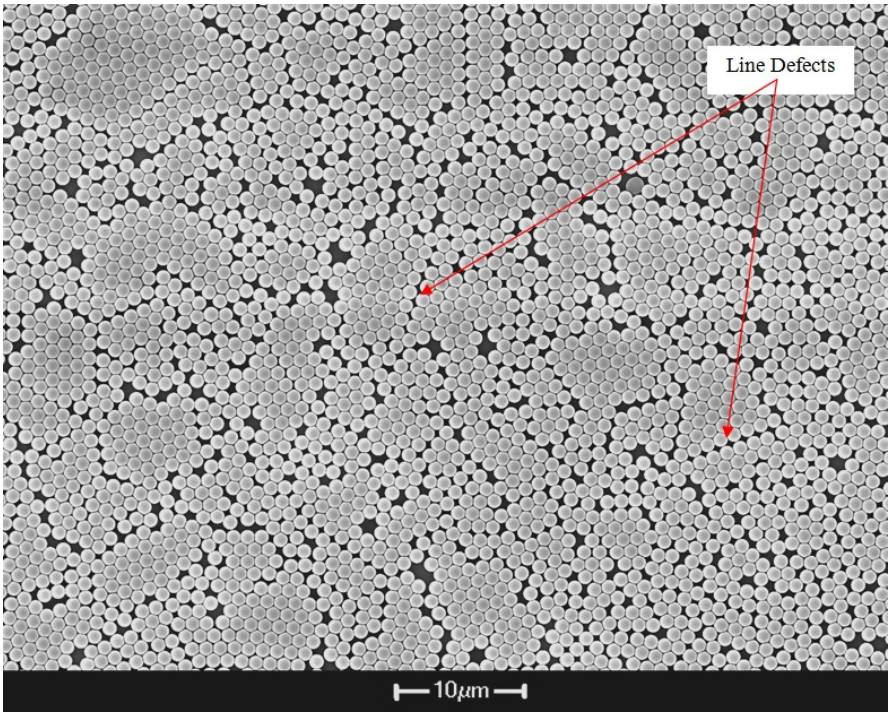

Figure 3-11 SEM image of obtained template after treatment in AZ developer for 30 seconds.

Although some line defects are observed in **Figure 3-11,** an improvement was achieved in comparison to **Figure 3-10** in which many empty islands are detected.

3.5.2.2 Effect of Evaporation Rate

Apart from surface treatment of the substrate, controlling the evaporation rate of water is the other important factor that effects the quality of the obtained template in the self assembly process [112]. The self assembly process was undertaken under different sizes of petri dishes to slow down the evaporation rate. Performing the assembly process under a closed condition, keeps the temperature of the surrounding area almost constant and prevents any external airflow disrupting the homogeneity of

evaporation. Several experiments were conducted over a levelled surface in different petri dishes. The effects of assembly in a closed condition using petri dishes with different sizes are given in **Table 3-6**. The other parameters were kept identical while the petri dishes were changed. The investigation showed the smaller the size of petri dishes, the slower the evaporation rate.

Table 3-6 Effect of evaporation rate on quality of template formation.

Petri dishes sizes (mm)	120×15	100×15	80×15	60×15
Evaporation time (minutes)	~ 80	~ 120	~ 200	~ 290
Quality of template	moderate	moderate	good	good

The prepared colloidal template in a petri dish with diameter of 100 mm showed partial improvement in respect of the results achieved after the surface treatment; but, the most obvious improvement was obtained when the total evaporation time of the assembly process reached above three hours. A good monolayer of PS microspheres formed over the photoresist surface without the existence of any empty islands and line defects. **Figure 3-12** illustrates the achieved result when a petri dish with a diameter of 80 mm was applied in the self assembly process. Some dot defects are still detected in the result which is unavoidable due to the capillary forces in between the particles.

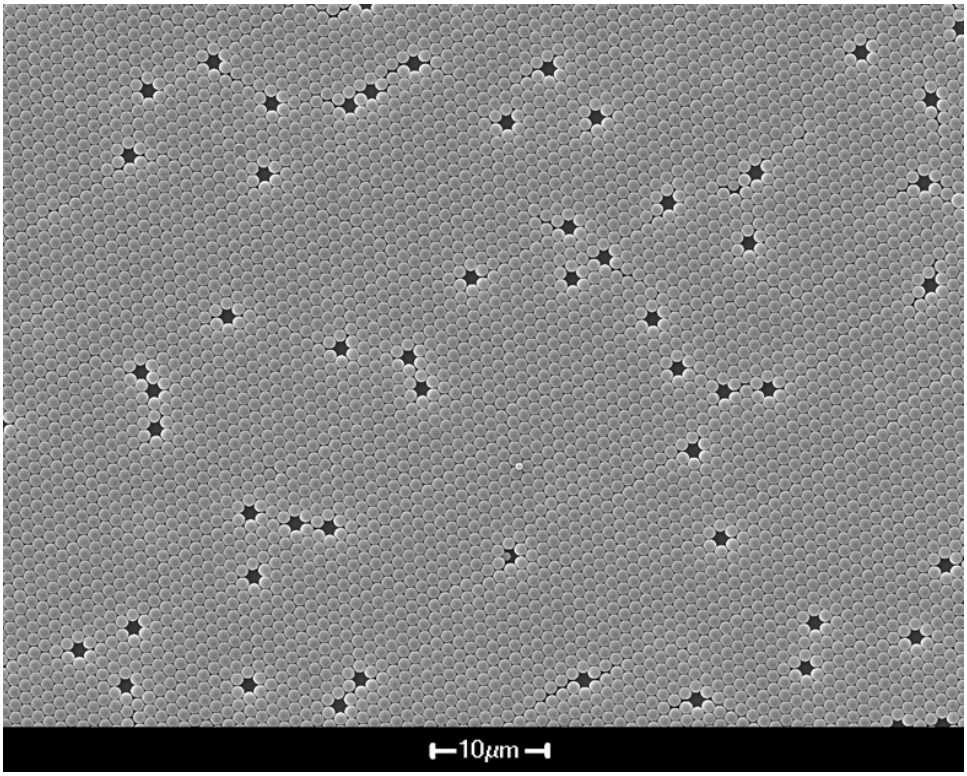

Figure 3-12 Self assembled PS microspheres over photoresist by controlling the evaporation rate.

3.5.3 Results of Monolayer Colloidal Lithography

After preparation of the colloidal mask over the photoresist, the sample was exposed to UV light using a conventional mask aligner. A Canon mask aligner, type PLA-501FA, equipped with a mercury lamp with an optical power of 12.6 mW/cm^2 was applied in these experiments. The colloidal spheres arrays were employed as a photomask to transfer the focused light for production of nanopatterns over the resist surface. The UV exposure process was carried out for only few seconds. The main reason for applying a short exposure time is to ensure that only those resist areas which are exactly located beneath the PS spheres are subjected to UV exposure. Furthermore, the simulations in Section 3.3.1 confirmed that the intensity of focused

light at the shadow-side surface of the sphere is about 5 times stronger than the input light. It should be mentioned that all the exposure experiments were operated with the aid of a LG-39 filter. Since the Canon mask aligner covers a spectral range of 320 to 500 nm, this filter was used to cut off the radiation wavelengths below 350 nm. Although AZ 5214-E resist has low UV absorption at wavelengths below 360 nm [110], using this filter makes the achieved results more reliable. Once the UV exposure was finished, the process is followed by removing the PS microspheres from the samples.

This step was carried out utilising an ultrasonic bath. The samples were immersed in a glass beaker of deionised water and placed in an ultrasonic system for less than 90 seconds. This time was sufficient for cleaning the resist surface from colloidal particles. Next, the samples were dipped into a beaker of AZ developer while gentle agitation by hand was applied to the beaker. The developer dissolves those areas of the resist which are exposed by UV light. The developing time of the resist was found to be less than 1 minute due to the short exposure. Finally, the process was completed by hard baking the samples at 110 ºC for 2 minutes. A scanning electron microscope (Jeol 7000F) was used to inspect the results. It should be noted that a less than 5 nm thin layer of gold was coated on the samples using a sputtering machine to increase the conductivity and consequently the image sharpness. **Figure 3-13** shows the top view of the SEM image of the ordered arrays of nanoholes after the development process.

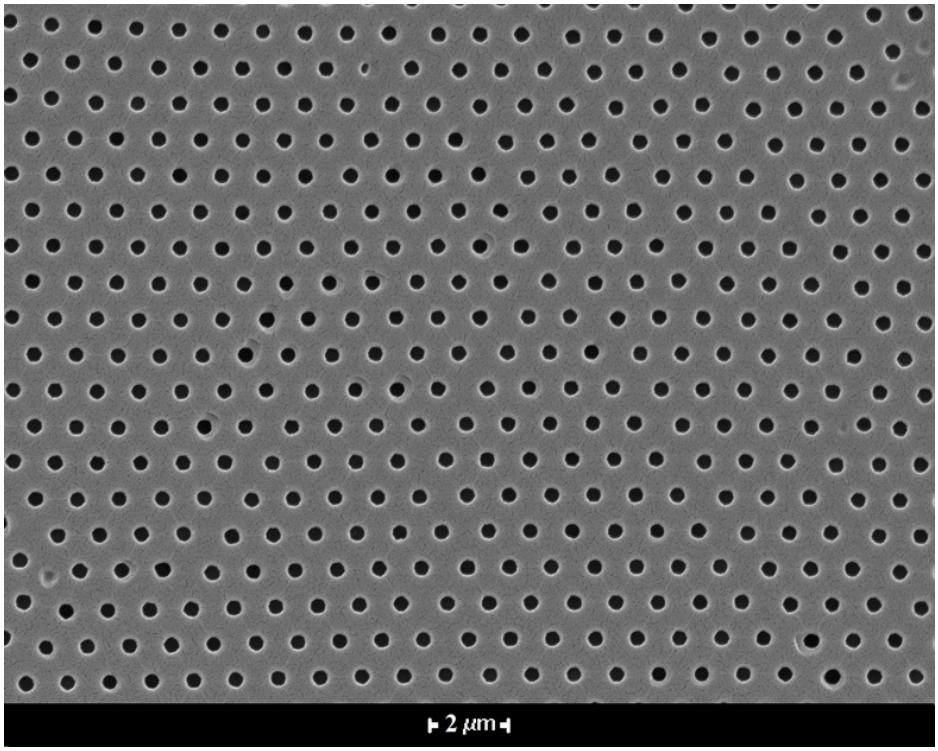

Figure 3-13 Uniform arrays of nanoholes over photoresist.

As expected, each polystyrene sphere acts as a near field lens to focus UV light. The exposure dose of 63 mJ/cm^2 was applied to obtain ordered arrays of nanoholes with a mean diameter of 390±5 nm. The period of the created nanoholes' array is about 1.1 μm, which is the same as the diameter of the microspheres.

A series of experiments were performed to examine the effect of different exposure doses on the resulting nanostructure. **Table 3-7** presents the experimental parameters from the investigation of different exposure doses while other parameters were kept constant. In these experiments, three groups of samples were exposed by three different exposure doses. Each group consists of ten samples. Samples of group A were exposed with an exposure dose of 25.2 mJ/cm^2. Samples of group B were

exposed using an exposure dose of 75.6 mJ/cm^2. Samples in group C were exposed with an exposure dose of 126 mJ/cm^2.

Table 3-7 The experimental parameters for investigation of exposure doses effects.

Groups	**Soft baking**	**Exposure doses** (mJ/cm^2)	**Spheres removal** (seconds)	**Developing time** (seconds)	**Hard baking**
A	100ºC/50 seconds	25.2	90	40	110ºC /2 minutes
B	100ºC/50 seconds	75.6	90	40	110ºC /2 minutes
C	100ºC/50 seconds	126	90	40	110ºC /2 minutes

The results showed that the diameter of a nanopattern is increased by enlarging the exposure dose. Shallow nanoholes with diameter of 210±5 nm were achieved for an exposure dose of 25.2 mJ/cm^2. The results became more obvious, in terms of pattern size, for stronger exposure energy. As is illustrated in **Figure 3-14**, the size of nanopatterns is 450±5 nm when the exposure dose was 75.6 mJ/cm^2, and the diameter of nanoholes reached to 750±8 nm for an exposure dose of 126 mJ/cm^2.

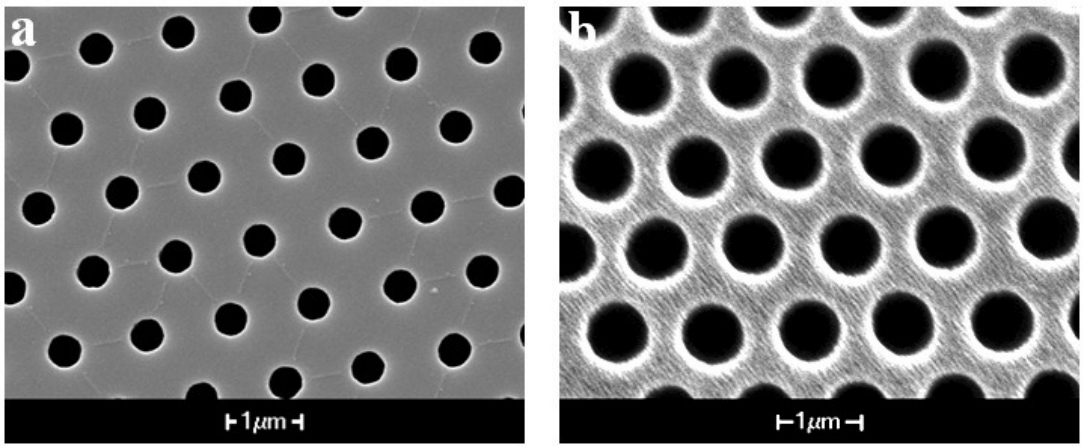

Figure 3-14 Ordered arrays of nanopatterns with different sizes are shown using different exposure doses: a) nanoholes with mean diameter of 450±5 nm (75.6 mJ/cm^2), b) nanoholes with mean diameter of 750±8 nm (126 mJ/cm^2).

3.6 **Fabrication of Dual Arrays of Nanoholes using BCL**

The fabrication steps are schematically illustrated in **Figure 3-15**. Similarly to the MCL method, a clean silicon substrate is first coated with a thin layer of AZ 5214-E resist followed by a soft baking. Afterwards, a double layer of PS microspheres is assembled on the photoresist coated substrate. As in the MCL method, treatment of the surface is essential prior to the assembly process to achieve hexagonal close packed spheres. The sample is then exposed to UV light using a mask aligner. Next, the PS spheres are removed from the sample by ultrasonication in deionised water. After the development step, uniform arrays of binary nanoholes are formed onto the sample. As the final step, a hard baking is applied to the sample.

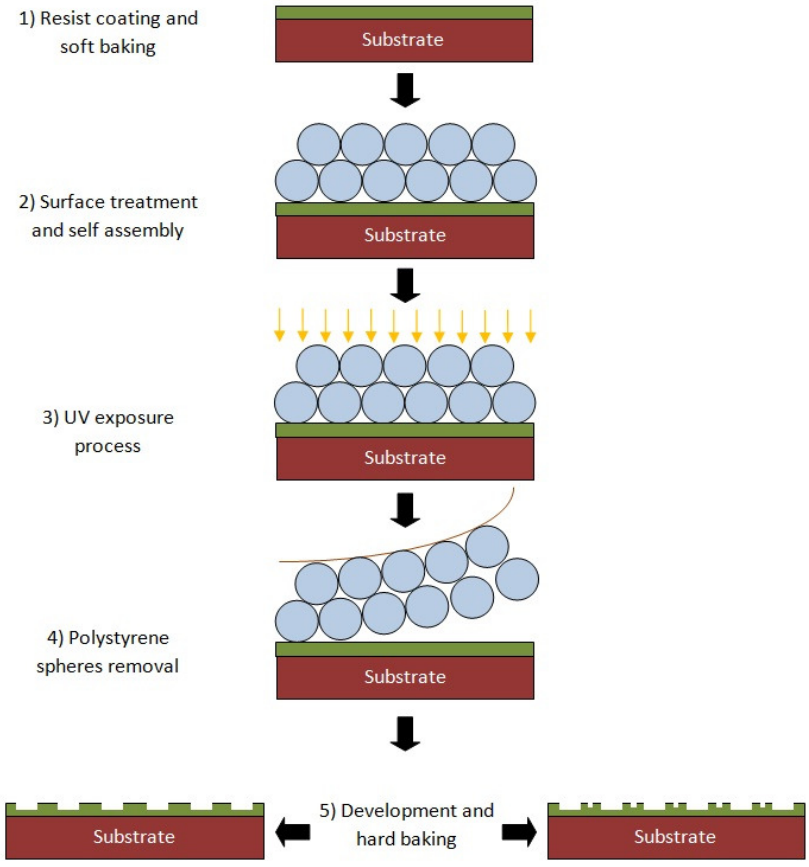

Figure 3-15 A schematic diagram of fabrication steps using BCL technique.

3.6.1 Photoresist Coating

A silicon wafer was cut into small pieces of 1.5 cm × 1.5 cm prior to the resist coating process. This step was carried out using a dicing saw machine. Although the cutting step can be performed after the coating, appearance of small cracks on the resist surface is the consequent of this act. Next, these pieces were cleaned with acetone and Isopropanol (IPA) while they were being spun over a spinner at 800 rpm. Afterwards, they were dipped into deionised water and their surfaces were dried using nitrogen gas. The cleaning process was finalised by placing the samples over a hotplate at 150 ºC for 10 minutes. The spin coating technique was used to cover the surface of the samples with AZ 5214-E photoresist. A thin film of 1.14 µm was coated using a spinner. The AZ 5214-E resist was dispensed to cover 40% of each sample and then they were spun coated at 6000 rpm. The samples wer then baked over a levelled hotplate for 50 seconds at 100 ºC.

3.6.2 Self Assembly of Double Layer PS Spheres

The assembly of the double layer colloidal microspheres over the photoresist coated substrate was started by the preparation of a latex/water dilution. The latex/water proportions and the required amount of droplet to cover the surface area of the substrate were calculated based on the equations which were presented in Section 3.5.2. It should be mentioned that a surface treatment was conducted to make the resist surface more hydrophilic before the PS spheres' deposition; where, the resist coated substrate was immersed into the AZ developer for 30 seconds. A micropipette

was used to place a droplet of prepared latex/water dilution onto the substrate. The bilayer of self assembled PS spheres was obtained by performing two different approaches. The first approach is called the tilting method and the second is called the spin-coating method.

3.6.2.1 Tilting Method

In the tilting method [39], the treated sample was first placed over a tilted base with a specified angle. A droplet of prepared dilution was then dispensed onto the sample. Next, the sample was left under a 75 ml petri dish to slow down the evaporation. Finally, a double layer of assembled microspheres was achieved. An investigation was carried out to optimise the covering area of the double layer spheres. For this investigation, different angles were used as the sample base while the other parameters were kept constant. The change in the coverage area of the bilayer due to varying the tilting angle of the base is illustrated in **Figure 3-16**. The applied angle for this investigation was in the range of 3º to 13º, in intervals of 2º. As observed from the figure, the largest area of bilayer PS spheres was obtained when the self assembly process was conducted over the tilted base of 9º. The covering area of double layer spheres is noticeably reduced when the angle reached 13º. It should be noted that the largest coverage area of about 90000 μm^2 was achieved through the tilting method. It is worth noting that a Jeol 7000 SEM was used to inspect the coverage area of the bilayer PS spheres for each sample.

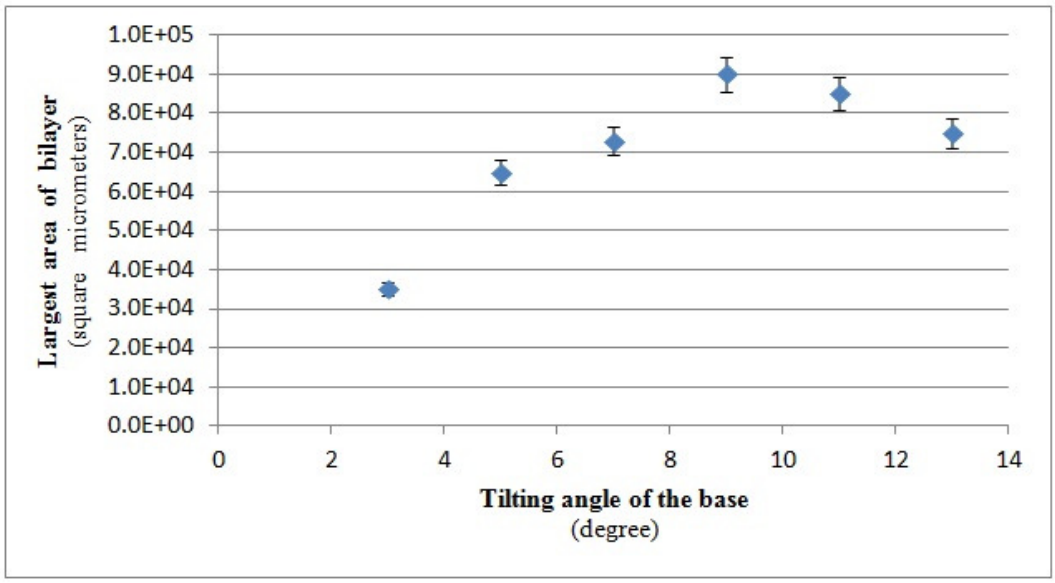

Figure 3-16 The coverage area of assembled bilayer of PS spheres as a function of base's tilting angle.

3.6.2.2 Spin-Coating Method

Since the largest area of the achieved bilayer using the tilting method was relatively small, the alternative method, spin-coating [41], for multi-layer assembly was employed [60, 113]. In this method, the treated sample was first placed into a spinner chuck and a droplet of prepared dilution was dispensed over it. The effect of spin speed was investigated in this experiment to optimise the coverage area of bilayer spheres. The spin speeds of 100 rpm to 800 rpm, with intervals of 100 rpm, were examined. For each required spin speed, the speed was first increased at a constant ramp to the specified speed. The speed was then kept constant for 30 seconds. Finally, the spinning process was finished by decreasing the speed at a constant ramp. The total time for the spinning process was 60 seconds. After finishing the spin-coating, the sample was left over the spinner chuck to prevent any undesirable disturbance of the self assembly process. Lastly, the sample was covered by a 75 ml

petri dish to slow down the evaporation rate. **Figure 3-17** shows the experimental results for different spin speeds.

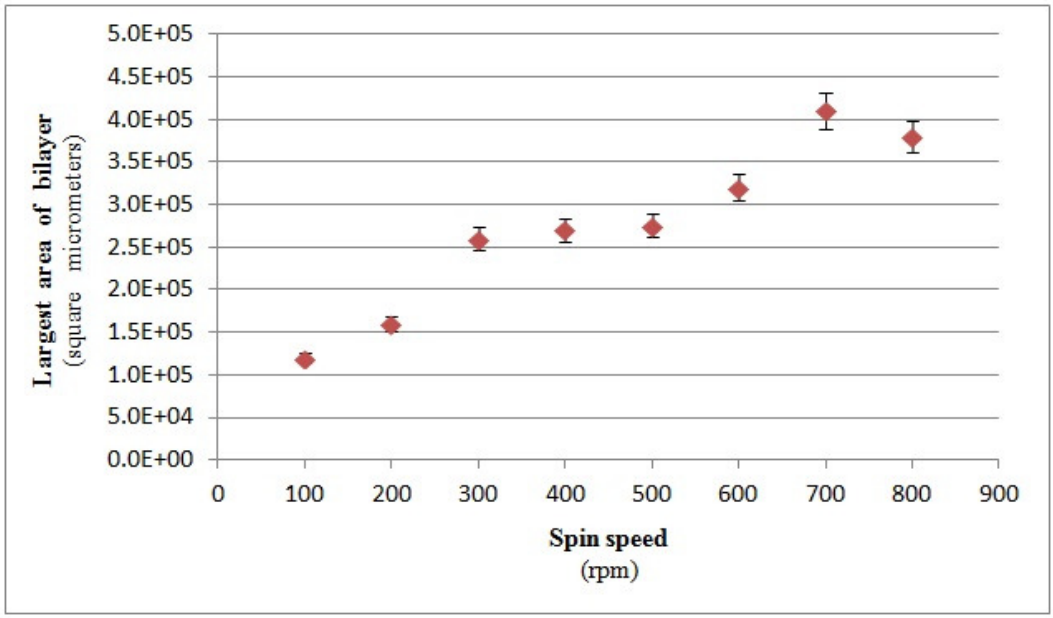

Figure 3-17 The coverage area of assembled bilayer of PS spheres as a function of spin speed.

As observed from the above figure, the largest area of bilayer PS spheres was obtained when the self assembly process was conducted using a spin speed of 700 rpm. The covering area of double layer spheres using the spin-coating method is noticeably increased in comparison to the achieved results for the tilting method. The largest coverage area of about 400000 μm^2 was obtained through the spinning method. **Figure 3-18** shows an SEM image of the achieved result. A double layer of PS microspheres are assembled onto the AZ 5214-E photoresist. The lower layer of assembled microspheres is clearly visible through the gap of the upper layer from the zoom in view (inset in **Figure 3-18**).

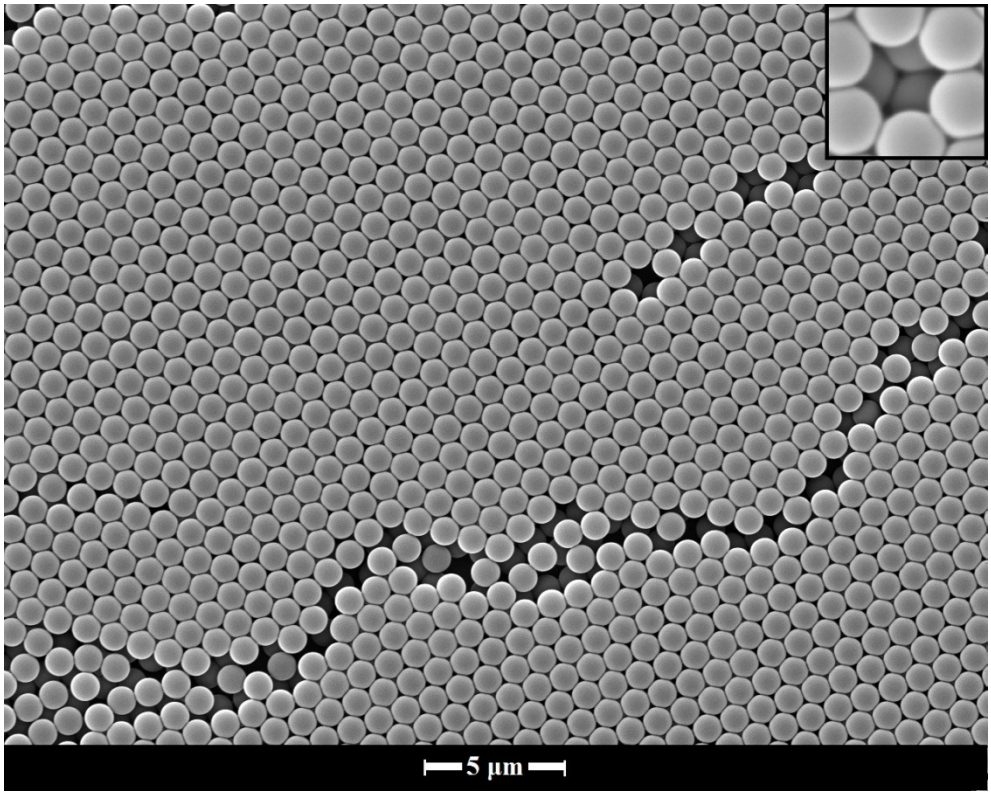

Figure 3-18 The SEM image of double layer PS microspheres over photoresist coated substrate.

3.6.3 Results of Bilayer Colloidal Lithography

After the preparation of the bilayer colloidal mask onto the resist coated substrate, the sample was exposed to UV light using a conventional mask aligner with an optical power of 12.6 mW/cm^2.The double layer of colloidal spheres was employed as a photomask for production of nanopatterns over the resist surface. The UV exposure process was performed for only a few seconds, similarly to the MCL technique. It should be mentioned that all of the exposure experiments were operated with the aid of an LG-39 filter for cutting off the radiation wavelengths below 350 nm. After the UV exposure, the process is followed by removing the double layer of PS microspheres. This step was similarly performed with the assistance of an

ultrasonic system. The samples were first placed in a beaker of deionised water followed by ultrasonication for about 3 minutes. This time was sufficient for washing off the colloidal particles from the resist surface. Next, the samples were dipped into a beaker of AZ developer while gentle agitation was applied to the beaker by hand. Since positive resist is used, the developer dissolves those areas of the resist which are exposed by UV light. The developing time of the resist was found to be less than 1 minute due to the short exposure. Lastly, the process was completed by hard baking of the samples at 110 ºC for 2 minutes. **Figure 3-19** shows the SEM image of the ordered arrays of nanoholes after the development process. Uniform arrays of nanoholes with a mean diameter of 640±5 nm were achieved when a bilayer of spheres was employed as the photomask. The exposure dose of 37.8 mJ/cm^2 was applied for this experiment. The period of the created nanoholes array is about 1.1 μm, which is the same as the diameter of the microspheres. The size of nanoholes agrees with the simulation results in Section 3.3.2. Hence, instead of having nanoholes with a narrow diameter, nanoholes with broader diameters are fabricated.

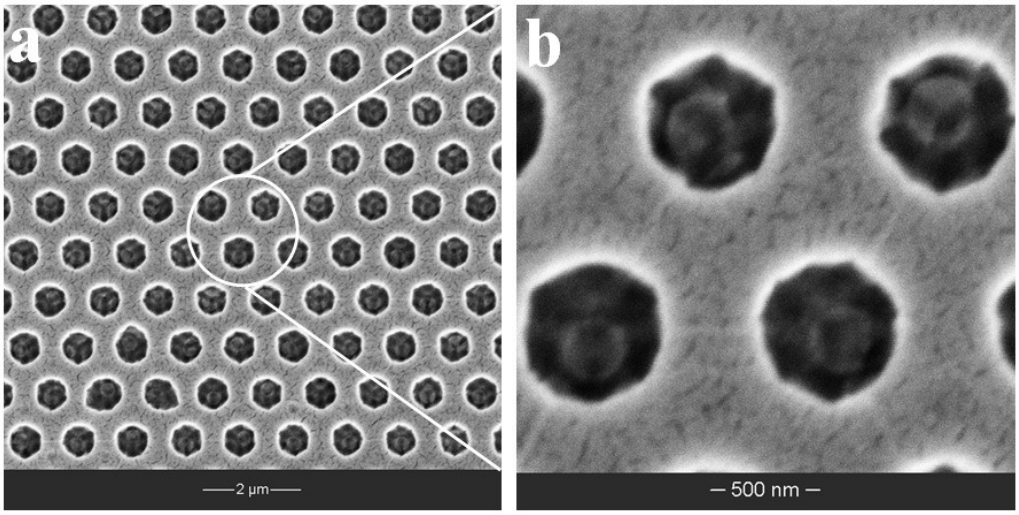

Figure 3-19 Top view SEM images: a) single arrays of uniform nanoholes, b) magnified image of uniform nanoholes' arrays.

As observed from the above figure, the achieved nanopatterns using the BCL technique are not as round as the obtained nanopatterns using the MCL technique. Here, I would like to stress that the main novelty and advantage of this technique lies in the fabrication of two sets of ordered nanoholes with different sizes, in one process. As illustrated in **Figure 3-20**, the smaller holes are placed between the bigger holes when the exposure dose of 75.6 mJ/cm^2 was applied.

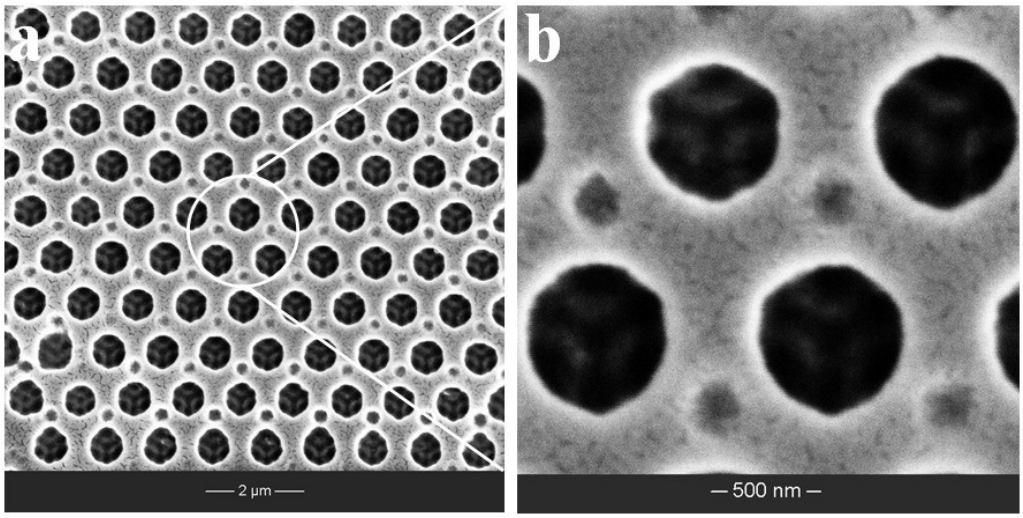

Figure 3-20 Top view SEM images: a) arrays of binary uniform nanoholes, b) magnified image of uniform nanoholes arrays.

The creation of the second array of nanoholes can be explained as follows: UV light is first collected and focused by the top layer spheres. Then, it is directed partly to the bottom layer spheres and partly to the photoresist through the voids between the bottom layer spheres. It is observed from **Figure 3-21a** that the bottom surface of the nanoholes contains some finer features. These features can be considered as the result of the three hot spots of the electric field, as discussed in the simulation section. As shown in **Figure 3-21b**, the arrays of big holes are located directly underneath the bottom layer spheres. Hence, it verifies that the arrays of small and

big nanoholes are generated by the top and bottom layers of microspheres, respectively.

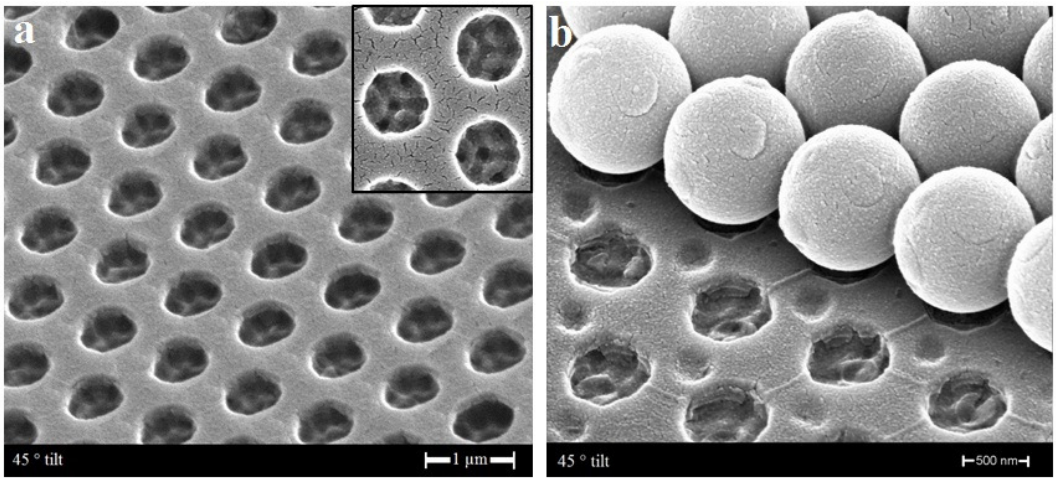

Figure 3-21 Tilted SEM images: a) finer features at the bottom of nanoholes, b) arrays of binary nanoholes in the presence of bottom layer spheres.

A series of experiments were performed to examine the effect of different exposure doses on the resulting nanostructure. **Table 3-8** presents the experimental parameters from the investigation of different exposure doses while other parameters were kept constant. In these experiments, three groups of samples were exposed to three different exposure doses. Samples of group D were exposed to the exposure dose of 37.8mJ/cm^2. Samples of group E were exposed to the exposure dose of 75.6mJ/cm^2. Samples in group F were exposed to the exposure dose of 113.4 mJ/cm^2.

Table 3-8 The experimental parameters for investigation of exposure doses effects.

Groups	**Soft baking**	**Exposure doses** (mJ/cm^2)	**Spheres removal** (minutes)	**Developing time** (seconds)	**Hard baking**
D	100ºC/50 seconds	37.8	3	40	110ºC /2 minutes
E	100ºC/50 seconds	75.6	3	40	110ºC /2 minutes
F	100ºC/50 seconds	113.4	3	40	110ºC /2 minutes

The results showed that the diameter of the secondary nanopatterns is increased by enlarging the exposure dose. The arrays of big nano-cavities appeared when the exposure dose was about 38 mJ/cm^2. At this exposure energy, there are no signs of small nano-cavities. **Figure 3-22a** indicates the appearance of small nano-cavities with a shallow diameter when the exposure dose is about 50 mJ/cm^2. The size of the small nano-cavities is changed from 220±5 nm to 380±5 nm by varying the exposure dose from about 75 mJ/cm^2 to 113 mJ/cm^2, as illustrated in **Figures 3-22b** and **3-22c**. The investigation shows the slight changes in the diameter of the big nano-cavities in respect to the changes of the small nano-cavities' diameter.

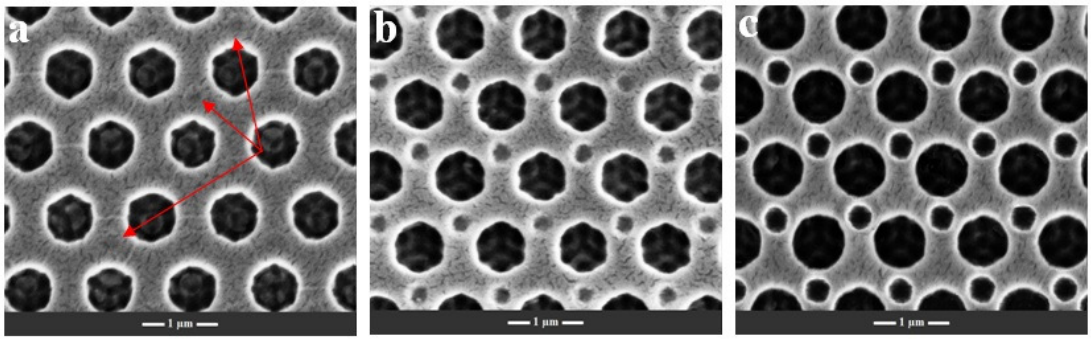

Figure 3-22 Ordered arrays of dual featured nanopatterns with different sizes are shown using different exposure doses: a) appearance of small nanoholes in between big nanoholes at exposure dose of 50 mJ/cm^2, b) arrays of small nanoholes with mean diameter of 220±5 nm in between arrays of big nanoholes, c) arrays of small nanoholes with mean diameter of 380±5 nm in between arrays of big nanoholes.

The aforementioned results present the fabrication of two sets of ordered nanoholes with different sizes using bilayer colloidal lithography. Apart from the exposure energy which made the patterns' size tuneable, it is worth noting that the periodicity of arrays of binary nanoholes can be controlled by varying the sphere size. Since the exposure time directly controls the amount of resist cured and thus the diameter of

the cavities, it is possible to produce various patterns through the proposed method. **Figure 3-23** schematically illustrates how the features vary from cavities to pillars when both types of nanoholes are big enough to overlap.

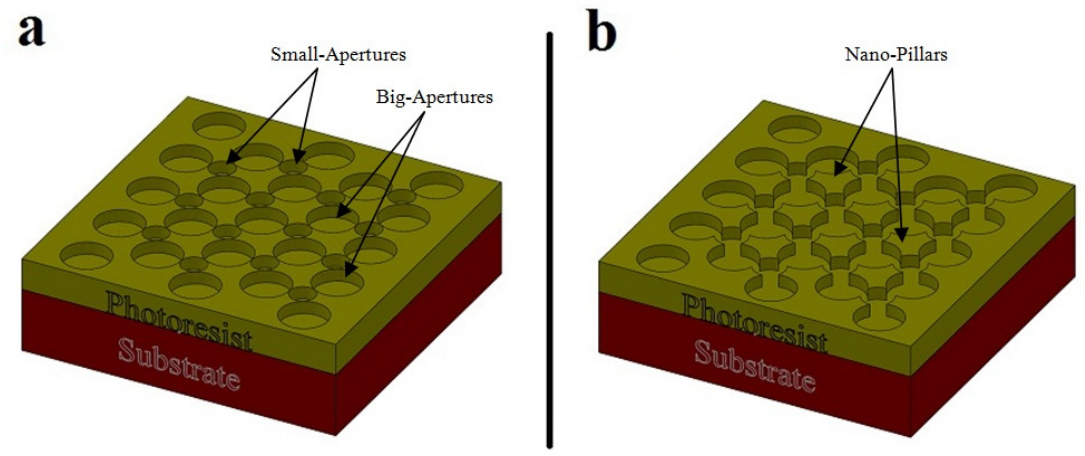

Figure 3-23 Shows the switching moment in which: a) arrays of binary nanoholes turn to b) arrays of triangular-shaped nanopillars.

The experimental results confirmed that arrays of nanopillars are achievable by increasing the exposure time. When the exposure dose was about 113 mJ/cm^2, uniform arrays of binary nanoholes were the resulting structure. When the exposure dose of about 138 mJ/cm^2 was applied, ordered arrays of nanopillars were achieved. As shown in **Figure 3-24**, arrays of triangular-shaped patterns with a side length of 750±10 nm and side-wall height of 210±5 nm are produced.

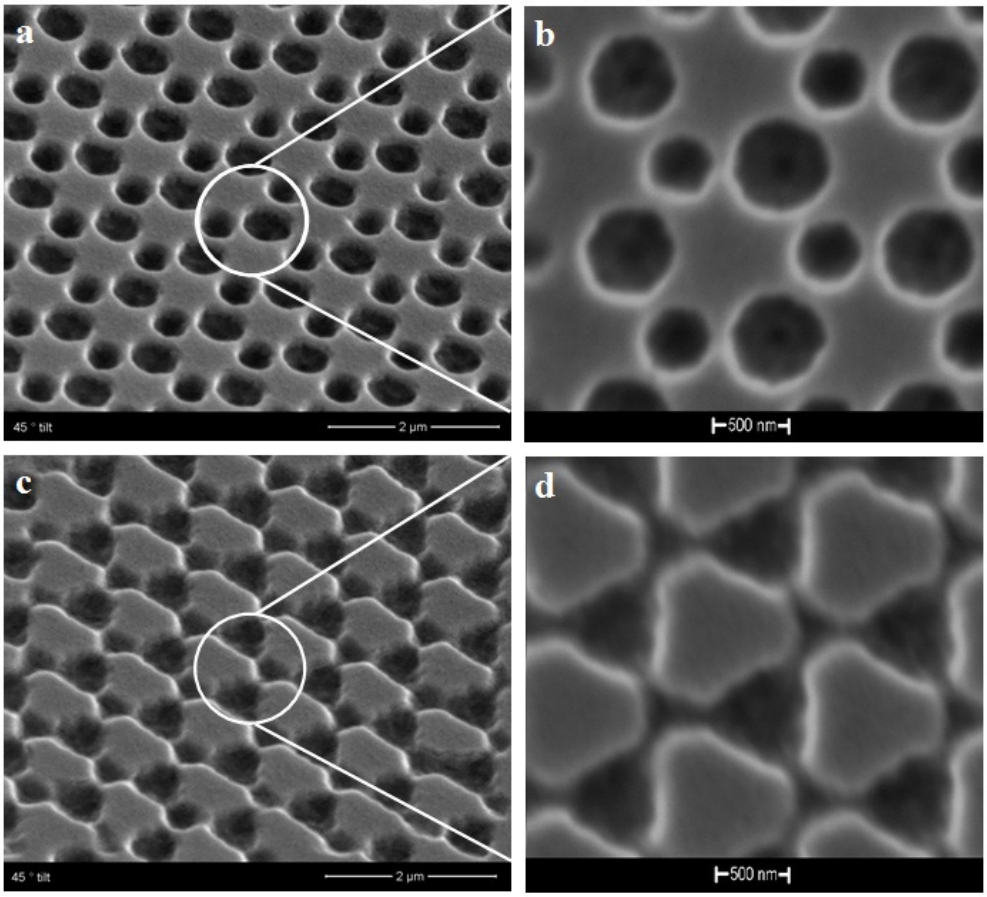

Figure 3-24 Tilted SEM images of experimental result; a) arrays of uniform binary nanoholes, b) magnified image of arrays of binary nanoholes, c) ordered array of triangular-shaped nanopillars, d) magnified image of triangular-shaped nanopillars.

3.7 **Summary**

In this chapter, both a monolayer and bilayer of self assembled polystyrene microspheres were used as a photomask for the production of ordered arrays of nanopatterns. The investigations were carried out using CST Microwave Studio software to understand the behaviour of UV light at the inside and near-outside of PS microspheres. It shows that polystyrene microspheres can act as near field lenses for the creation of a periodic nanostructure. Both single and arrays of uniform binary

nanoholes were successfully fabricated and characterised by using MCL and BCL techniques, respectively. In comparison with the resulting patterns of monolayer colloidal lithography and bilayer colloidal lithography, it can be found that:

- The bigger nanoholes can be obtained through the BCL technique in respect to the MCL technique, when a similar exposure dose is applied.
- The BCL method has the potential of creating two sets of ordered patterns, while in the MCL method a set of uniform patterns only is achievable.
- It was found that the resulting nanopatterns of both MCL and BCL techniques are adjustable by using different exposure doses.
- Apart from the fabrication of arrays of binary nanoholes using the BCL method, this method revealed its potential for the production of triangular-shaped nanopillars.

This is the first report of creating arrays of binary nanopatterns through one colloidal lithography process. The proposed approach shows its potential for the fabrication of mixed arrays of nanopatterns with tuneable size. The periodicity of nanopatterns can be controlled by varying size of microspheres. The approach presented in this chapter can be extended for the fabrication of arrays of single or binary nanopillars with controlled size for chemical and biomedical applications, using a negative phase of photoresist.

CHAPTER 4: PS SPHERES AS A TEMPLATE

4.1 Introduction

This chapter explains the use of polystyrene microspheres as template for the fabrication of both 2D and 3D periodic nanostructures. Combination of monolayer self assembly, soft lithography and metal deposition is applied for this study. The chapter begins by presenting a general overview of both fabrication strategies in Section 4.2. Materials that are used in the fabrication process are presented in Section 4.3. The assembly process for making a PS spheres template and preparation of a PDMS soft mould are described in Section 4.4. Fabrication details, experimental results and characterisation approaches for production of 2D and 3D periodic nanostructures are discussed in Section 4.5 and Section 4.6, respectively. Lastly, this chapter is summarised in Section 4.7.

4.2 General Overview of Fabrication Processes

A general overview of the fabrication approach is presented in this section. In this approach two different strategies are followed. The first strategy is mainly devoted to fabricated ordered arrays of periodic micro/nano structures based on PDMS/PDMS replica moulding. The second strategy is focused on creating periodic metallic

nanopatterns over a replica PDMS micro-patterned mould. In both strategies a combination of self assembly and soft lithography processes is utilised to produce such periodic features at micro/nano scale. Since both strategies require a soft PDMS mould in their fabrication processes and this mould is prepared using a similar method for both strategies, the general overview of the fabrication steps is presented in two subsections. The first subsection describes those steps which are held in common for both strategies, and the second subsection explains further steps which are distinguished. The following indicates the fabrication steps for the preparation of a PDMS mould:

❖ Subscriber steps for both strategies

1. Monolayer self assembly of colloidal spheres over substrate.
2. Casting the self assembled colloidal template with PDMS slurry.
3. Curing and peeling off PDMS soft mould.

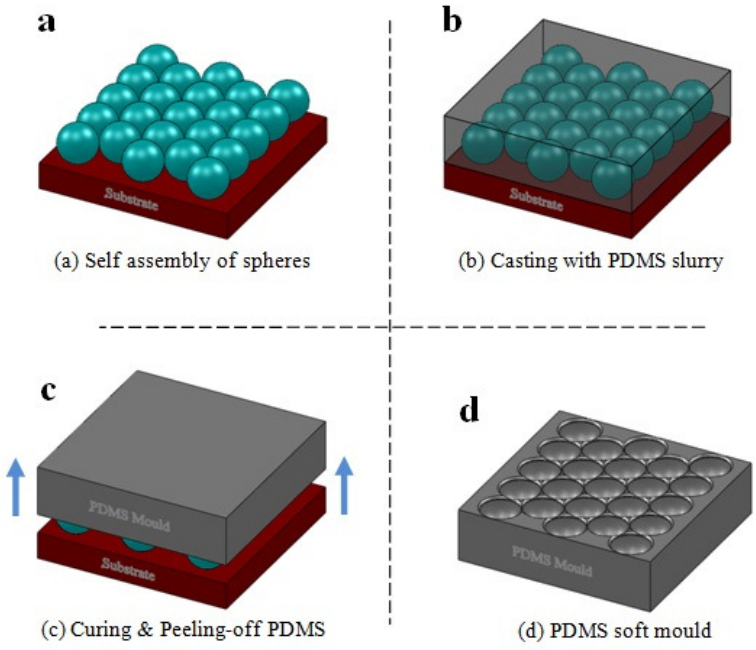

Figure 4-1 A schematic diagram shows the preparation steps of a PDMS soft mould.

Figure 4-1 shows the fabrication steps for creating a PDMS mould. A substrate with a covering monolayer of PS spheres is used as a template for this procedure. The prepared PDMS mould is then used as the foundation for both proposed strategies. The following separately indicates the fabrication steps for both nanofabrication strategies. **Figure 4-2** schematically illustrates a general overview of fabrication process for both strategies.

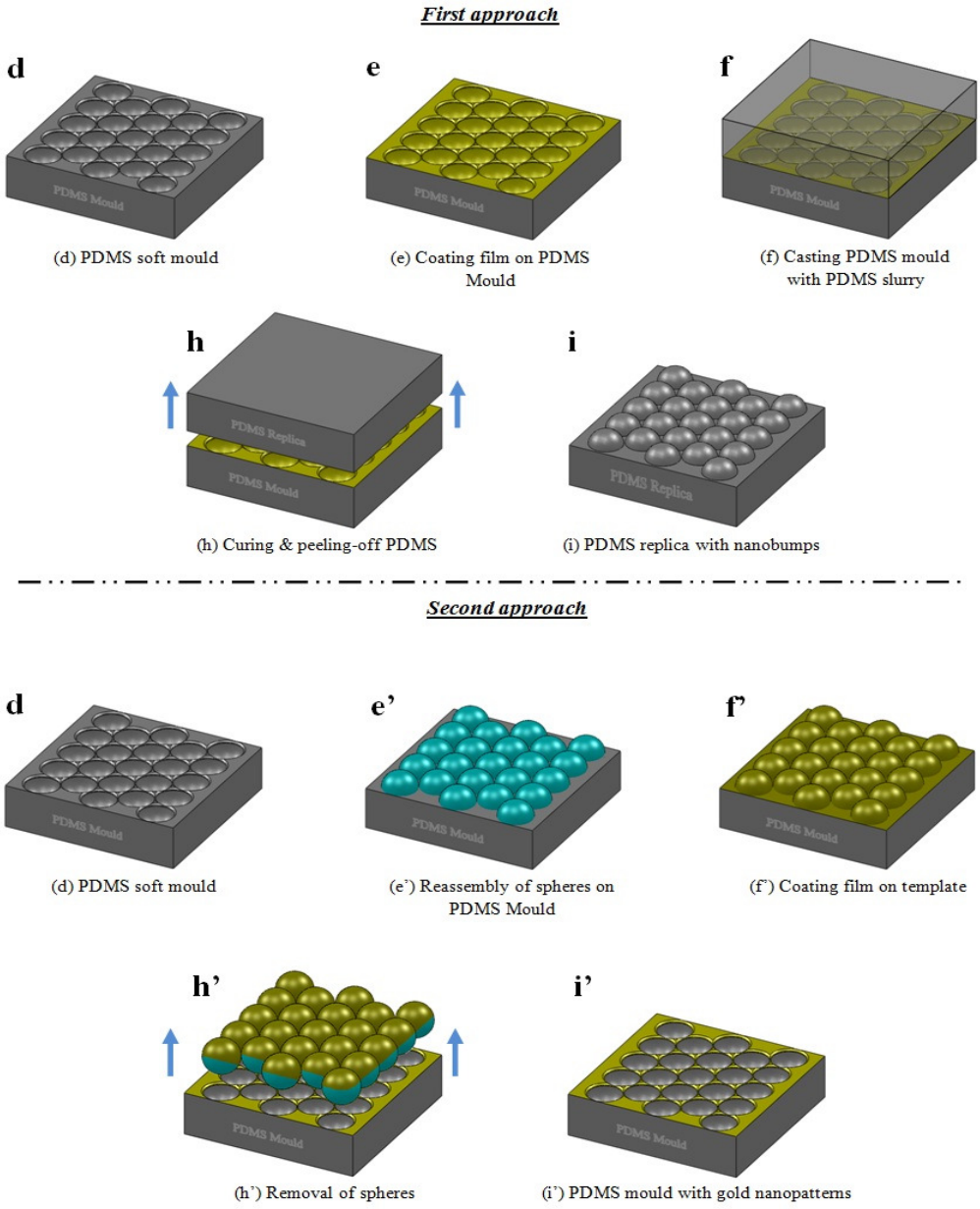

Figure 4-2 Schematic diagrams of both proposed nanofabrication strategies: 1) nano-replication process (top), 2) nanopatterning process (bottom).

❖ Non- subscriber steps

- First Strategy:
  1. Cleaning the prepared PDMS mould.
  2. Coating thin film of metal onto the PDMS mould.
  3. Casting the PDMS mould with PDMS slurry.
  4. Curing and peeling off PDMS replica.
- Second strategy:
  1. Cleaning the prepared PDMS mould.
  2. Reassembly of colloidal spheres over the PDMS mould.
  3. Metal deposition over the reassembled colloidal spheres mask.
  4. Removal of colloidal spheres from the PDMS mould.

Polystyrene microspheres and PDMS are proposed as suitable materials for these fabrication techniques. Modification and optimization are performed throughout the fabrication steps to achieve high resolution nanopatterns over a relatively large area.

4.3 **Materials Used in Experiments**

4.3.1 Polydimethylsiloxane (PDMS)

PDMS is a well-known elastomer in soft lithography processes. PDMS is a silicone-based polymer which is composed of an inorganic siloxane and organic methyl

groups [114]. Among other soft lithographic materials, PDSM is normally preferred due to its advantages. In general, PDMS is non-toxic and non-flammable. PDMS is an electrically non-conductive material and it is optically clear. It is a flexible material which helps to render more complicated structures and it has a low surface energy which helps in the demoulding process. Sylgard 184 is the nominated type that was used in the following experiments. The commercial elastomer of Sylgard is supplied as two part liquid kits including a base material and a curing agent. When both liquid parts are thoroughly combined, a PDMS pre-polymer is formed. Some PDMS pre-polymers are designed to cure at room temperature, while others require to be cured in an oven.

4.3.2 Mono-Dispersed Spheres

Similarly to the previous experiments, polystyrene microspheres are the nominated type used in the following experiments. The size-standard category was selected due to its high precision in terms of size; 1 wt% diluted aqueous suspensions of polystyrene spheres with a mean diameter of 1.1 μm and a size distribution of 1% were purchased from the Duke Scientific Corporation.

4.4 **Preparation of a PDMS Soft Mould**

The preparation steps for producing a PDMS soft mould are shown in **Figure 4-3**. The preparation steps begin with surface treatment of a silicon wafer. Next, a monolayer of polystyrene spheres is self assembled onto the treated silicon substrate. This substrate is then used as a primary template. Next, PDMS slurry is prepared and poured onto the primary template to cover the entire surface. Afterwards, the PDMS pre-polymer is cured by heating. The cured PDMS is gently peeled off from the template. As the final step, the fabricated PDSM soft mould is cleaned from any residual materials.

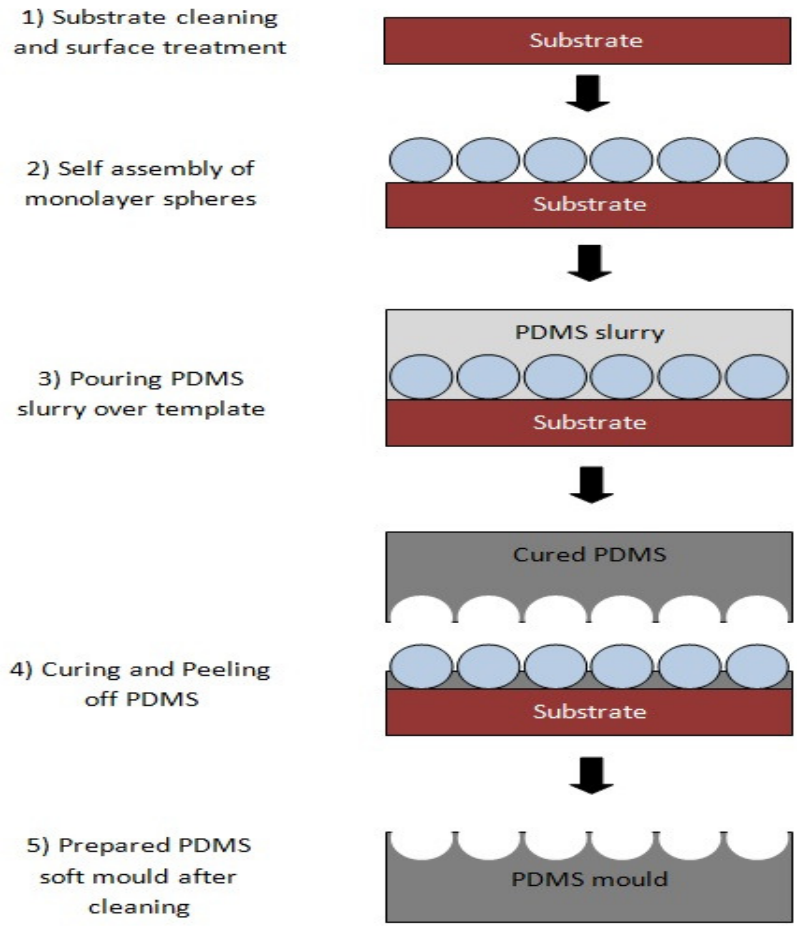

Figure 4-3 The diagram shows the preparation steps for producing a PDMS mould.

4.4.1 PS Pattern Template

Preparation of a PS pattern template is the initial step of the experimental work which is described here. This step consists of substrate treatment and MSA process. Single side polished silicon wafer was firstly cut into 1.5 cm × 1.5 cm pieces and cleaned with acetone. These pieces were used as templates for the monolayer self assembly process. Next, the cleaned substrates were treated by piranha solution. Surface treatment using piranha solution is a popular treatment method in the semiconductor industry. When concentrated sulphuric acid (H_2SO_4) and hydrogen peroxide (H_2O_2) are mixed, the mixture is called piranha solution [115]. Although different ratios are normally applied for the preparation of piranha solution, we used piranha solution with a ratio of 1 to 3 (H_2O_2 30%: H_2SO_4 98%) in this research. Piranha solution is commonly used to clean a sample surface from any organic contaminants. This treatment helps to obtain a hydrophilic surface and consequently achievement of better monolayer self assembly. After soaking the silicon substrates in the piranha solution at 80 ºC for 30 minutes, the substrates were rinsed with copious amounts of deionised water. Next, the treated substrates were placed in a glass beaker of H_2O:NH_4OH:H_2O_2 solution and sonicated for about 45 minutes. This mixture is known as RCA solution because of its development by the Radio Corporation of America (RCA Co.) [116]. When ammonium hydroxide (NH_4OH), hydrogen peroxide (H_2O_2) and deionised water (H_2O) are mixed with the ratio of 1:1:5, the mixture is called RCA solution. RCA solution puts many OH groups onto a sample surface which make the sample surface even more hydrophilic [62, 117]. Next, the treated substrate was rinsed repeatedly with deionised water and then stored in deionised water until used. The self assembly of the monolayer PS

microspheres over the treated substrate was started by the preparation of a latex/water dilution. The latex/water proportion and the required amount of the droplet needed to cover the entire substrate surface were calculated based on the equations which are presented in Section 3.5.2.

A micropipette was used to place a 10 µl droplet of prepared dilution with 2 wt% PS spheres suspension onto the substrate. The self assembly process was undertaken in a sealed area to slow down the evaporation rate by using different sizes of petri dishes. **Table 4-1** gives the investigation results. The quality of the systematic hexagonal arrays of spheres improves, as the volume of the sealed area gets smaller. The results showed, for an identical situation, the assembly process over silicon substrate takes a slightly longer time than the assembly process over resist coated substrate. **Figure 4-4** illustrates the prepared PS pattern template when a petri dish with diameter of 60 mm was used in the self assembly process.

Table 4-1 Effect of the volume of sealed area on the quality of spheres template formation.

Petra dishes sizes (mm)	120×15	100×15	80×15	60×15
Evaporation time (hours)	~ 1.5	~ 2.5	~ 3.5	~ 5
Quality of template	moderate (with defects)	moderate (with less defects)	Good (only dot defects)	Very good (less dot defects)

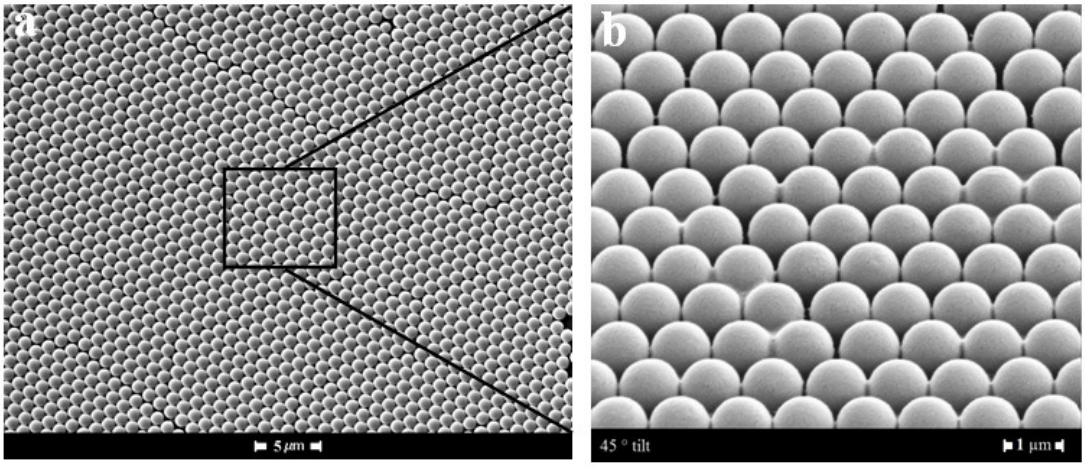

Figure 4-4 Self assembled arrays of PS microspheres over treated silicon substrate: a) top view SEM image, b) magnified tilted SEM image.

4.4.2 PDMS Experiments

The PDMS soft mould with the inverted PS pattern was prepared using a replica moulding process. The required thickness of a PDMS mould is about 3 mm. As mentioned above, Sylgard 184 prepolymer was used in the experiments and the preparation steps are reported here. The curing agent (cross-linking agent) and the base material (monomer) were thoroughly mixed in the weight ratio of 1 to 10 using a mechanical stirrer for 15 minutes. The prepared PDMS slurry was then de-aired in a vacuum chamber for 30 minutes to remove air bubbles from the mixture. For casting the PDMS slurry onto the PS pattern template, a plastic box with dimensions of 20 × 20 × 5 mm was used. First, the PS pattern template was placed in the plastic box. The PDMS slurry of approximately 3 mm thickness was then poured onto the plastic box to cover the entire surface of the template. Afterwards, the plastic box was put into a vacuum chamber for 3 hours to de-air the bubbles on the pattern interface and the PDMS slurry.

There are two typical procedures for curing PDSM slurry as suggested by the manufacturer. The PDMS slurry can be cured either by heating at 70 °C for 1 hour or by keeping at room temperature for 24 hours. In this experiment, the PDMS slurry was cured at 50 ºC for 2 hours followed by cooling at normal room temperature. The curing process has been done at a temperature lower than recommended to prevent any adverse deformation of the PS spheres which subsequently affects the quality of the PDMS mould. After finishing the curing process of the PDMS slurry, the cured PDMS should be released from the PS pattern template. For this reason, a stainless steel blade was first used to separate the cured PDMS from the plastic box. Next, the cured PDMS was gently peeled off from the PS pattern template. This step was successfully performed without the aid of any release agent. The low surface energy of PDMS provides an easy releasing process. It is worth noting that the peeling off process is only feasible for a PDMS layer with a thickness of about 2 mm or more. Any attempts at releasing the PDMS layer with a lesser film thickness caused the appearance of a tear in the PDMS layer. The fabricated PDMS soft mould was then sonicated in an acetone bath to clear off any residual materials followed by rinsing in deionised water. Finally, the PDMS soft mould was dried using a nitrogen stream.

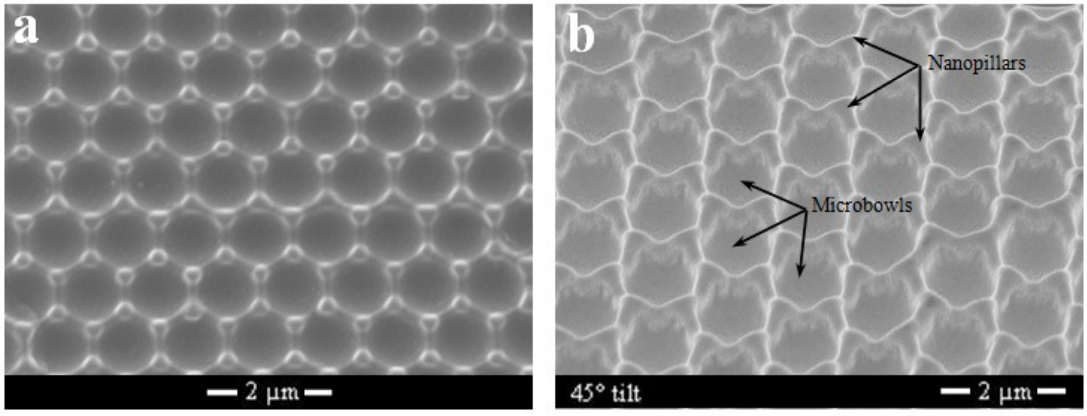

Figure 4-5 Obtained PDMS soft mould after demoulding process: a) top view of order arrays of hybrid nanostructure, b) side view is specified microbowls and nanopillars.

The resulting PDMS mould was inspected using SEM. **Figure 4-5** illustrates the arrays of PDMS hybrid nanostructure. It can be clearly observed that the patterned hemispherical microbowl structures are uniformly formed with a smooth concave surface. In addition, triangular shaped nanopillars are located at the junction of the microbowls. Both the microbowls and nanopillars are highly ordered, preserving the PS template surface topography. This soft mould is used as the foundation in the fabrication process of the following proposed strategies which will be discussed in the next two sections.

4.4.3 Structural Characterisation

Both an SEM stereoscopic technique and FIB milling method are used to characterise the morphology of the PDMS soft mould. Three-dimensional reconstruction through SEM stereoscopic images is used to perform volume analysis, while FIB milling is used to perform cross-sectional analysis.

4.4.3.1 Three-Dimensional Reconstruction through SEM Stereoscopic Imaging

This method is based on computing 3D points from 2D matched points in two images, one tilted with respect to the other. These images are taken by SEM with a normal tilting angle of between 5° to 10°. The presented method has been successfully employed for surface characterisation of various structures [118, 119]. The principle of the stereo imaging process is schematically described in **Figure 4-6**.

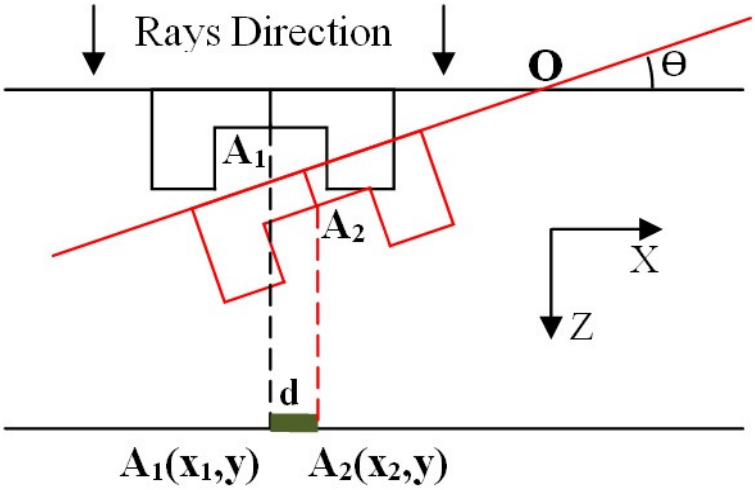

Figure 4-6 Stereo images of an object before (black) and after (red) tilting. Tilting about *O* transforms A_1 to A_2.

This figure shows points A_1 which is the original position of point A before tilting and A_2 which is the secondary position after tilting in a 3D coordinate system. Considering angle (Θ) and centre of tilting (O), the Z coordinate of A is a function of disparity between points A_1 and A_2. The points X_1 and X_2 are the X coordinates of A_1 and A_2, respectively [120]. Then Z_A can be computed from the following equation:

$$Z_A = \frac{(X_2 - X_1) + X_1\,(1 - \mathrm{Cos}\Theta)}{\mathrm{Sin}\Theta} \qquad \textbf{Eq. 4-1}$$

This process can be carried out for all of the other points of both images and will find the shape of the structure. In order to get the best performance of the presented method, several parameters should be considered: (a) tilting object at eucentric level, (b) reduce noises of SEM images, (c) take images at the proper magnification, (d) maintaining the same working distance for both SEM images, and finally (e) increasing disparity by best choice of tiling angle.

4.4.3.2 Cross-Section Characterisation through FIB Milling

The FIB system uses a liquid-metal ion source in its column to produce ions, typically Ga+. The ions are emitted and focused into a beam by an electric field and passed through apertures. They subsequently bombard the sample surface which results in milling away material from the surface [121]. For detailed cross-sectional analysis, milling a trench is essential to create a smooth side wall. A rectangle is required to be milled through high ion beam energy to create a trench. Important parameters for the milling are voltage and current.

The accelerating voltage should be as high as possible, for instance 30 kV (FEI FIB/SEM STRATA 235 DB), to achieve the optimum resolution. The current needs to be high enough to remove a volume of around 2 μm^3. Since soft materials are very sensitive to ion bombardment, an ion beam with a current higher than 50 pA would damage the surface of the sample [121].

4.4.3.3 Characterisation Results

An SEM stereoscopic technique is used to determine the three dimensional surface of the PDMS micro-bowl structure. Two high resolution SEM images were obtained at a eucentric level of 5 mm with a tilt angle of 10° as shown in **Figure 4-7a** and **Figure 4-7b**. The commercial software package, MeX 5.1 (Alicona Imaging), was

used for 3D reconstruction and geometrical analysis [122]. These SEM images were used to make the digital elevation model (DEM) which is shown in **Figure 4-7c**.

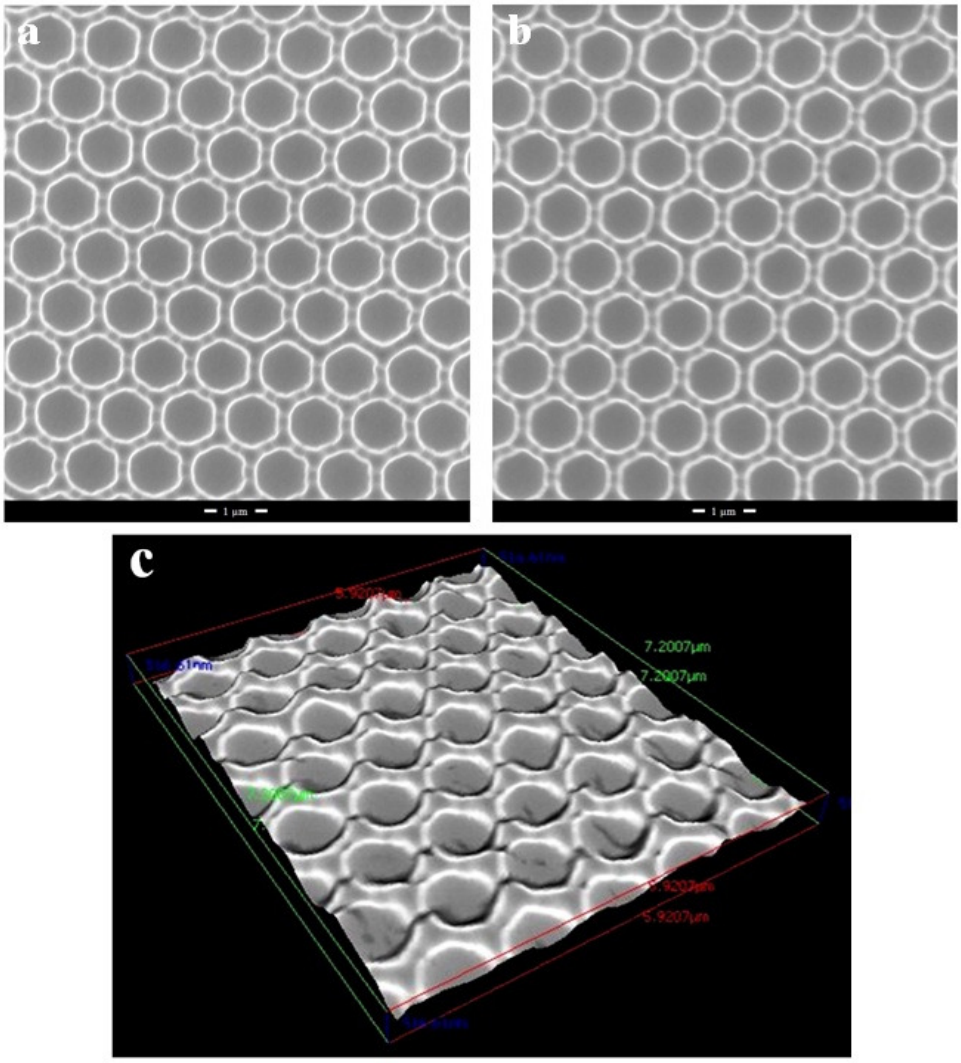

Figure 4-7 Pair of SEM stereo images of a microbowl PDMS surface taken with tilt angle of 10º and its 3D reconstruction model: a) left image, b) right image, and c) the digital elevation model of PDMS microbowl structure (Green, red and blue colour dimensions correspond to 7.2 µm × 5.4 µm × 0.5 µm respectively).

The average volume of the pyramids is about 1.86×10^7 nm^3 which is approximately equal to the volume of a pyramid with a 350 nm side length. This achieved side length for the pyramid is in agreement with the interstitial spaces between PS spheres with a diameter of 1.1 µm. The average of maximum peak to valley distance

was found to be 516 nm, which matches well with the half diameter of the spheres. A less than 50 nm thick layer of gold was coated on the PDMS mould using a sputtering system to increase the conductivity and consequently the image sharpness before milling the structures. **Figure 4-8** illustrates the results after FIB milling. The dashed line shows the bottom of the bowl-shaped structure. The dark flat surface underneath the dashed line is formed as the result of the ion bombardment. The height of a single pyramid has been measured from the tip, just below the gold layer, to the point where the arched shape thin wall meets the support wall of the pyramid. In this manner, the average height of the pyramids was found to be 325 nm.

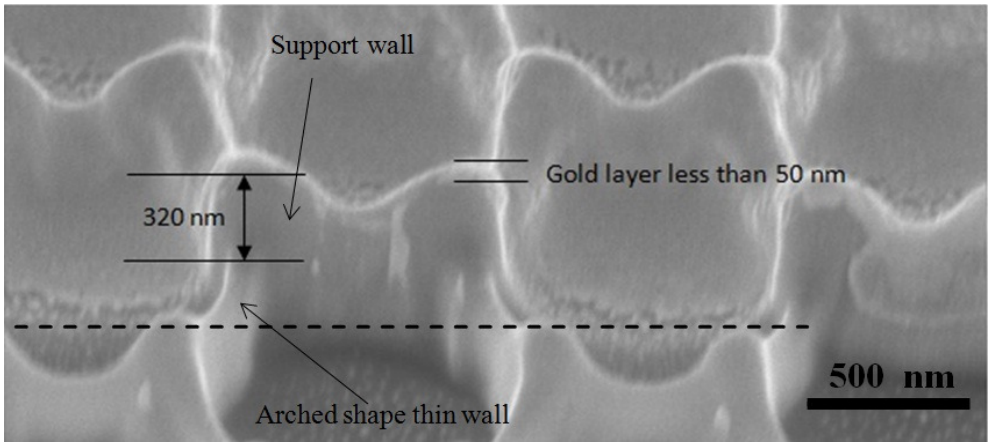

Figure 4-8 A PDMS microbowl structure after FIB milling. The dashed line shows the bottom of the microbowls.

4.5 **Fabrication of 2D Periodic Nanostructure**

After preparation of the PDMS soft mould, a metal film is sputtered onto the top surface of the PDMS mould. In this experiment, another replica moulding soft lithography process is performed to fabricate a PDMS replica. For this reason, the PDMS soft mould is cast using PDMS slurry followed by a curing process of the

PDMS slurry. When the PDMS pre-polymer is cured in the oven, a peeling off process is performed to release the cured PDMS replica from the PDMS mould. Lastly, the fabricated PDSM replica is cleaned from any residual particles of metal which are stuck to it. The fabrication steps are schematically illustrated in **Figure 4-9**.

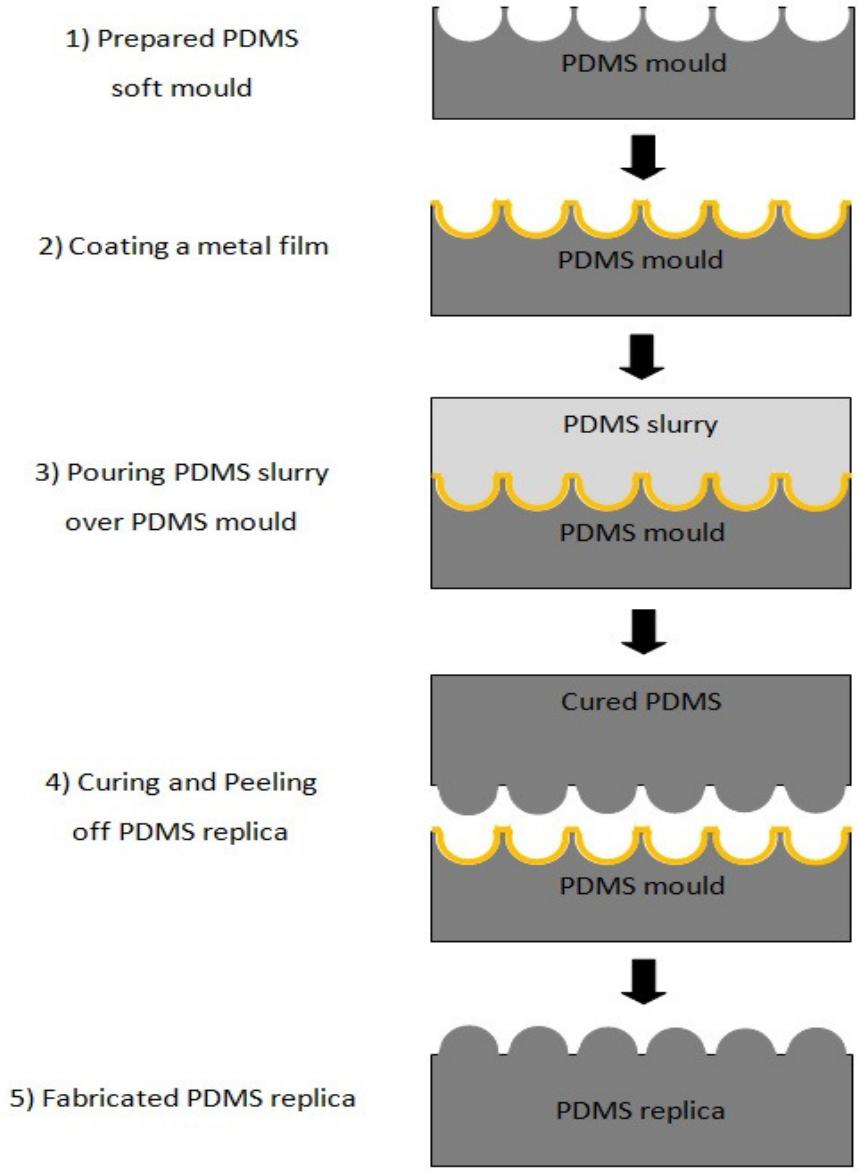

Figure 4-9 The diagram shows the proposed fabrication process using PDMS/PDMS replica moulding.

4.5.1 PDMS/PDMS Replication Process

The PDMS soft mould was reinforced by the adhesion of a supporting glass or plastic plate. From here, the phrase 'PDMS master template' refers to the PDMS soft mould. The supported PDMS master template was then coated with a gold or platinum film using a sputter coater at 0.1 Torr and 20 mA current in an argon atmosphere. Coating PDMS with gold or platinum film for a PDMS/PDMS replication process has not yet been explored in the nanofabrication community. Therefore, the effect of sputter coating on the surface topography is essential before performing the PDMS/PDMS replication process. Different coating thicknesses were applied to the PDMS template samples and the surfaces were examined. The thickness of the deposited layer was tuned directly from the sputter coater by controlling the deposition duration.

After the metal coating process, the PDMS slurry was cast onto the PDMS master template. As previously, a similar plastic box was used as a container in this process. After pouring the PDMS slurry on the PDMS master template, the plastic box, which contains both the master template and PDMS slurry, is placed in a vacuum chamber for 5 hours. A long vacuum duration is needed to ensure that the PDMS patterns are filled with the PDMS slurry. The desired PDMS replica was then cured at 60 °C for 2 hours, followed by the demoulding process in which the PDMS replica was released from the PDMS master template with the aid of a stainless steel blade.

4.5.2 Surface Characterisation

Two challenges need to be addressed in developing a PDMS/ PDMS replication process. First, to improve the surface wettability nature; a conformal contact between the PDMS slurry and the PDMS master template is necessary to achieve nanopattern transfer. The other challenge is to improve the peeling off ability and to introduce a clean demoulding process. With respect to the first challenge, the flatter the PDMS slurry drop shape (low contact angle), the better the wetting of the nanopattern interface. As for the second challenge, it is important to reduce the adhesion between the PDMS master template and its replica after curing and to keep them undamaged during demoulding.

The contact angle, peeling ability, and surface topography of the surfaces of PDMS samples were studied to characterise the replication process. Eight sets of PDMS/PDMS replication experiments were grouped according to their surface nature. Firstly, in set A, was the PDMS master template in which sample surfaces were left unpatterned and uncoated. Secondly, in set B, sample surfaces were nanopatterned and uncoated. Then, in set C, sample surfaces were left unpatterned and coated with a 20 nm platinum film. In set D, sample surfaces were left unpatterned and coated with a 20 nm gold film. In set E, sample surfaces were nanopatterned and coated with a 20 nm platinum film. In set F, sample surfaces were nanopatterned and coated with a 20 nm gold film. In set G, sample surfaces were nanopatterned and coated with a 40 nm platinum film. Finally, in set F, sample surfaces were nanopatterned and coated with a 40 nm gold film.

The aim of studying the contact angle is to investigate the wettability of the PDMS master template by the PDMS slurry. An average of ten contact angle readings was taken. The peeling off ability was performed after the pair of contacted PDMS samples were cooled down to room temperature to allow a similar curing condition. In the experiments, two PDMS pairs were peeled off manually and the sample quality was visually inspected. When each of the two PDMS pairs, the master template and the replica, are complete and not damaged after peeling off, the process is recorded as being successful; otherwise it is recorded as unsuccessful. At least ten samples were made on each set. The peeling off ability is defined as follows.

$$\text{Peeling off ability} = \frac{Number\ of\ undamged\ samples}{Total\ number\ of\ samples} \times 100\% \qquad \textbf{Eq. 4-2}$$

Both the contact angle and the peeling off ability experiments were carried out in a clean environment to avoid contamination of particles in the air. Surface topography, size uniformity and periodicity of all samples were observed using the Jeol 7000 SEM operated with an acceleration voltage of 20 kV. The SEM samples were prepared by attaching the prepared PDMS samples to an aluminium stub using conductive adhesive tape.

4.5.3 Results of Patterning 2D Nanostructure

As mentioned earlier, the achieved PDMS master template was coated with either a gold or platinum layer. The deposited layer of the gold on the surface of the PDMS template was assumed to be uniform in simulation. In particular, the film thickness

was assumed constant throughout the topography of the PDMS template. Experimental validation was performed by generating various thicknesses of the deposited layer. The simulation and experimental results for various deposition thicknesses are illustrated in **Figures 4-10** and **4-11**, respectively.

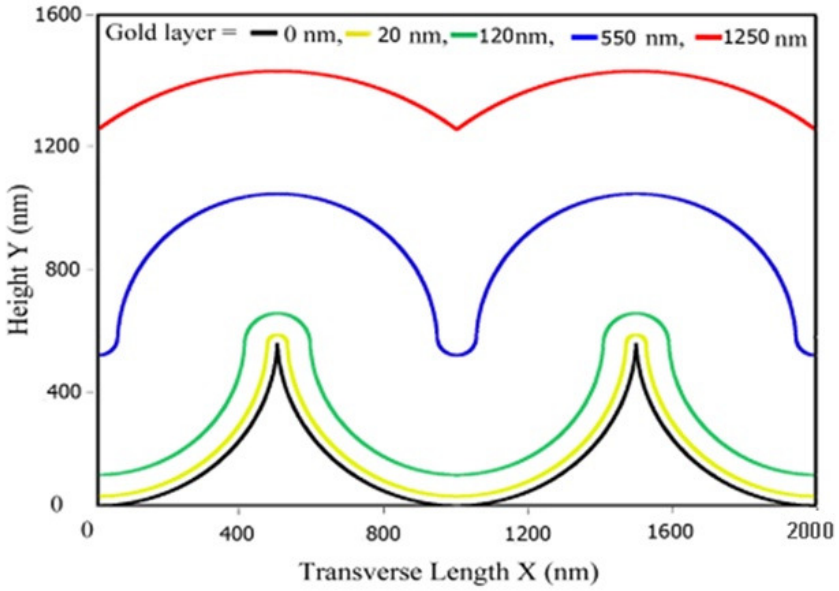

Figure 4-10 Surface topography of PDMS master template as a function of the deposited layer.

It can be clearly seen that the thickness of the deposited layer significantly affects the PDMS template topography. The higher the deposited thickness means the lower the bowls' diameter and the higher the nanopillars' diameter. Both the simulation and experimental results show that the depth of the microbowls remains constant when the layer thickness is less than or equal to 550 nm, which is equivalent to half of the PS spheres' diameter. In addition, the geometry of the bowls changes gradually from nearly hemisphere to conical, with inward curvature increasing with the deposited thickness. By further increasing the layer thickness, the bowls and the nanopillars become shallower. Thus, the variation of the coating thickness can be used together

with the size of the PS spheres to tune the nanostructures' PDMS master template. The simulation and experimental analysis prove the assumption of a uniformed deposition.

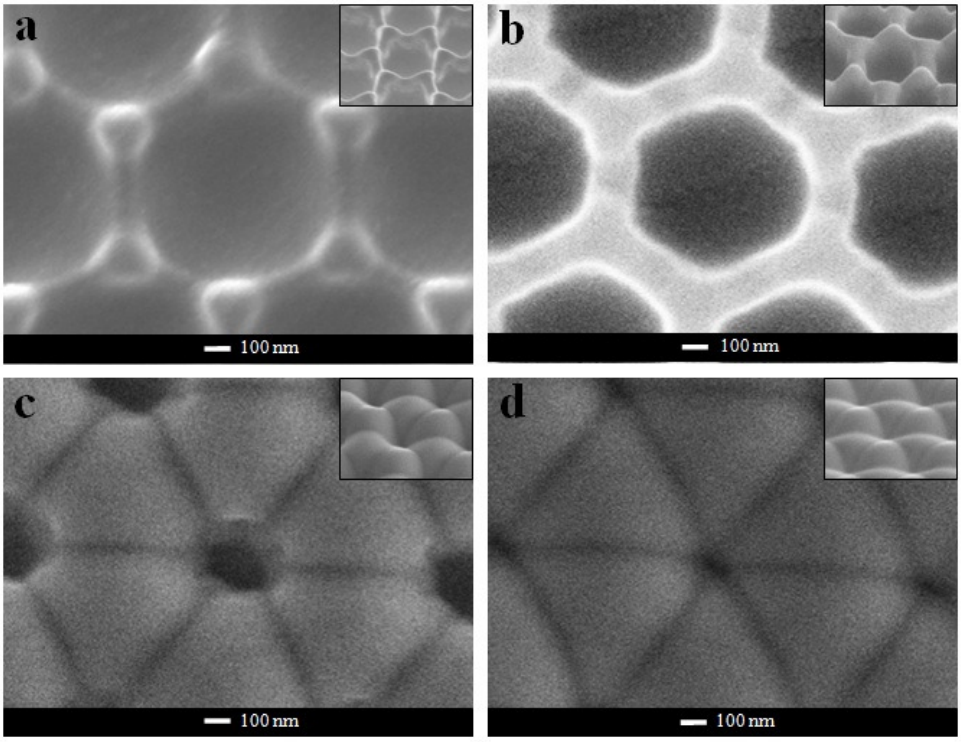

Figure 4-11 The SEM images of PDMS template which are coated with different gold film thicknesses: a) layer of 20 nm, b) layer of 120 nm, c) layer of 550 nm, and d) layer of 1250 nm.

The contact angle measurement and peeling off ability results are listed in **Table 4-2**. In addition, photos of the contact angle measurement are shown in **Figure 4-12**. The average contact angle of a PDMS slurry drop on an unpatterned and uncoated PDMS surface is 14º. The low contact angle indicates a good wetting property between the PDMS plain surface and the PDMS slurry, unlike the hydrophobic behaviour of the PDMS surface when in contact with water where the contact angle ranges from 89º to 120º [123]. No samples were successfully demoulded, and the peeling off ability is 0%.

Table 4-2 The contact angle and peeling off ability of the replication process.

Group	Description	PDMS contact angle	Peeling off ability
A	unpatterned and uncoated	14°	0%
B	nanopatterned and uncoated	31°	0%
C	unpatterned and 20 nm platinum coated	10°	80%
D	unpatterned and 20 nm gold coated	6°	100%
E	nanopatterned and 20 nm platinum coated	12°	60%
F	nanopatterned and 20 nm gold coated	8°	100%
G	nanopatterned and 40 nm platinum coated	12°	100%
H	nanopatterned and 40 nm gold coated	8°	100%

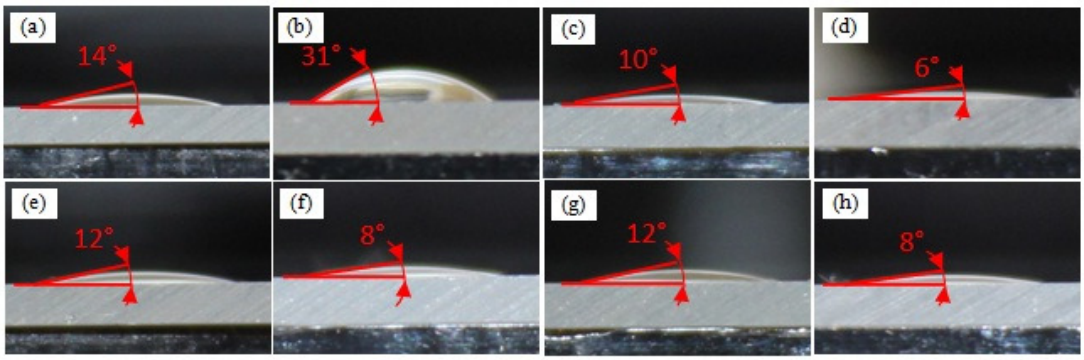

Figure 4-12 The contact angle images for different sets: a) group A, b) group B, c) group C, d) group D, e) group E, f) group F, g) group G, and h) group H.

With the presence of nanopatterns on the PDMS surface, the surface's wetting properties are degraded where the average value of the contact angle is 31°. This may be attributed to the specific characteristics of nano-topography. The nanopatterned surfaces of the untreated PDMS resisted the outward spread of the PDMS slurry and helped to maintain a higher contact angle. These results are similar to those in the literature, where the presence of patterned structures has been proven to enhance the hydrophobic nature. On the other hand, the peeling off ability remains at 0%. All the

peeling attempts failed with the uncoated PDMS samples, due to the high bonding force between the PDMS pair impeding demoulding associated with the adhesive interaction between the PDMS slurry and the PDMS master template during the curing step.

For the unpatterned and coated samples in groups C and D, the decrease of the contact angle and the increase in the peeling off ability is abrupt when the samples are coated with either a gold or platinum layer. The best results are achieved for samples coated with gold where the contact angle is decreased to about 6º and the peeling off ability is improved to about 100%, while samples coated with platinum have a contact angle of about 10º and a peeling off ability of about 80%.

Similarly, in set E, where samples are nanopatterned and coated with 20 nm platinum, the contact angle is decreased to about 12º and hence the surfaces' wetting properties are improved. On the other hand, the peeling off ability is only about 60%. SEM images of set E topography are shown in **Figure 4-13**. It can be noted that the pattern of the PDMS master template is partially transferred to the PDMS replica. The bowls can be identified in the PDMS template with notable distortion. In addition, the nanopillar pattern cannot be identified on the PDMS template and are presented on the surface of the PDMS replica. On the other hand, the bump arrays on the PDMS replica are visually distinguished.

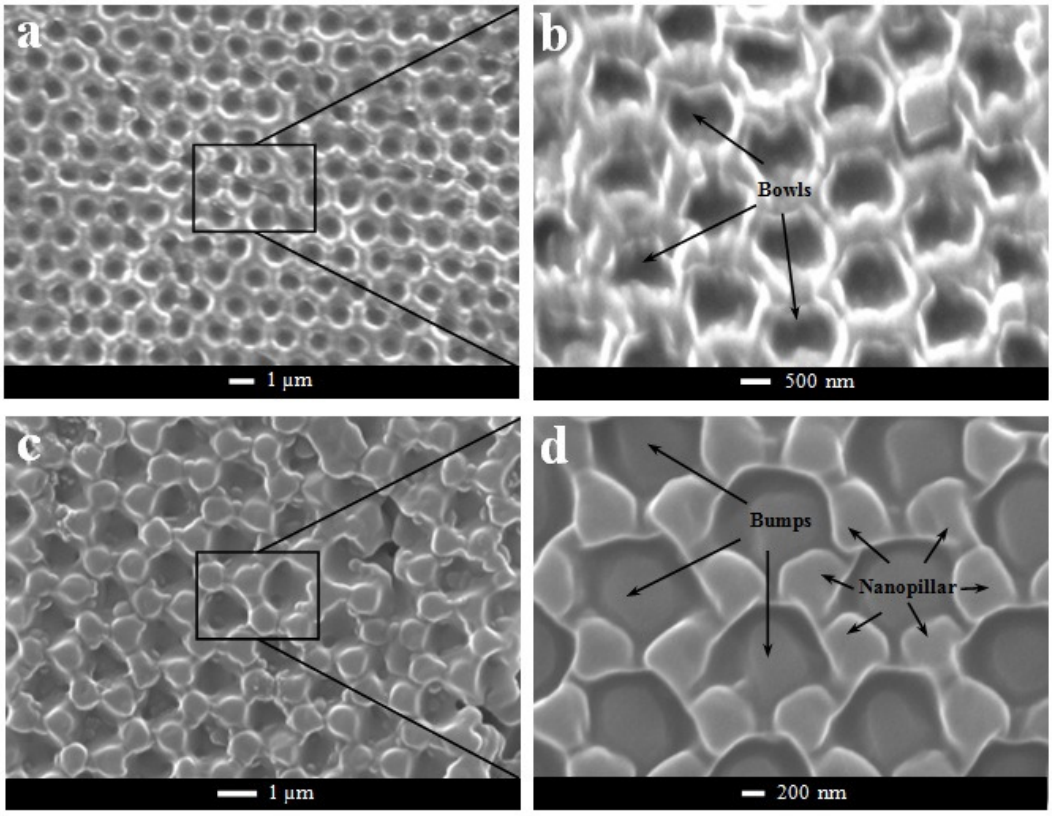

Figure 4-13 The SEM images of PDMS nanopatterned after peeling off for set E coated with a 20 nm platinum film: a) PDMS master template, b) magnified image of PDMS template shows damaged bowls, c) PDMS replica, and d) magnified image of PDMS replica shows damaged bumps and pillars.

In set F where samples are coated with a 20 nm gold layer, the surface wetting properties of the nanopatterned PDMS master template were significantly improved. The average value of the contact angle decreased to about 8º while the peeling off ability of the samples is significantly improved to 100%. All samples were demoulded easily and both the original and the copy remained intact. Samples coated with 20 nm gold not only had improved wetting properties against the PDMS slurry, but also reduced the molecular adsorption to PDMS surfaces, which enhanced the peeling off ability. SEM images of the gold-coated PDMS master template and the PDMS replica are shown in **Figure 4-14**. Contrary to set E, the PDMS replica shows

complete and uniformly patterned bump arrays. In addition, the bowls and nanopillars of the PDMS master template are kept intact after demoulding.

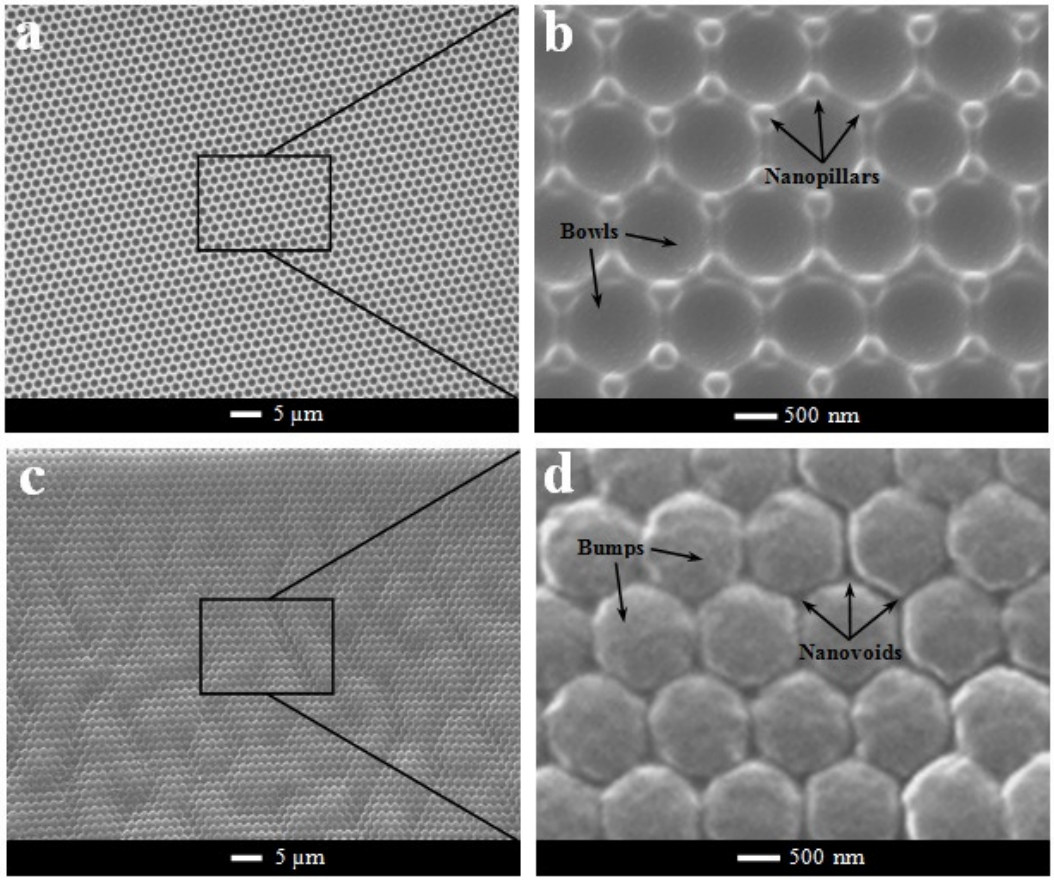

Figure 4-14 The SEM images of PDMS nanopatterned after peeling off for set F coated with a 20 nm gold film: a) PDMS master template, b) magnified image of PDMS template shows perfect bowls and pillars, c) PDMS replica, and d) magnified image of PDMS replica shows perfect bumps and voids.

The influence of average thickness of the deposited metal film, on the wetting behaviour of the sample surface and the peeling off ability was studied experimentally for sets G and H. SEM images of the PDMS topography of the samples in sets G and H are shown in **Figure 4-15** and **Figure 4-16**, respectively. With further increasing the platinum thickness from 20 nm to 40 nm, the average value of the contact angle remained unchanged at 12º, while the peeling off ability of the samples improved from 60% to 100%. Both the PDMS master template and the

PDMS replica were demoulded without distortion, as shown in **Figure 4-15**. On the other hand, when the gold thickness was increased from 20 nm to 40 nm, both the contact angle and the peeling off ability remained unchanged. **Figure 4-16** demonstrates the results of both the PDMS master template and the PDMS replica of set H that are similar to those illustrated in **Figure 4-14**. A slight decrease in the diameter of the bowls and increase in the nanopillar thickness can be noticed when compared to the results obtained using 20 nm layer thicknesses.

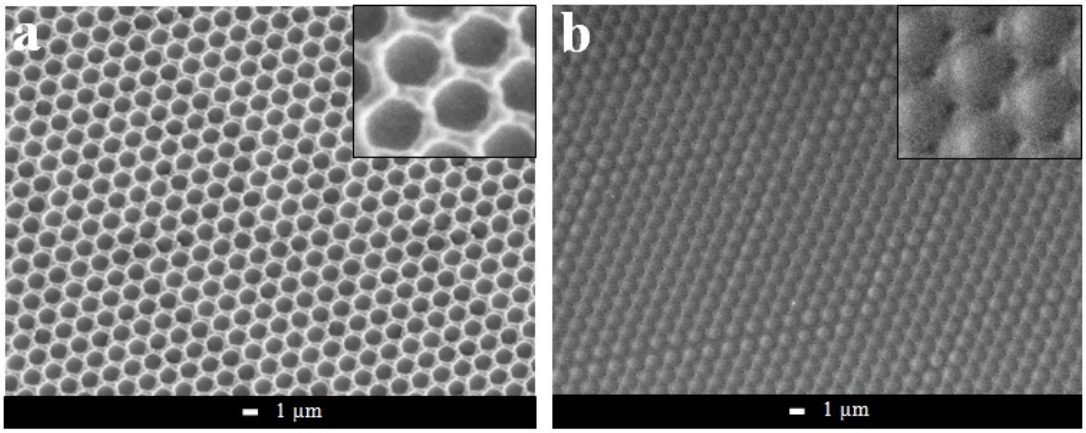

Figure 4-15 SEM images of PDMS nanopatterned after peeling off for set G: a) PDMS master template, b) PDMS replica.

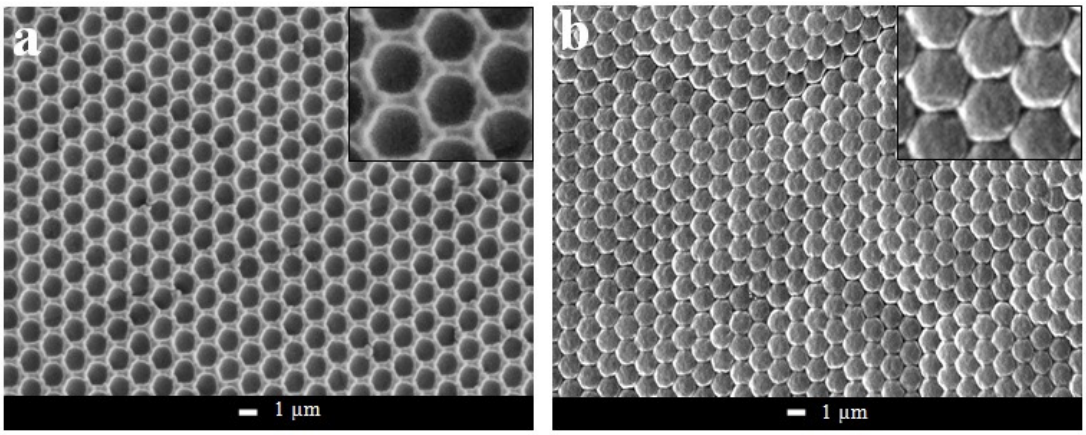

Figure 4-16 SEM images of PDMS nanopatterned after peeling off for set H: a) PDMS master template, b) PDMS replica.

By comparing **Figure 4-13** and **Figure 4-15**, for samples coated with 20 nm and 40 nm platinum layers, it can be noted that the replication process is significantly improved and the results similar to those of the gold coated samples. A schematic explanation of the peeling off mechanism for samples in sets E and F is illustrated in **Figure 4-17** and **Figure 4-18**, respectively.

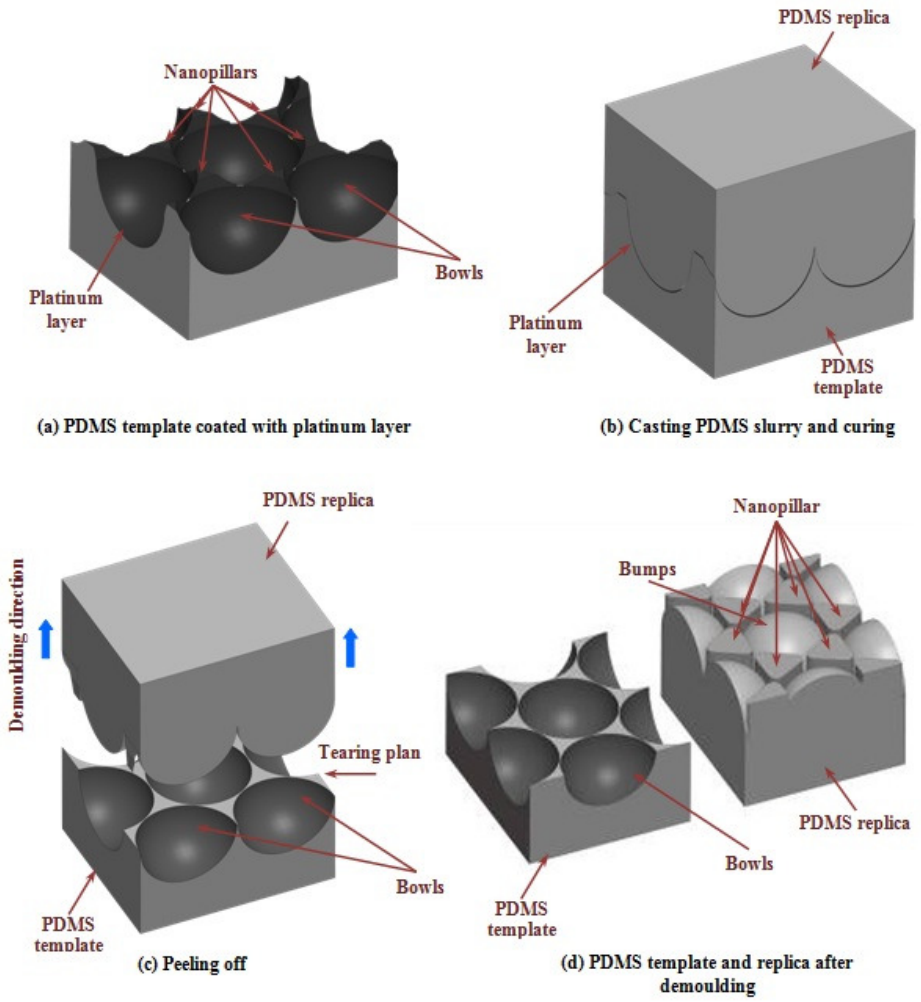

Figure 4-17 A schematic explanation of demoulding mechanism of platinum coated samples.

It can be said that when the average thickness of the platinum is close to 20 nm, the formed layer of platinum on the PDMS topography may not be able to cover the entire surface of the nanopillar tips of the PDMS master template. This results in an

adhesion between tips of the master template and the PDMS replica during curing. Afterwards, the nanopillars were broken from the PDMS template and attached to the replica during peeling off. Consequently, the PDMS template contains only the microbowls' pattern and does not contain any of the nanopillars, see **Figure 4-13**. The replication process was significantly improved with further increasing of the platinum layer to about 40 nm. At such high deposition thickness, the platinum particles were able to form on all the PDMS topography including the tips of the nanopillars, which eases the peeling off ability and hence improves the perfection of the resultant nanostructures.

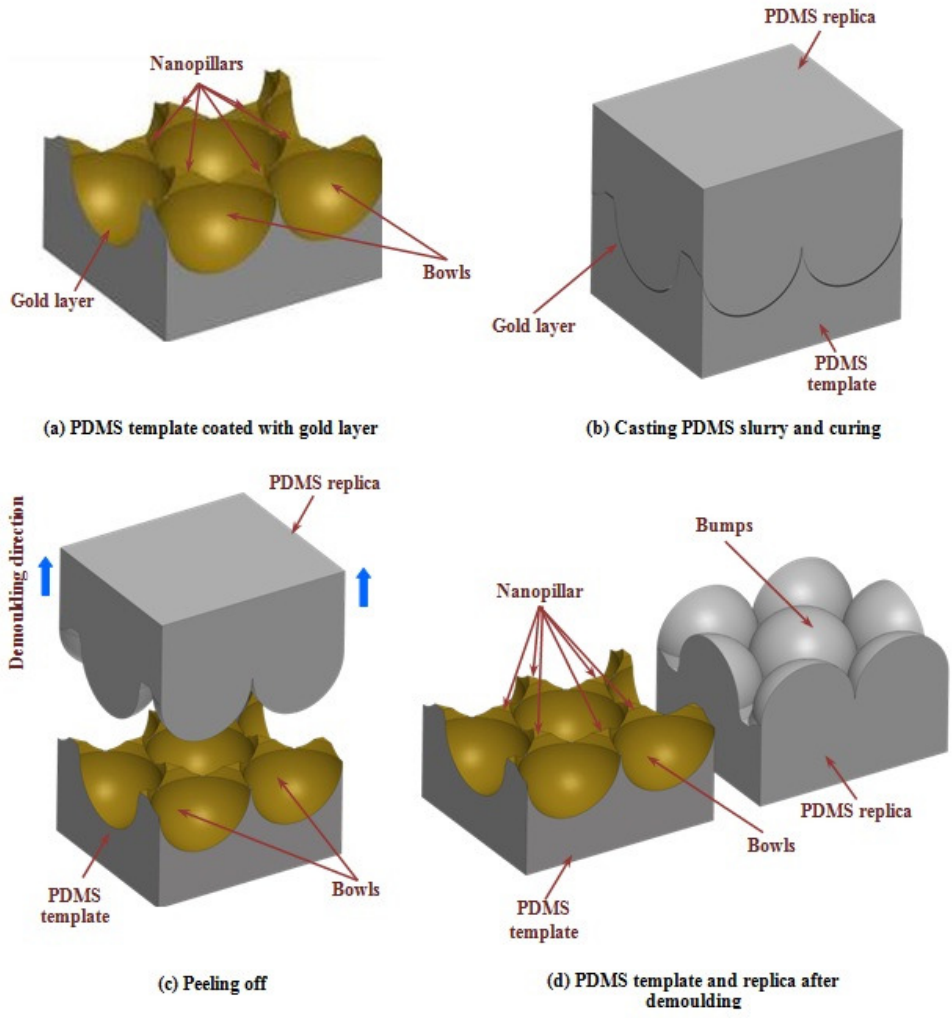

Figure 4-18 A Schematic explanation of demoulding mechanism of gold coated samples.

4.6 **Fabrication of 3D Periodic Nanostructure**

After preparation of the PDMS soft mould, another self assembly process is conducted over the top surface of the PDMS mould. Surface treatment of the PDMS mould is required prior to the reassembly process. Next, a metal film is coated onto the top surface of the reassembled monolayer of the PS microspheres. The polystyrene microspheres are then removed from the surface of the PDMS mould by using ultrasonication bath for a short time. At last, the PDSM soft mould is cleaned from any residual particles which are stuck to it. The fabrication steps are schematically illustrated in **Figure 4-19**.

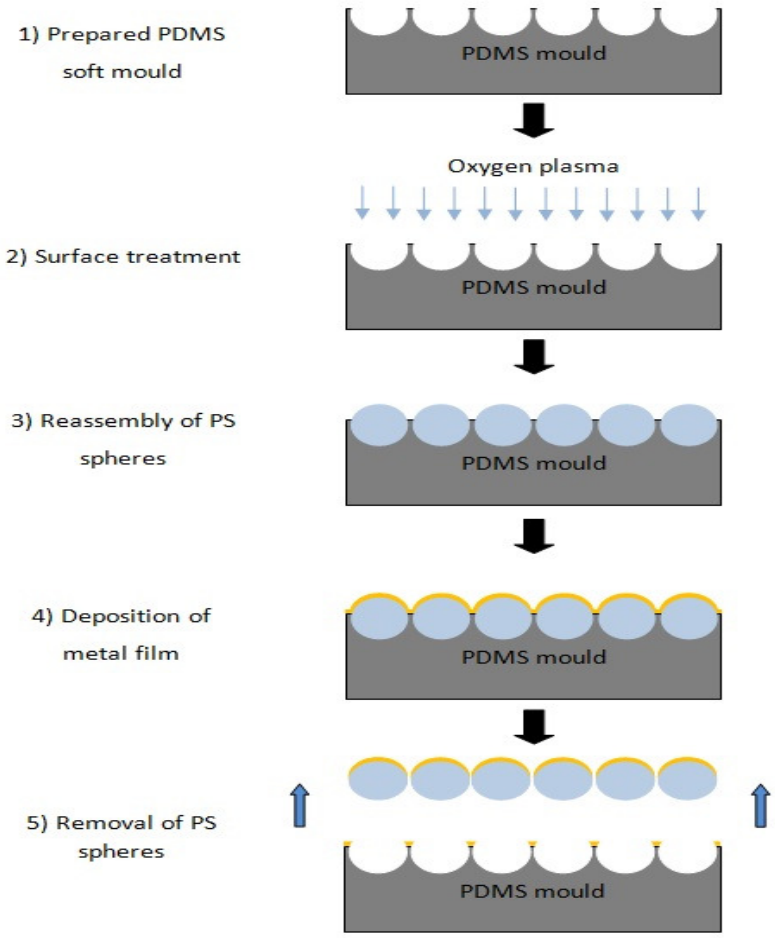

Figure 4-19 Diagram shows the proposed fabrication process using microspheres reassembly process.

4.6.1 PS Spheres Reassembly Process

The PDMS soft mould was reinforced by the adhesion of a supporting glass or plastic plate. From here onwards, the phrase of 'PDMS master template' refers to the PDMS soft mould. The supported PDMS master template was then treated using oxygen plasma at a working pressure of 40 mTorr. To optimise surface properties of the PDMS template, several experiments were performed using different oxygen plasma treating times. After plasma treatment the PDMS templates were kept in deionised water until they were used. Next, the same sized PS microspheres (1.1 μm) were used for a monolayer self assembly process over the structured PDMS template.

A droplet of prepared latex/water dilution was placed onto the PDMS template using a micropipette. A megasonic system was used to assist the spreading process of the PS spheres over the master template for only few minutes. The relative humidity in the clean room was 49% at 21 ºC and the self-assembly process was undertaken in a 75 ml sealed petri dish. Subsequently, a thermal evaporation system was used to coat a 50 nm gold film over the PDMS template which had self-assembled microspheres on the top. In fact, the self assembled spheres over the PDMS master template act as a protective layer and assist the deposition process, so the gold particles are only deposited on the uncovered area. This process was finally followed by the removal of the PS spheres from the surface of the PDMS template by sonicating samples in an ethanol bath for 4 minutes.

4.6.2 Surface Treatment of the PDMS Template

The most challenging part of the proposed fabrication technique was the self assembly of the polystyrene spheres onto the structured PDMS template. Since PDMS is inherently considered as a hydrophobic material, it is demanding to perform even a good MSA process onto a plain PDMS mould. Surface treatment of PDMS micro/nano structures using oxygen plasma has been extensively studied by different research groups for decades. It is a popular treatment technique for PDMS micro-fluidic devices. Treatment of PDMS using oxygen plasma adds many silanol groups (SiOH) to the PDMS surface which causes the PDMS surface be more hydrophilic [124]. A series of experiments were performed to examine the effect of different plasma-treatment times on the surface properties of the PDMS master template. **Table 4-3** presents the experimental results from the investigation, while other operating parameters were kept constant. In these experiments, four groups of samples were treated using different treatment times. Each group consists of five samples that were all placed into a low pressure radio frequency (RF) chamber at once.

Table 4-3 The experimental results provide the effects of different plasma-treatment times.

Group	**Gas flow** (sccm)	**Plasma power** (W)	**Treatment time** (seconds)	**Contact angle**
A	50	800	30	75º
B	50	800	60	63º
C	50	800	120	37º
D	50	800	180	23º

A contact angle of almost 115º was achieved for a PDMS master template without applying oxygen plasma treatment. The contact angle of the treated PDMS template reached almost 75º when the sample was treated for only 30 seconds. In general, the contact angle of the treated PDMS template is reduced by increasing the treatment time. A contact angle of 23º was obtained when three minutes of plasma treatment was performed. Although the obtained contact angle is not quite as good as for MSA process and further treatment may result in better surface properties, it should be noted that a long-term oxygen plasma treatment may change the surface topography of sample [125, 126] which is not desirable for this research.

4.6.3 Results of Patterning the 3D Nanostructure

An environmental scanning electron microscope (ESEM) was applied to inspect the result of the experiments described above. As explained earlier, each PDMS master template consists of ordered arrays of microbowls. The morphology of the microbowls is included in the reverse profile of the top half of the microspheres and the distributed pillars at the corners of each hexagonal bowl structure. As shown in **Figure 4-20**, the vertices of each hexagonal pattern are curvilinear triangular in shape and they are placed slightly above other parts. These pillar arrays are formed by the interstitial spaces between the PS spheres. The aim of this proposed method is to create gold nanopattern over these pillar arrays.

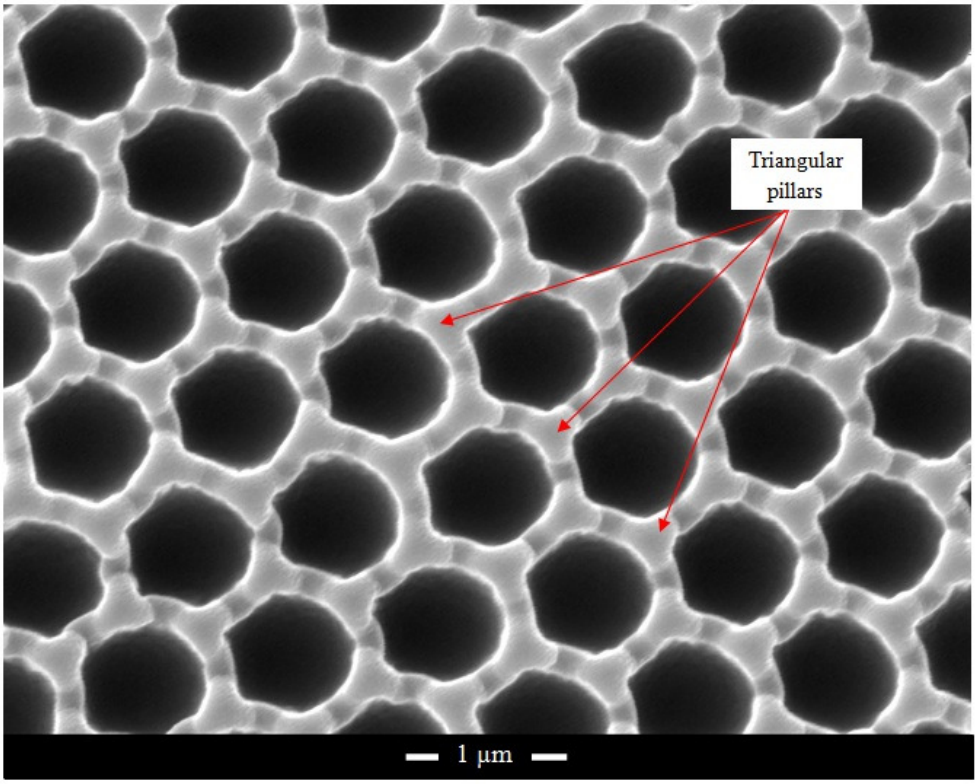

Figure 4-20 The SEM image shows arrays of curvilinear triangular pillars slightly above the microbowl structures.

To create gold nanopatterns over these distributed pillars, another self assembly process is required. The initial result of the self assembled PS spheres over the PDMS template is illustrated in **Figure 4-21**. As it is observed, microspheres do not entirely cover the PDMS template due to the hydrophobicity of the PDMS template. It is also perceived that those PS spheres which are placed onto the PDMS template are structurally deformed. The presence of nanopatterns beneath the PS spheres and the existence of empty spaces in the neighbourhood of the PS spheres are the main reasons for the occurrence of the spheres' deformation.

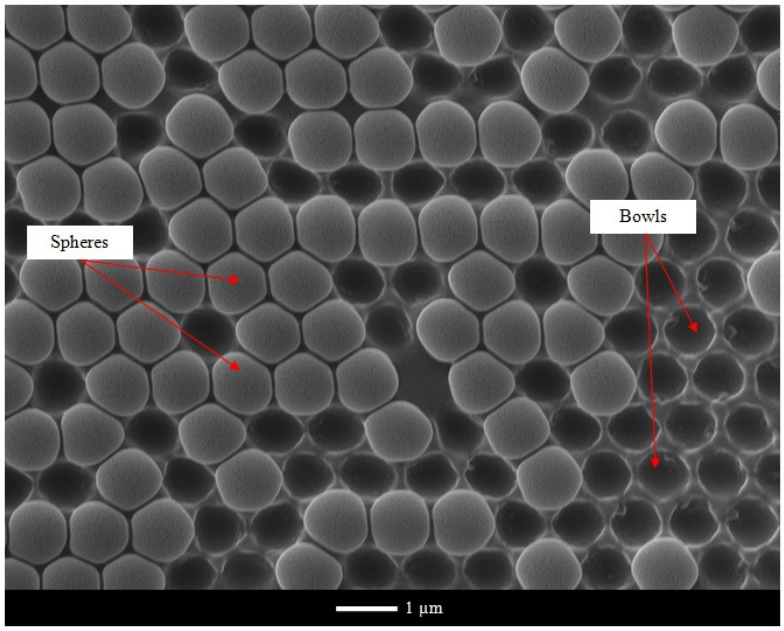

Figure 4-21 SEM image shows assembled PS spheres over a PDMS template without treatment.

As mentioned above, the surface of the PDMS master template was treated using oxygen plasma prior to the MSA process. A monolayer of self-assembled PS spheres on treated microbowl structures is shown in **Figure 4-22b**. Although the shape of the PS spheres is hexagonal instead of circular, they are perfectly self assembled over the PDMS template. Furthermore, as it is clearly observed from this SEM image, the voids between the assembled spheres over the PDMS template are narrower in comparison to the voids between the assembled spheres over silicon substrate in **Figure 4-22a**. This phenomenon happens due to the existence of the underneath patterns since spheres of the same diameter have been used. It should be noted that sphere distortion is the consequence of those forces generated by PDMS nanopillars which are located beneath of each sphere. In other words, each six nanopillars which surrounded a PS sphere generate equal forces in order to accommodate a high quality hexagonal close packed structure.

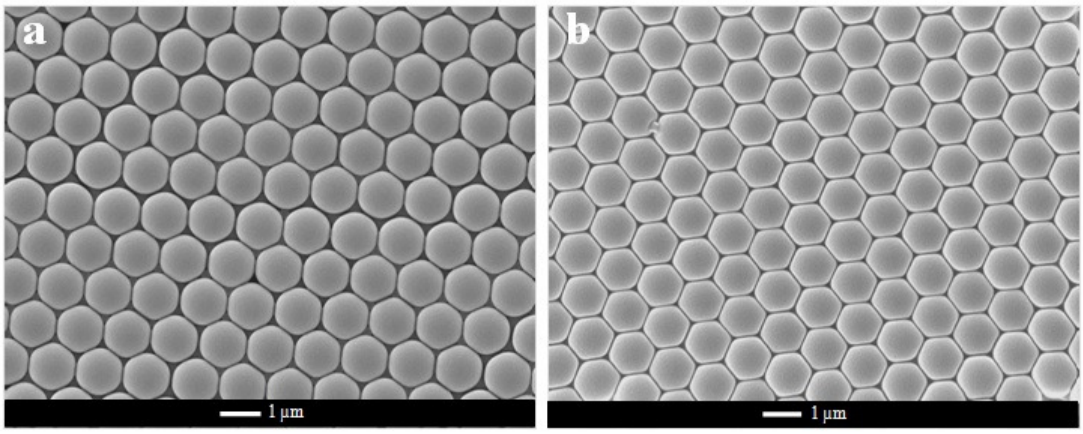

Figure 4-22 SEM images of self-assembled PS microspheres: a) over treated silicon substrate, b) over treated PDMS master template.

Following the self-assembly of the spheres, gold is then deposited by thermal evaporation. In fact, the spheres over the microbowl structures act as a protective mask to prevent the deposition of gold particles on the entire surface. Hence, the gold nanopatterns are only formed on the tips of the nanopillars after removal of the PS mask. The geometry of the structure can be controlled by changing the size of the spheres in the self assembly process. The effect of the sphere's size on the curvilinear triangular profile is illustrated in **Figure 4-23**.

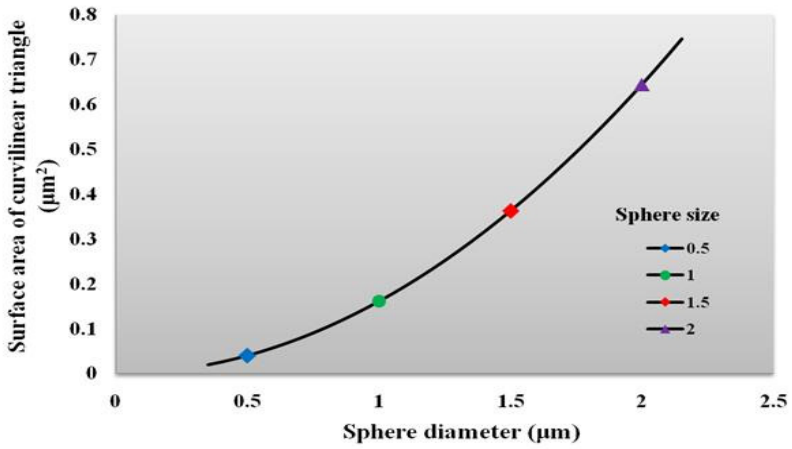

Figure 4-23 Effect of the sphere's size on the curvilinear triangular profile.

As can be seen, the surface area of the curvilinear triangle increases exponentially with the size increase of the PS spheres. The following geometric calculation also shows the relationship between the surface area of the curvilinear triangle, A_{ct}, and the microsphere radius, r.

$$A_{ct} = \left[\sqrt{3} - \frac{\pi}{2}\right] r^2 \qquad \textbf{Eq. 4-3}$$

After gold deposition, the PS sphere mask is removed by sonicating the entire sample in a solvent, leaving behind the deposited gold over the PDMS pillars with a curvilinear triangle shape. **Figure 4-24** shows the SEM image of the gold nano features. Arrays of highly ordered gold nanopatterns over hexagonal pillars with a perpendicular bisector of 210 nm on average are observed. The height of the gold nanopatterns can also be tuned by controlling the thickness of metal deposition while its surface area can be controlled by utilizing different sized spheres.

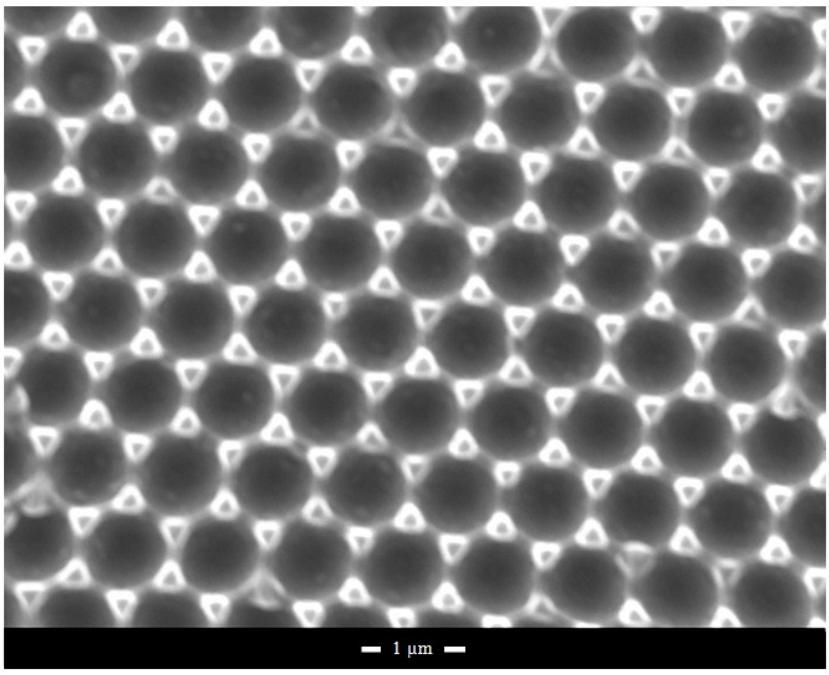

Figure 4-24 The SEM image of the gold nanopatterns above curvilinear triangular pillars.

4.7 **Summary**

In this chapter, the overviews of both fabrication methods to make 2D and 3D periodic nanostructures have been introduced. Next, the MSA process and the preparation of a PDMS soft mould from a PS spheres' template have been discussed. SEM stereoscopic imaging technique and FIB milling technique have been used to characterise the morphology of the prepared PDMS mould. The fabrication process of PDMS nanobumps' arrays using PDMS/PDMS replica moulding and the patterning process of metallic features over PDMS nanopillars' arrays have been presented.

In the first approach, the use of different film thicknesses for the fabrication of PDMS nanobumps arrays has been examined in detail. The surface wettability of the PDMS template and the peeling off ability of PDMS pairs, as the challenges of the proposed approach, have been fully inspected. The contact angles of the PDMS slurry were decreased from 31º to 8º and 12º when the nanostructured PDMS samples were coated with a 20 nm gold layer or a 40 nm platinum layer, respectively. In addition, the peeling off ability improved from 0% to 100%. In the experiments, the effects of different film thicknesses of a gold or platinum layer have been checked and the achieved results have been compared. This study shows that a thickness of at least a 20 nm gold layer or a 40 nm platinum layer on the nanostructured PDMS template works best as a release layer. Both experimental and simulation results of the coating process show that the gold sputter coating produces uniform film coating.

In the second approach, the feasibility of patterning distributed nanopillars with a metal film has been investigated. For the creation of gold nanopatterns over distributed pillars of a PDMS template, a monolayer self assembly process has been identified as a proper strategy. Hydrophobicity of the prepared PDMS template, due to the nature of the material, and the presence of nanostructures were found as the main challenges of the MSA process. The fabrication process to obtain metallic features over PDMS nanopillars' arrays has been optimised through extensive investigation. In the optimisation, the effect of different oxygen plasma-treatment times on surface properties of a PDMS template has been studied. The contact angle of the PDMS template was reduced from 115º to 23º when the sample was treated for three minutes.

The proposed strategies provide a versatile way of developing a functional PDMS substrate. Consequently, uniform arrays of nanostructures have been successfully fabricated using simple and convenient approaches without the need for expensive or sophisticated patterning instruments.

CHAPTER 5: NANOSTRUCTURE FABRICATION BY NICKEL ELECTROFORMING

5.1 Introduction

This chapter explains nickel electroforming as a reliable technique for production of metallic nanostructures. The fabrication methods to create uniform arrays of periodic nanopatterns using colloidal lithography were presented in detail in previous chapters. Ordered arrays of metallic nanopatterns have generally attracted the interest of the nanofabrication community due to their advantages in the nanoimprint lithography process. This chapter begins in Section 5.2 with presenting a brief introduction to the electroforming process and its theory. A general overview of the fabrication process and details of the electroforming setup are presented in Section 5.3 and Section 5.4, respectively. Experimental details for the production of metallic nanostructures are then explained in Section 5.5. The challenges of the electroforming process at nanoscale are discussed and alternative solutions for overcoming these challenges are suggested in Section 5.6. This chapter continues by presenting and discussing the electroforming results in Section 5.7 and the chapter is finally summarised in Section 5.8.

5.2 **Electroforming Background**

In general, electroforming refers to a process in which a metallic structure can be generated or regenerated through electrodeposition upon a mould followed by a separation process [127]. Electroforming uses a facile and cost-effective technique to produce any complicated geometry at high precision [128]. The electroforming process using different metals and alloys has been widely studied in the micro and nano community. Some metals like nickel, copper and gold and some alloys like NiFe and NiCo are the most common ones which have been chosen for electroforming process [129]. An electroformed nickel structure is generally stronger than wrought metal because of its smaller grain size [130].

5.2.1 Theory of Electroforming

A typical electroforming process consists of two electrodes which are submerged in an electrolyte bath. These electrodes are externally connected to a DC power supply and their internal sides, which are located in the electrolyte, are linked to a metal block (anode) and a desired mould (cathode). In the course of electroforming, electrons cause cations reduction in the electrolyte bath and subsequently deposit them onto the cathode side. Simultaneously oxidisation occurs on the anode side to compensate cations for the electrolyte [131]. For instance, as is schematically illustrated in **Figure 5-1**, the Ni^{2+} cations are reduced by obtaining electrons at the cathode side and the Ni^{2+} cations are increased by losing electrons at the anode side. This sequence provides an effective transfer of nickel from a metal block towards a

desired mould. The information on ingredients of the nickel electrolyte bath used in the electroforming process is given on **Table 5-2**.

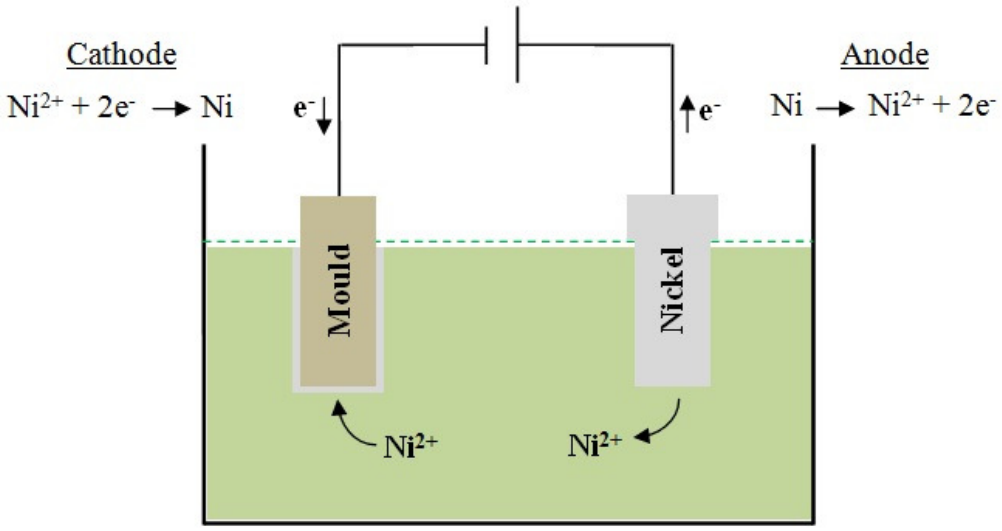

Figure 5-1 A schematic diagram showing the electrodeposition process.

5.2.2 Thickness Control through Electroforming

It is possible to achieve the desired thickness of an electroformed structure by controlling the timing and current density of the electrodeposition process. Based on Faraday's laws of electrolysis, the following equation can be presented to determine the relation between the aforementioned parameters.

$$h = \frac{t\,I\,M}{\rho\,S\,F\,z} \qquad \textbf{Eq. 5.1}$$

The height, h, of an electroformed structure is calculated using **Equation 5-1**, where F is the Faraday Constant, M is the molar mass of substance, z is the valence number of ions of the substance, I is the current, t is the time, ρ is the density, and S is the surface area. **Table 5-1** gives the values of specified parameters for nickel electroforming.

Table 5-1 Required specifications for thickness control in nickel electroforming.

Name	Value	Description
F	96485.31 (C/mol)	Faraday Constant
M	58.69 (g/mol)	Molar Mass
z	2	Atomic Valence
ρ	8.908 (g/cm^3)	Density

Since the nickel electroforming process is performed over a periodic nanostructure with symmetric patterns, a uniform thickness of the electroformed structure is the consequence of this process. It is worth noting that for those processes in which the size or the shape of patterns are not uniform over the entire surface of the mould, electroformed patterns with different heights would be achieved through an electrodeposition process. This issue happens because free electrons in a conductive film of a mould are only permitted to conduct through the uncoated surfaces of the conductive film of the mould. Hence, deeper thicknesses are obtained for narrower patterns due to the existence of higher local current density. **Figure 5-2** schematically compares electroforming progress for two different moulds, one with

uniform patterns and one with non-uniform patterns. As it is shown, the thicknesses of electroformed structures are regular in the mould with uniform patterns, while the electroformed thicknesses are irregular in the mould with non-uniform patterns. It is also observed that heights of electroformed structures are varied among different patterns due to the difference in local current densities.

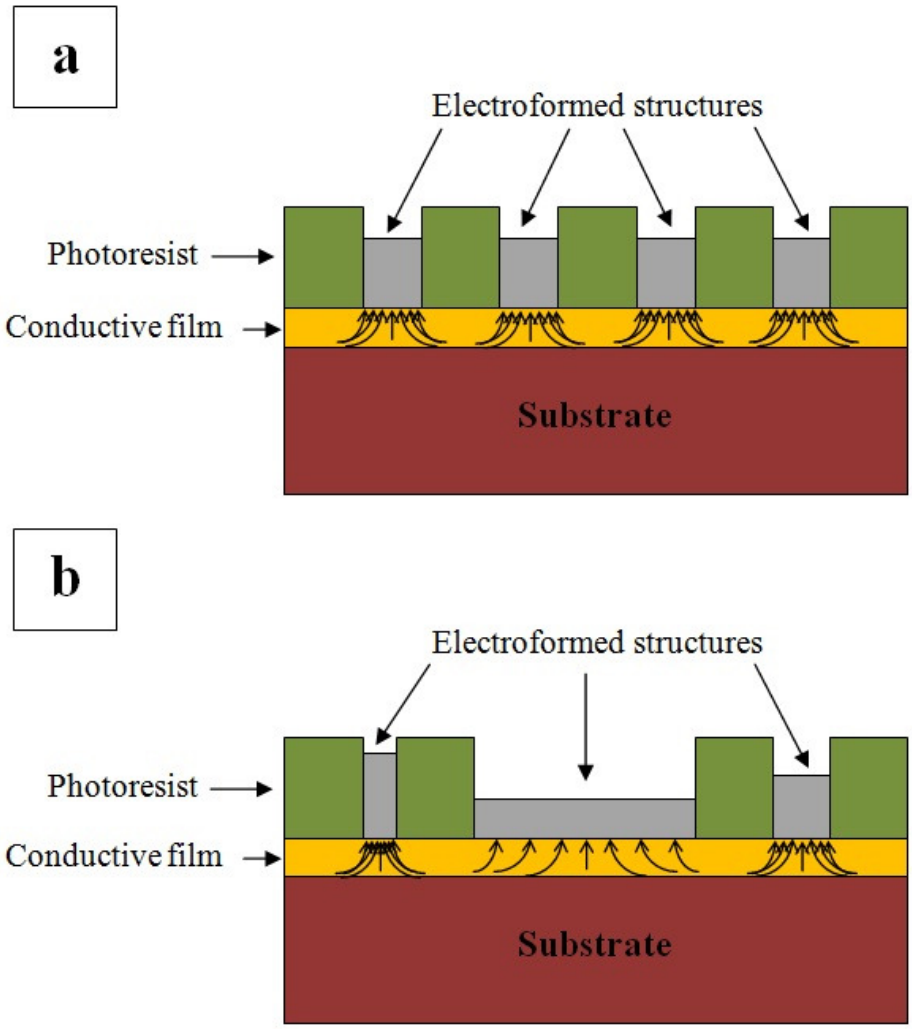

Figure 5-2 A schematic illustrates different local current densities and electroformed thicknesses for: a) a uniform nanopatterned structure, b) a non-uniform nanopatterned structure.

5.3 **General Overview of Fabrication Process**

The general process for the fabrication of metallic arrays of nanopatterns is schematically illustrated in **Figure 5-3**. The following steps clarify the complete fabrication method using an electroforming process over a uniform nanostructure template:

1. Coating the prepared nanostructure template with a thin conductive film.
2. Filling up the nanostructure template using electrodeposition.
3. Releasing a metallic electroformed structure from the template.
4. Removing the thin conductive layer through chemical etching.

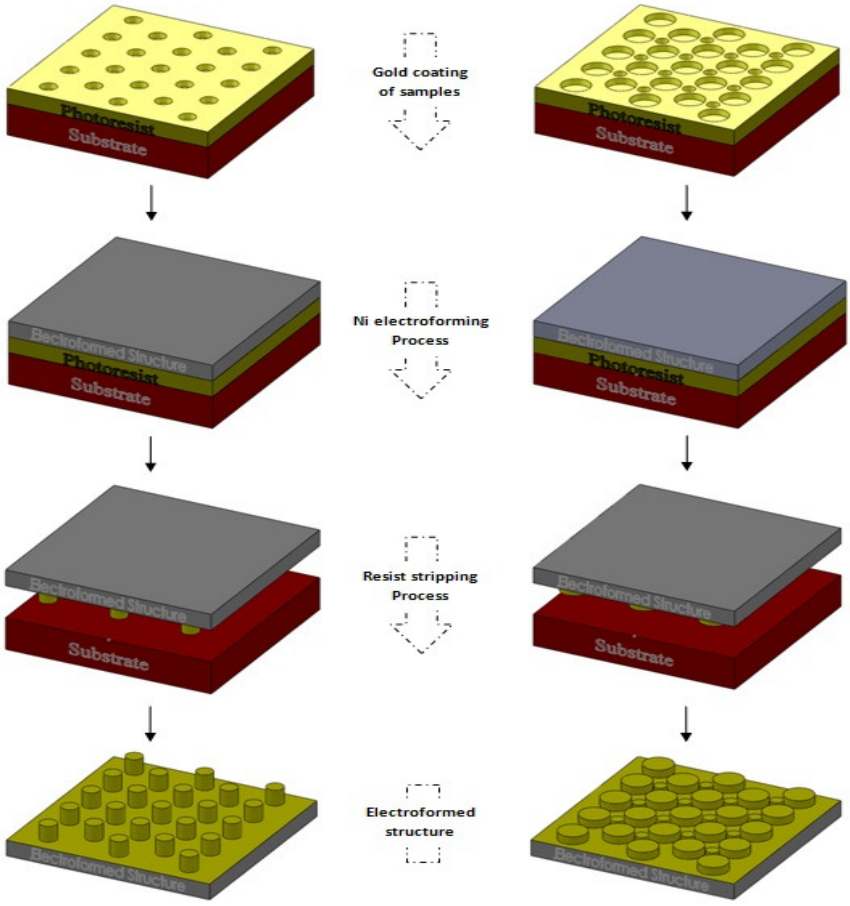

Figure 5-3 A schematic picture shows the nano electroforming process.

In a typical electroforming process, a thin metallic film which acts as a conductive layer is generally applied underneath the photoresist layer, while in the aforementioned technique, the conductive film is coated over the uniform nanostructure template. The only reason for this issue is to get a good measure of the height of the achieved patterns without applying any changes in the profile of the fabricated nanostructure.

5.4 **Electroforming Setup**

To run the electroforming process and create a metallic nanostructure, a simple setup was designed and built. It is worth noting that all electroforming experiments were performed in a laboratory fume cabinet. The electroforming setup is comprised of different components which are introduced in more detail here. A Tenna DC72-6153 power supply was used as the energy source to drive the electrodeposition process. A glass beaker containing the electrolyte is used as an electrochemical cell for the electrodeposition process. A plastic lid with two fixed arms of 8 cm height was applied to cover the glass beaker in the course of the electroforming.

Anode and cathode electrodes are attached to these fixed arms to prevent any undesirable dislocation of electrodes. When the electrodes are in their parallel positions relative to each other, there is a 5 cm gap in between them. A nickel plate with a surface area of 2 cm^2 was used as the anode. The fabricated nanostructure was coated with a thin gold layer which was used as the cathode. A dual function

hotplate-agitator was used to control both the temperature and the stirring-speed of electrolyte bath in the course of the electroforming. A magnetic bar was placed inside the glass beaker to assist the agitation process. **Figure 5-4** shows the physical image of the setup for the electroforming experiments.

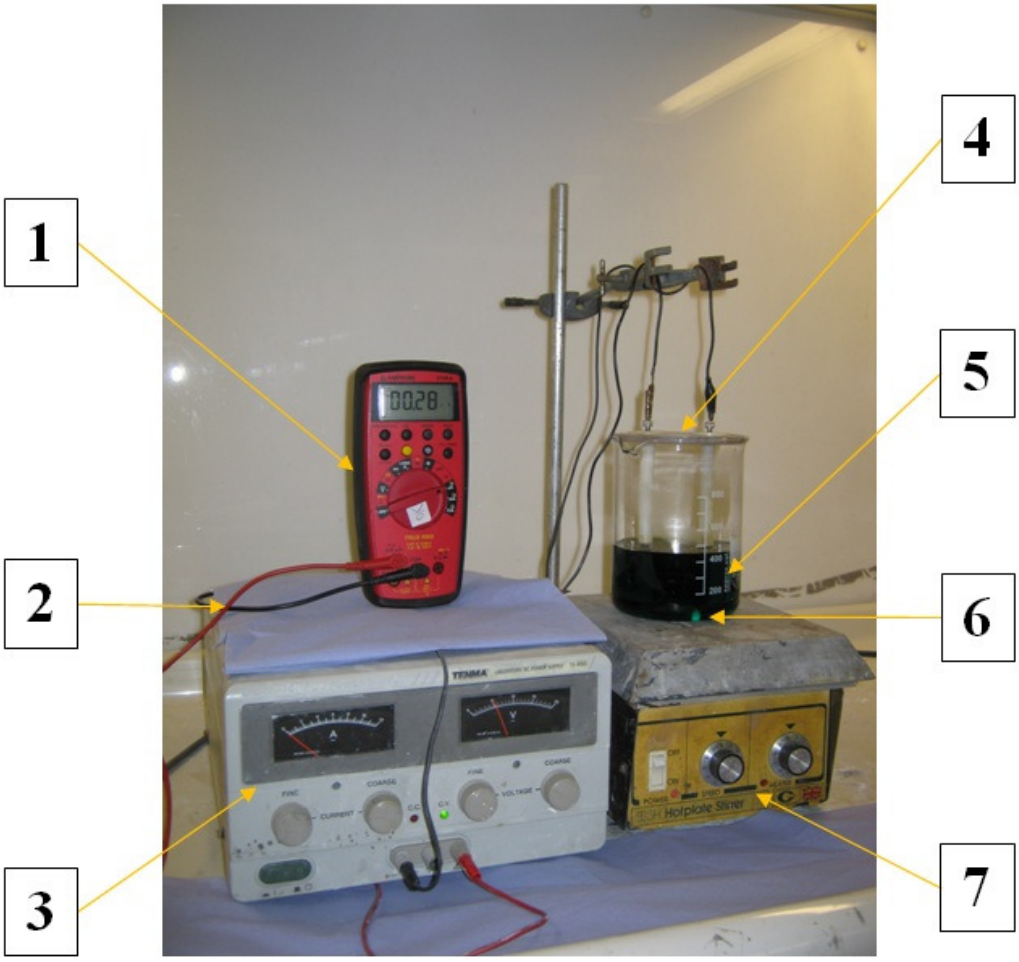

1. Multimeter
2. Electrical wires
3. DC power supply
4. Plastic lid with two fixed arms
5. Electrochemical cell
6. Magnetic bar
7. Dual function hotplate-agitator

Figure 5-4 Digital image of electroforming setup along with its components details.

5.4.1 Nickel Electrolyte Solution

There are different types of electrolyte solution which have been used in nickel electroforming processes for decades. In this research, a commercial nickel sulfamate provided by PMD Chemicals Ltd was used as the electrolyte solution for the experiments. The commercial nickel sulfamate is known as a ready to use product, and in this study no further treatment was applied to it. The major advantages of nickel sulfamate over other electrolyte solutions like nickel sulphate are its capability for high current plating and low stress plating processes. This product is comprised of nickel (85~95g/L), nickel chloride (8~12g/L) and boric acid (25~35g/L). Nickel carbonate or sulphamic acid can independently be used to increase or decrease the pH value of electrolyte solution, respectively.

5.5 Experimental Details for Production of a Metallic Nanostructure

The fabricated nanostructures using colloidal spheres as micro-lenses are to be used as the template for the electroforming process. As discussed in Chapter 3, these ordered arrays of nanoholes are generated through a facile and cost-effective method. First, a standard 4 inch silicon wafer was cut into small pieces of 1.5 cm by 1.5 cm, followed by a cleaning process. The cleaned silicon substrate was then coated with a thin layer of AZ 5214-E photoresist. Next, a soft bake was applied to the resist coated substrate. The surface of the prepared sample was chemically treated as mentioned in Chapter 3, to make it more hydrophilic. MSL and BSL techniques were then used to obtain a single and a double layer of colloidal spheres, respectively. The

sample was then exposed by UV light, followed by removal of colloidal spheres using an ultrasonication bath. After a developing and cleaning process, ordered arrays of nanoholes were obtained over the entire surface of the photoresist coated substrate. This sample was then coated with a thin film of gold as a conductive layer. A gold sputtering system was used to get a 30 nm gold film. The sputtering process was run in three steps to ensure that all areas of the sample including the side-walls of the nanoholes were covered by a conductive film.

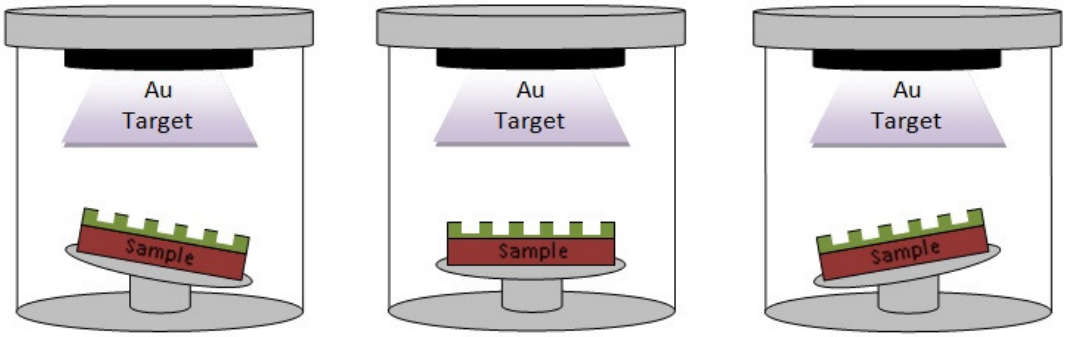

Figure 5-5 A schematic diagram illustrates the three steps for gold sputtering process.

Sputtering was first applied when the sample was placed inside a vacuum chamber at a parallel position in respect to a target gold source. The sample was then placed inside the chamber with 15º tilting angle in respect to the target gold source, once to the left and once to the right as is schematically illustrated in **Figure 5-5**. After the gold coating step, the sample was immersed into the electrolyte bath while it was attached to the cathode arm. Operating parameters, like pH and temperature of the electrolyte and current density are directly influential to the quality of electroformed patterns. All these parameters are tuneable and they have been controlled in the course of the electroforming process. In these experiments, the nickel electrolyte was

agitated using a magnetic stirrer while it was heated on the hotplate for 30 minutes prior to the electrodeposition process. The temperature and the pH value were maintained at 50 °C and 4.5±0.1 for the duration of experiment, respectively. The measurement was performed using a pH meter (type HI98127) which was purchased from Hanna Instruments. Nickel electrodeposition was conducted to fill in the nanoholes structure using a current density of 10 mA/cm^2. The height of the electroformed structure can be found according to the equation in Section 5.2.2.

After finishing the nickel electroforming process, the sample was brought out from the electrolyte bath. Next, the sample was rinsed with copious amounts of deionised water and this was followed by drying using a thermal blow dryer. The electroformed structure was then released from the resist coated substrate through a demoulding process. For the demoulding process of AZ 5214-E resist, there are several effective methods, such as using AZ stripper, oxygen plasma, acetone solution and piranha solution that can be applied, depending on the underlying layer [132]. In this research, acetone solution was chosen as a stripper for the demoulding process. The sample was soaked in the acetone solution for about 10 minutes to get rid of the AZ 5214-E resist. Next, a gold etchant (nickel compatible) purchased from Sigma Aldrich, was used to remove the thin conductive layer from the electroformed structure. Finally, the resultant metallic nanostructure was cleaned in deionised water.

5.6 **Challenges of Nickel Electroforming at Nanoscale**

In the course of electroforming at nanoscale, there are several common problems that normally occur. These problems, which are generally known as structural defects, are studied here in two categories. The first category investigates the structural defect related to the template, while the second category investigates the structural defect related to the electroformed structure. In this study, these defects are firstly introduced as the main challenges of this research and subsequently their proper solutions are presented in the following subsections.

5.6.1 Defects in the Master Nanotemplate

The first challenge was the weak photoresist adhesion to the silicon substrate. The experimental work shows that the resist film was stuck to the substrate for only 30 minutes after being placed in the electrolyte bath and it gradually started to swell. Although the cleaning process had been applied prior to the resist coating process to promote the adhesion ability of the resist, the weak bonding between the resist and the substrate had been observed throughout the electroforming process. It is worth noting that an alternative chemical treatment was also applied to improve the adhesion problem using nitric acid, but the same result has been detected in the course of electroforming. Apart from substrate treatment which has been reported as an effective way to prevent resist adhesion problems, resist hard baking is another method for promoting resist bonding to substrate [133]. As mentioned earlier in chapter 3, the prepared sample had been subjected to a hard baking at 110º for 2

minutes. The investigations began with increasing the hard baking time in the photoresist processing. Different baking conditions were applied to the samples and the electroforming experiments were then carried out to inspect the results. Surprisingly, no improvement occurred. Since the obtained results were in contrast with the proposed techniques, the author looked to the other stages of fabrication for the cause of this problem. Removal of colloidal spheres using ultrasonication was found as the only reason for this adhesion problem. The sample was placed in a glass beaker of deionised water inside an ultrasonic system to get rid of any colloidal particles. Since this step is run ahead of the hard baking step, it is observed that the thin film of AZ 5214-E is released from the substrate shortly after placing in the electrolyte bath. **Figure 5-6** illustrates the digital images of two samples where both are damaged in the electroforming process. One of the images shows that some part of the resist layer along with the gold film are removed from the substrate, while the other one shows the imperfect electroformed structure next to its substrate.

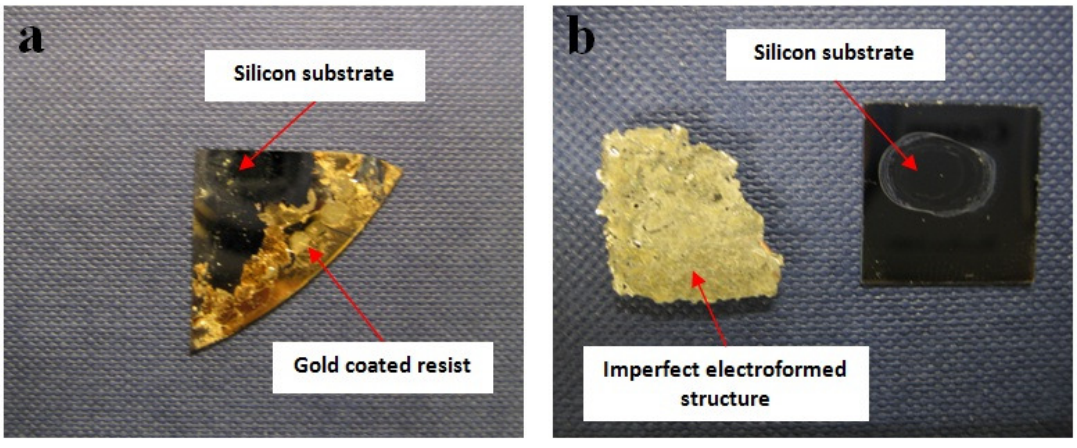

Figure 5-6 Digital images show two imperfect samples: a) some areas of gold coated resist are swollen and other areas are removed, b) right corner of the electroformed structure is totally missing.

To overcome this challenge, a transparent adhesive tape was used as an alternative approach. Therefore instead of using an ultrasonication system for removing PS spheres, Scotch tape did the same job without affecting the adhesion of the resist. It should be mentioned that to achieve a clean resist surface without the existence of PS spheres, at least three attempts are required for sticking and peeling off the tape. It should be also considered that the Scotch tape should not cover the entire surface of the sample in the course of this action, since this may cause some damage to the resist film. Using Scotch tape confirmed that the resist film can be securely stuck to the substrate for the entire period of the electroforming process.

5.6.2 Defects in the Electroformed Nanostructure

Apart from the photoresist swelling challenge, which has been successfully solved, there were other challenges which prevented the production of a good electroformed structure. As is shown in **Figure 5-7**, several defects are visible in the nickel nanostructure at first glance. The observations indicate the existence of nanopatterns only in some areas of the electroformed structure. The reason for this issue was found in the wettability of the sample. Although the surface of AZ 5214-E photoresist is covered by a thin layer of gold, it should be noticed that the surface of the sample is still considered as a hydrophobic surface. Hence, it is demanding for the nickel electrolyte to penetrate through the nanoholes' arrays of the sample. On the other hand, some random gas bumping (gas bubbles adhering to the sample surface) areas are formed on the cathode surface and cause the appearance of empty spaces on the electroformed structure as shown in **Figure 5-7**.

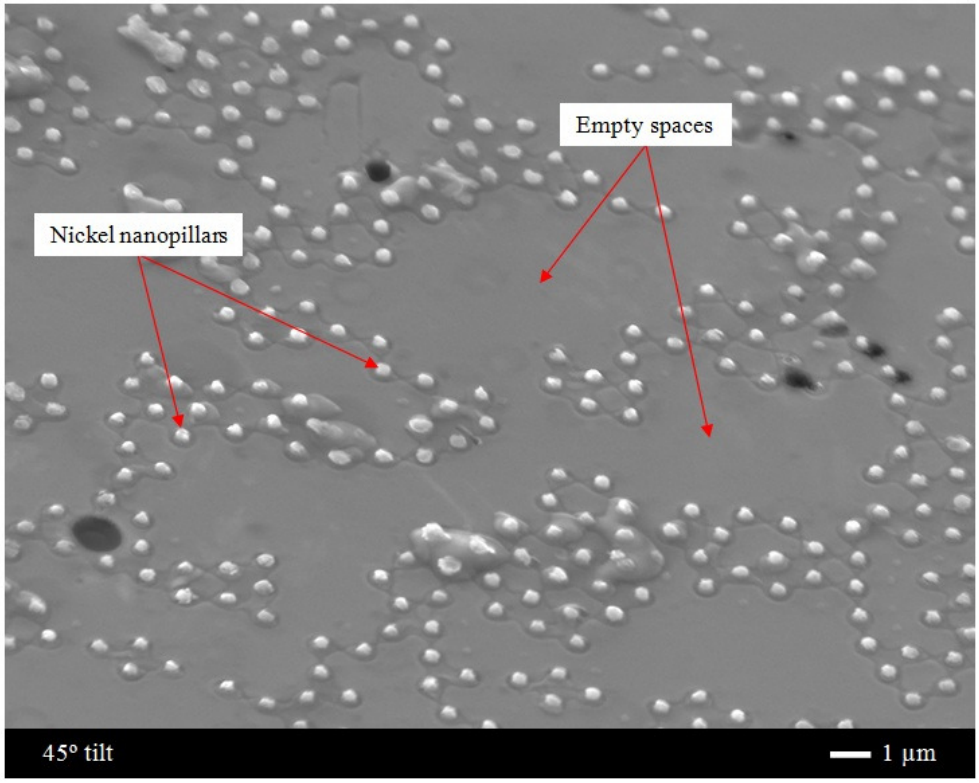

Figure 5-7 SEM image shows an imperfect nickel electroformed nanostructure.

The most common method to solve this problem and get rid of gas bumping is the use of a stirrer at high speed in the course of electroforming. However this method is only applicable for those processes which are conducted at microscale. The other recommended method is the use of a wetting agent to reduce the surface tension of the electrolyte solution. The most common wetting agent for the electroforming process is sodium dodecyl sulphate (SDS) which is an anionic surfactant [134]. **Figure 5-8** illustrates how a little concentration of SDS wetting agent significantly lowers the surface tension of the nickel electrolyte.

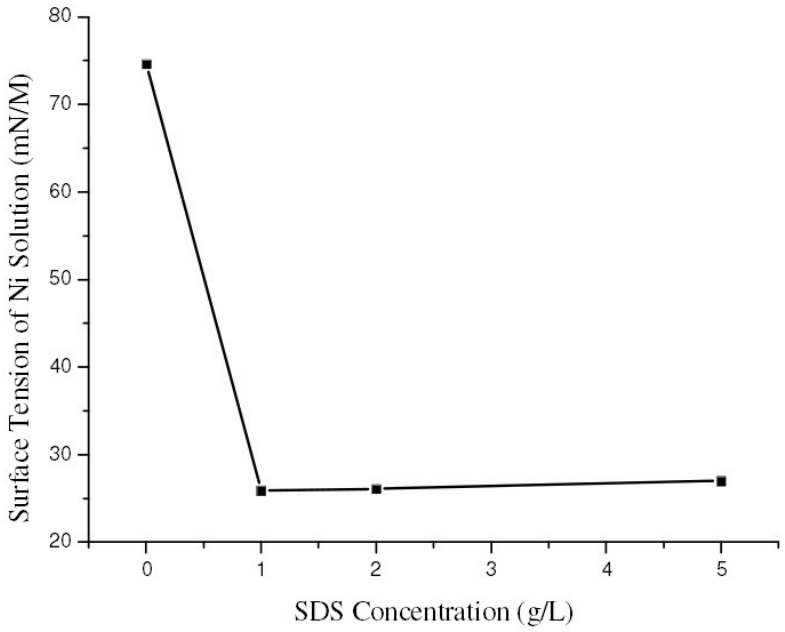

Figure 5-8 Changes of the surface tension of the nickel electrolyte by increasing SDS amount [135].

As is observed from the above figure, a small amount of SDS in the nickel solution can improve the wettability of the nickel electrolyte by decreasing its surface tension. Consequently, the surface of the nanotemplate can be wetted much easier when it is placed in the electrolyte bath containing SDS. This effect can be confirmed by comparing the contact angle measurements for two different droplets of the nickel electrolyte, one containing wetting agent and one without wetting agent. For this experiment, the contact angle of a nickel solution with SDS concentration of 1g/L was compared with a wetter-free nickel solution. The results showed that the contact angle decreased from 65º to 32º when the specified amount of SDS surfactant was added to the nickel electrolyte, as displayed in **Figure 5-9**.

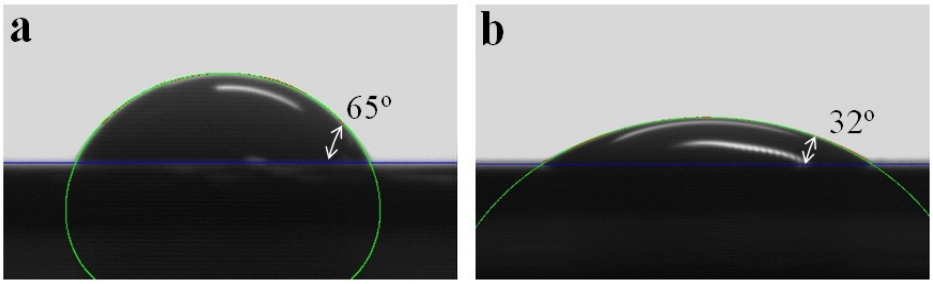

Figure 5-9 The contact angle measurements for different sets: a) wetter-free nickel solution, b) nickel solution containing SDS.

Figure 5-10 illustrates the nickel electroformed nanostructure using nickel electrolyte containing the SDS wetting agent. As it is shown in this figure, the ordered arrays of nickel nanopillars are evenly formed on the entire surface of the electroformed structure. No evidence of empty spaces is observed among the nanopillars due to the usage of the SDS surfactant.

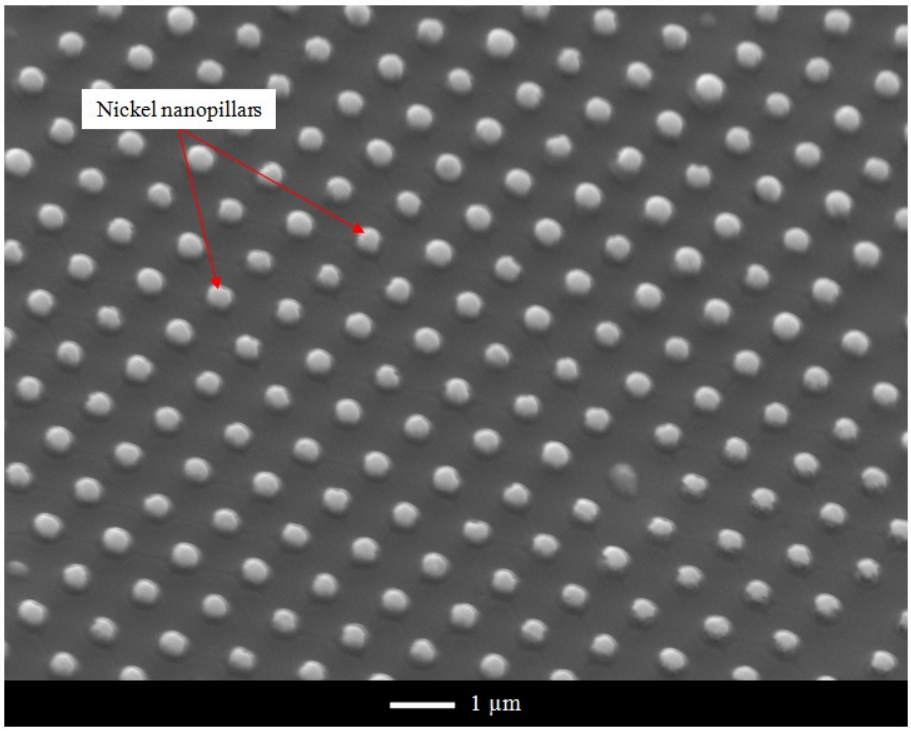

Figure 5-10 SEM image of a nickel electroformed structure using SDS surfactant in its process. The diameter of achieved nickel nanopillars is 390±5 nm which is in agreement with the size of nanoholes structure used as the master template.

5.7 **Experimental Results and Discussion**

Figure 5-11 shows the tilted SEM image of the uniform arrays of nickel nanopatterns over a relatively large area. This particular electroformed nanostructure was created using a current density of 10 mA/cm^2 in a nickel bath with a temperature and pH value of 50º and 4.5, respectively. The information on the ingredients of the nickel electrolyte bath, which had been used for this production, is presented in **Table 5-2**. It can be clearly seen in the inset of this figure that the average height of the obtained nanopillars is 100±5 nm.

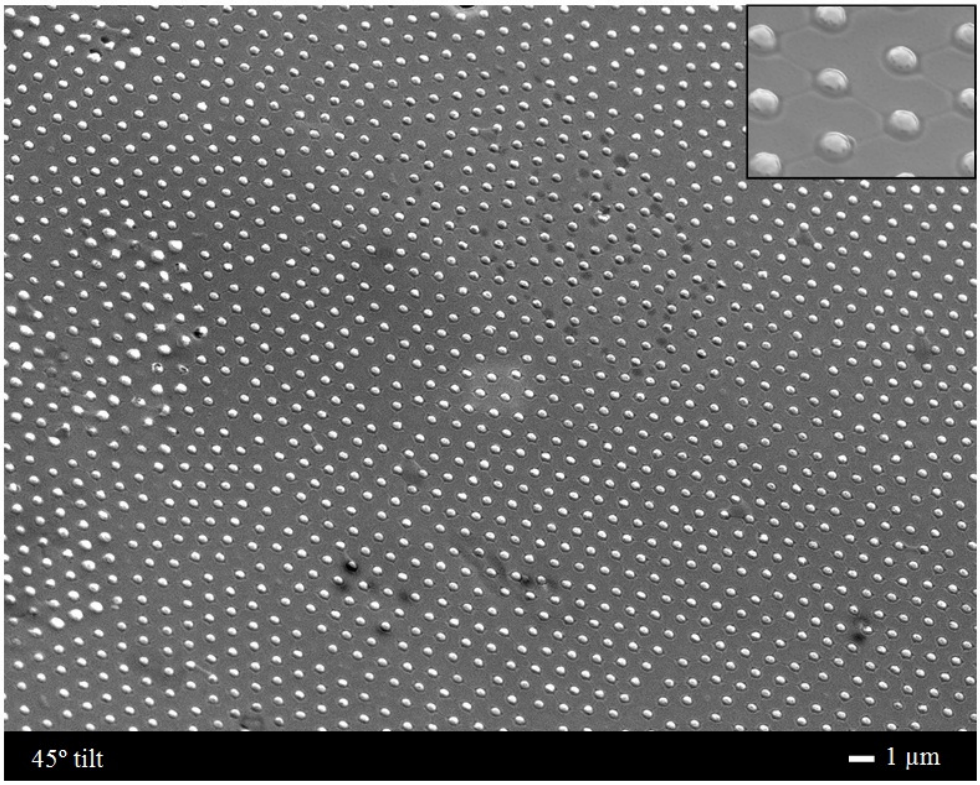

Figure 5-11 Tilted SEM image shows uniform arrays of nickel nanopillars with 100±5 nm height.

Table 5-2 The information on ingredients of the nickel electrolyte bath used in the electroforming process.

Symbol	Name	Value
$Ni(NH_2SO_3)_2$	Nickel Sulfamate	380-425 g/L
$NiCl_2$	Nickel Chloride	8-12 g/L
H_3BO_3	Boric Acid	25-35 g/L
$NaC_{12}H_{25}SO_4$	Sodium Dodecyl Sulphate	~1 g/L

Figure 5-12 and **Figure 5-13** show the FIB characterisation results for both nanostructures which had been fabricated using the single and double layer colloidal lithography methods, respectively. An FEI dual beam FIB (Strata DB235) was used for these experiments. The milling process was conducted using an FIB acceleration voltage of 30 kV and ion current of 30 pA. It is worth noting that the usage of lower ion current did not provide a good focusing on the samples due to the low energy of ions, and the usage of higher ion current caused the development of a re-deposition effect on the samples. An area of 2 µm by 3 µm was milled from the samples in 70 seconds.

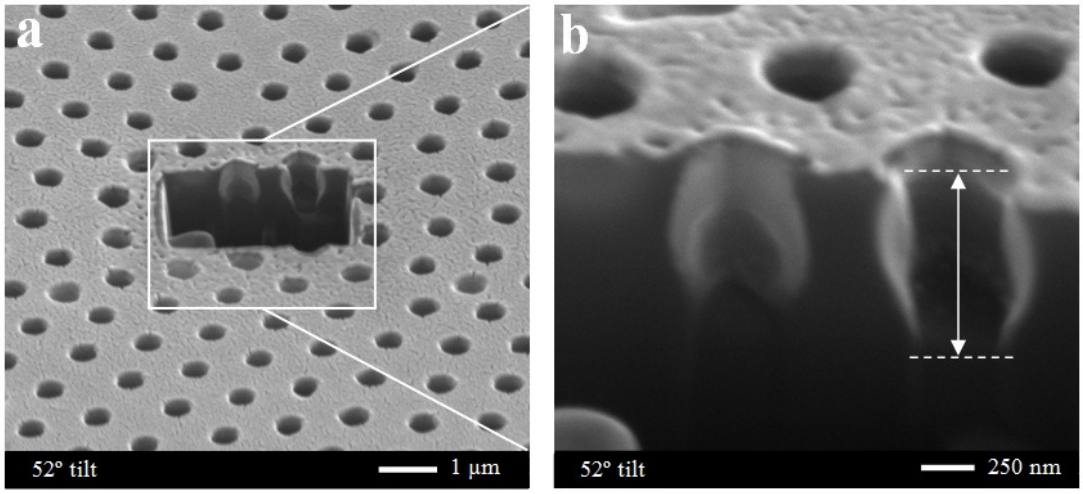

Figure 5-12 SEM images show milled arrays of nanoholes created by MCL method.

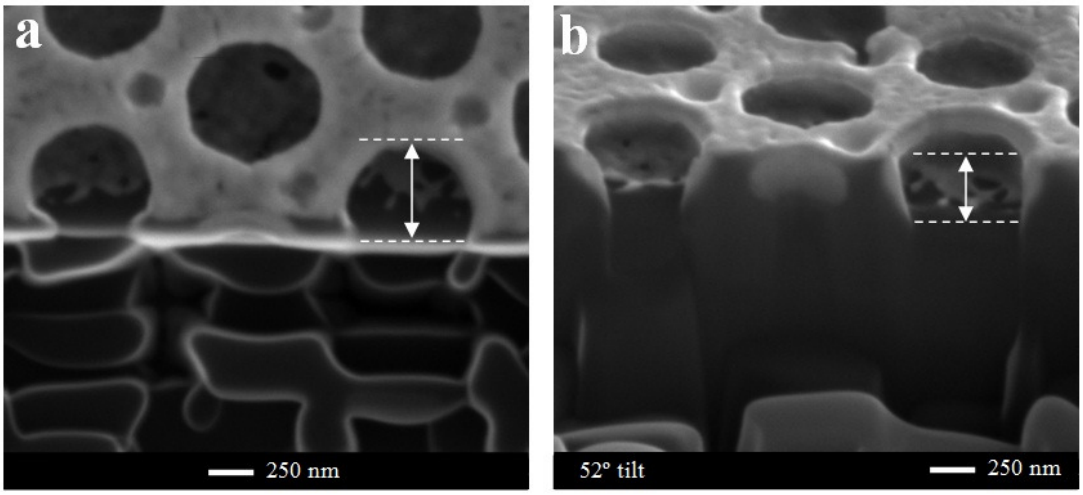

Figure 5-13 SEM images illustrate milled arrays of dual nanoholes created by BCL method.

A thin film of platinum was used as a protective layer to support the soft surfaces of the resist coated samples and reduce the re-deposition effect in the course of the FIB milling process. The depth of nanopatterns can be estimated using the FIB milling results. Random areas were examined on several samples for this investigation. **Figure 5-14** illustrates the resultant measurements of the nanoholes' depth. In this figure, the samples with single arrays of nanoholes are distinguished from the samples with dual arrays of nanoholes using different coloured symbols. The small and big blue squares represent the depth of the small and big nanoholes in the dual patterned structure, while the red triangle indicates the depth of nanoholes for the single patterned structure. As it can be seen in this figure, the average depth of nanoholes produced by the MCL method is 820±10 nm, while the average depth of nanoholes produced by the BCL method is 60±3 nm and 350±5 nm for the small and big nanoholes, respectively.

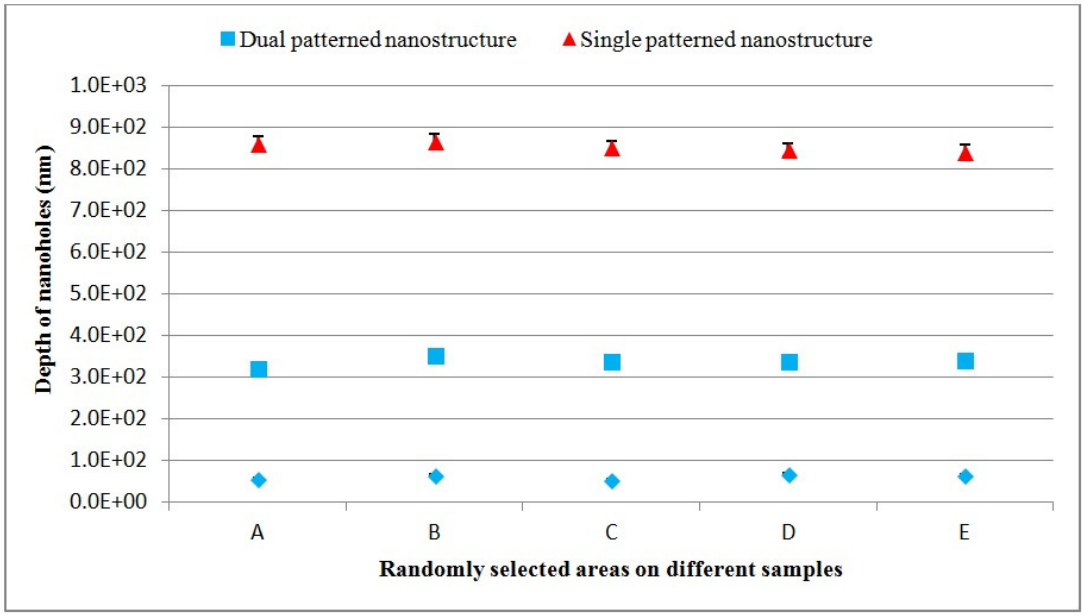

Figure 5-14 Comparison of the obtained height between single and dual patterned nanostructure.

As discussed earlier in this chapter, **Figure 5-11** displayed a nickel nanopillars structure which was fabricated through an electroforming process over a template with single arrays of nanoholes structure. The comparison between the height of nickel nanopillars and the depth of nanoholes shows a massive difference. The height of the nickel nanopillars is about one-eighth of the nanoholes' depth. The reason for this issue was found in the wettability of the nanoholes. Although SDS surfactant was used to decrease the surface tension of the nickel electrolyte and provide better conditions for the solution to wet the nanotemplate surface, it is difficult to completely fill the fine nanoholes with nickel solution due to the presence of the trapped air at the bottom of them. On the other hand, the higher the aspect-ratio of the nanopatterns, the lower the chance of electrolyte penetration. Since the depth of nanoholes created by the MCL technique is higher than the depth of nanoholes fabricated by the BCL method, it was necessary to use other elements to

get rid of the trapped air. The use of a vacuum was found as the proper solution. Hence, the desired nanotemplate was first immersed in the electrolyte bath followed by placing it in the vacuum chamber. The sample was then held inside the vacuum for about 30 minutes to ensure that all the fine nanoholes were filled by the nickel solution. Also, all residual bubbles were removed from the nanoholes using the vacuum. **Figure 5-15** and **Figure 5-16** illustrate the resultant nickel nanostructures. Highly ordered arrays of single and double patterned nanopillars were successfully produced using the nickel nano-electroforming process. As can be seen in **Figure 5-15**, the nanopillars are smoothly electroformed which indicates the quality of the initial nanotemplate.

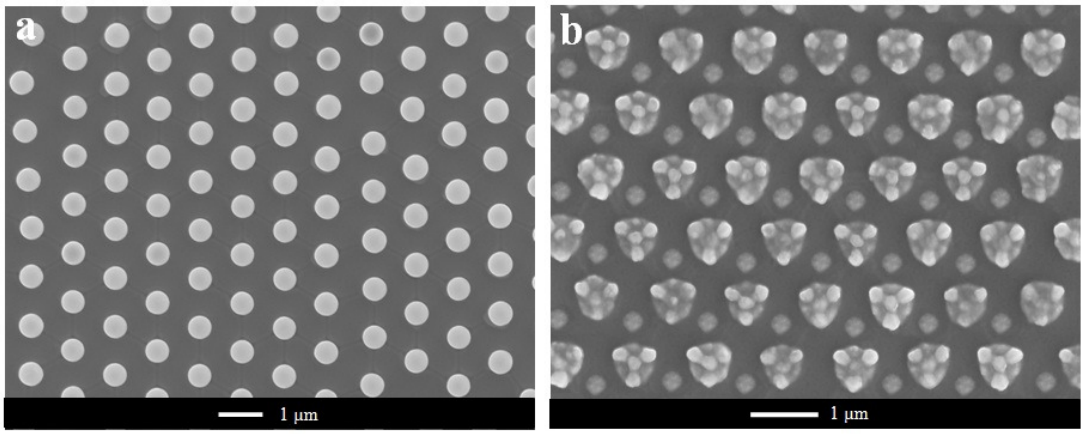

Figure 5-15 SEM images show the nickel nanopillars fabricated by electroforming process: a) single patterned metallic nanostructure, b) double patterned metallic nanostructure.

The top view SEM images show that the nickel nanopillars inherited the exact features of the photoresist surface. This issue can be clearly observed from **Figure 5-15b** in which bigger nanopatterns comprise several finer features on their surfaces. This confirms that the electroformed structures resemble the photoresist nanotemplate. Hence, nickel electroforming can be used as an effective tool to create

metallic nanostructures with high precision. The tilted SEM image of a single patterned nanostructure is demonstrated in **Figure 5-16**. It can be seen that the height of the nanopillars is greatly increased. The experimental results confirmed that a vacuum process can easily assist to improve the electroforming performance at the nanoscale level. Ordered arrays of metallic nanopillars with an average height of 815 nm were successfully fabricated using this technique. The achieved results of the electroformed structures are in a good agreement with the FIB characterisation results which were presented earlier in this chapter. The fabricated metallic nanostructures can be used as a nano-stamp for imprinting lithography.

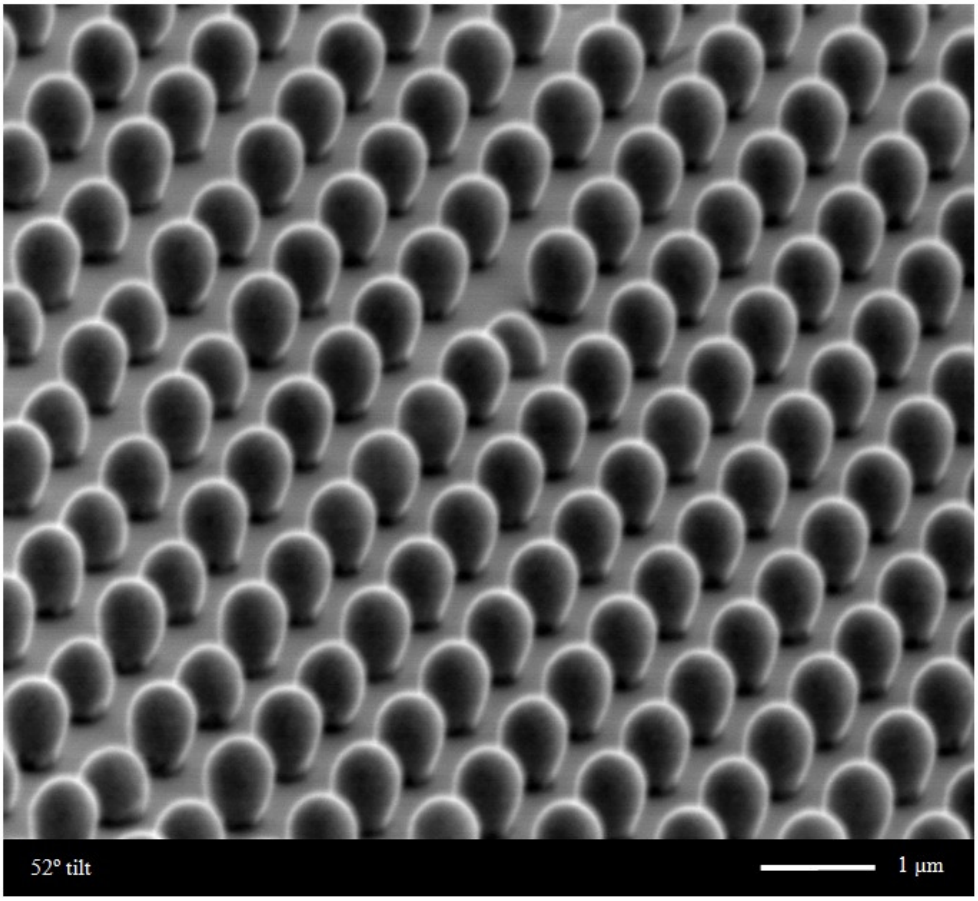

Figure 5-16 Tilted SEM image of a nickel nanostructure with periodic nanopillars arrays.

5.8 **Summary**

In this chapter, a nickel electroforming process was used for the production of ordered arrays of metallic nanostructures. A brief introduction was provided to explain the mechanism of electrodeposition. Next, a general overview of the fabrication process was introduced and the electroforming setup was illustrated. It was found that the operating conditions would directly influence the quality of the electroformed nanostructures. Several structural defects were identified as the challenges for the electroforming process at nanoscale. Different approaches were applied to overcome these defects followed by presenting the proper solution for each challenge. FIB milling was conducted to measure the dimension of the nanopatterns which were placed on the template. The characterisation results were subsequently used to justify the dimension of the obtained metallic nanostructures.

The resultant metallic nanopillars confirm that the process is able to mirror the profile of photoresist patterns even for very fine features. The proposed method provides a versatile way for creating metallic nanostructures with high dimensional accuracy. Uniform arrays of single and double patterned metallic nanostructures have been successfully fabricated using a simple and convenient technique without the need for expensive tools.

CHAPTER 6: CONCLUSIONS AND FUTURE WORK

6.1 Conclusions

The aim of this PhD project is to investigate the potential of colloidal lithography and explore its application for the creation of highly accurate periodic nanostructures. The project is furthermore aimed to achieve high-throughput and novel nanostructures by developing facile and precise fabrication approaches suitable for mass production. The current research intends to produce ordered arrays of nanopatterns on surfaces of photoresist and PDMS. The research has involved modelling and simulation to study the behaviour of electromagnetic waves for both monolayer and bilayer submicron spheres; fabrication of single and dual patterned nanostructures using polystyrene spheres as micro-lenses; preparation of PDMS soft moulds using self assembled colloidal spheres as a template; structural characterisation of PDMS soft moulds using SEM stereoscopic and FIB milling techniques; fabrication of 2D and 3D periodic nanostructures through PDMS/PDMS replication and monolayer reassembly processes, and finally patterning of ordered arrays of metallic nanopillars using an electroforming process.

The significant contributions of the research presented in this thesis in modified colloidal lithography as a versatile tool for fabrication of multi-material nanostructures can be summarised as follows:

A. Proposed a novel bilayer sphere fabrication method for creating uniform arrays of dual nanopatterns on photoresist surface

A bilayer of closely packed microspheres has been self assembled on a thin layer of AZ 5214-E resist for the fabrication of uniform arrays of nanoholes. Two sets of well ordered nanoholes with different sizes have been successfully created on the AZ 5214-E resist after exposing the sample by UV light. This is the first report of creating the arrays of binary nanopatterns through one colloidal lithography process.

B. Characterisation of PDMS soft mould using SEM stereoscopic and FIB milling techniques

Both an SEM stereoscopic technique and a FIB milling method have been used to characterise the morphology of PDMS soft moulds. The surface of a PDMS microbowl structure has been successfully reconstructed through the SEM stereoscopic technique and the geometrical analysis has been conducted using Alicona Imaging software. The measurement results have been validated with FIB milling characterization results.

C. Developed a PDMS/PDMS replication process for producing 2D periodic structure at nanoscale

A nanofabrication method has been presented for producing hybrid nanostructured arrays based on a novel PDMS/PDMS replication approach. A nanopatterned PDMS replica has been successfully constructed through a direct casting of PDMS slurry onto a surface treated nanopatterned PDMS template. Both the surfaces of the nanopatterned PDMS template and the nanopatterned PDMS replica remained undamaged after the demoulding process and can be employed for further fabrication processes.

D. Proposed a novel patterning technique for fabrication of 3D nanostructures with ordered arrays

A novel nanopatterning technique has been introduced on the basis of monolayer self assembly of PS spheres, PDMS nano-replication, reassembly of monolayer PS spheres and metal coating. Triangular gold nanopatterns have been successfully created over uniformly distributed pillars of a PDMS template.

E. Developed electroforming process for manufacturing uniform arrays of metallic nanopatterns

Metallic nanostructures have been produced using a nickel electroforming process. Uniform arrays of single and double patterned metallic nanopillars have been successfully fabricated using the aforementioned nanostructures as master templates.

All the project objectives have been achieved through systematic research in the project involving repeated nanofabrication processes, simulation and characterisation. The following conclusions can be drawn from this research.

1. It has been observed from the computer simulation that polystyrene microspheres can act as near field micro-lenses due to their appropriate values of optical index. It has been realised that the FWHM of the hot spot at the bottom of microspheres tends to be bigger as the wavelengths get bigger.

2. It has been proven that AZ 5214-E resist is a suitable choice to satisfy the fabrication requirements in terms of good assembly of PS spheres as the initial step of MCL and BCL techniques.

3. The proposed BCL method has been successfully developed for producing two sets of nanopatterns in one CL process. It has been found that the sizes of the resulting nanopatterns, created by either the MCL method or BCL method, are precisely adjustable by using different exposure doses.

4. The proposed BCL technique has been successfully extended for the production of other types of periodic nanostructure. Apart from fabricating uniform arrays of binary nanoholes using the BCL method, this method has revealed its potential for the manufacturing of triangular-shaped nanopillars.

5. A PDMS/PDMS replication process has been developed as an effective method for the production of periodic nanostructures. The surface wettability nature of a

PDMS template and the peeling off ability of PDMS pairs has been fully inspected. The experimental results confirmed that the contact angles of PDMS slurry were decreased from 31º to 8º and 12º when a gold film and platinum film were used as a releasing layer. It has been proven that the thickness of at least a 20 nm gold layer or a 40 nm platinum layer works best as the releasing film.

6. The usage of oxygen plasma for treating the surface of pre-patterned PDMS confirmed an extensive improvement on the hydrophobicity nature of the PDMS template and subsequently assisted reassembly process. Dimensions of PDMS nanopillars can be tuned by changing the spheres' size, while the thickness of gold nanopatterns can be adjusted by controlling the thickness of the metal deposition.

7. Nickel electroforming has been developed as a compatible and precise method for the production of metallic structures at nanoscale. The usages of SDS surfactant and a vacuum have been found as effective approaches to improve the quality of electroformed patterns at nanoscale. The resultant metallic nanopatterns confirmed that the proposed method is able to fabricate even small nano-features with high dimensional accuracy.

Based on the experimental and analysis works presented in this thesis, the proposed nanofabrication techniques using modified colloidal lithography prove to be repeatable, facile and effective. It is furthermore proven that high quality periodic nanostructures can be yielded through the proposed nanofabrication techniques without the need of either expensive or sophisticated patterning instruments.

Therefore, the research aims have been successfully reached. The methodology and analysis adopted in this project have led to the achievement of the project's aims. The proposed nanofabrication methods which have been studied through this research are qualified for those applications in which volume nanopatterning are required. In addition, this project opens up a new route for fabrication of periodic nanostructures with different materials. The presented approaches can be further extended to create other nanostructures, and thus have wider applications.

6.2 **Suggestions for Future Work**

This thesis represents some comprehensive research efforts to first modify the colloidal lithography method and next explore some alternative approaches for multi-material nanopatterning. As such, this research should be viewed as a solid foundation for further work. Future research is needed either to develop more applications or to complete works initiated in this PhD project but which were not completed because they are well beyond the project scope.

Here, the identified topics are listed as further research areas:

1. In this thesis, arrays of closely packed polystyrene spheres were fully studied as micro-lenses for production of uniform nanostructures using either monolayer or bilayer colloidal spheres. This work can be expanded for fabrication of order arrays of periodic nanostructures using ellipsoids in monolayer or bilayer

colloidal crystals. It is worth noting that several self assembly approaches have been recently developed to conveniently control the direction of ellipsoids.

2. Fabricated nanostructure using the MCL method can be used as the master template for the production of high aspect ratio PDMS nanopillars; as an effective and facile approach for creation a self cleaning film.

3. Since the proposed BCL method in this research is a new route for fabrication of arrays of binary nanopatterns, the introduced technique can be applied to other types of positive or negative tone resists. This method can be further developed by making the resist layer thinner and creating the binary nanopatterns on a surface of a glass slide to study its capability as a biological or optical device.

4. In the current research, platinum and gold have been used as a releasing film in the proposed PDMS/PDMS technique. The effects of different film thicknesses in both the surface wettability nature of the PDMS template and the peeling ability of PDMS pairs have been studied in detail. The approach presented in this project can be developed by using other metallic layers as a releasing film.

5. This thesis introduced a novel technique for patterning gold nanostructures on the top of a PDMS microbowl structure. The fabricated structure may attract the interest of researches for further investigation. The fabricated structure can be further modified and used as an alternative to those nanostructures in which ordered arrays of gold or silver nanoparticles are deposited on a glass slide and used to detect biological or chemical targets.

REFERENCES

[1] P. Buffat and J. P. Borel, "Size effect on the melting temperature of gold particles," *Physical Review A,* vol. 13, pp. 2287-2298, 1976.

[2] A. P. Alivisatos, A. L. Harris, N. J. Levinos, M. L. Steigerwald, and L. E. Brus, "Electronic states of semiconductor clusters: Homogeneous and inhomogeneous broadening of the optical spectrum," *The Journal of Chemical Physics,* vol. 89, pp. 4001-4011, 1988.

[3] J. C. Hulteen and R. P. Van Duyne, "Nanosphere lithography: A materials general fabrication process for periodic particle array surfaces," *Journal of Vacuum Science & Technology A: Vacuum, Surfaces, and Films,* vol. 13, pp. 1553-1558, 1995.

[4] N. Vogel, C. K. Weiss, and K. Landfester, "From soft to hard: the generation of functional and complex colloidal monolayers for nanolithography," *Soft Matter,* vol. 8, pp. 4044-4061, 2012.

[5] W. Moreau, *Semiconductor Lithography: Principles, Practices, and Materials (Microdevices)*: Plenum Press, 1989.

[6] M. Rothschild and D. J. Ehrlich, "Attainment of 0.13-μm lines and spaces by excimer-laser projection lithography in ``diamond-like" carbon-resist," *Journal of Vacuum Science & Technology B: Microelectronics and Nanometer Structures,* vol. 5, pp. 389-390, 1987.

[7] Y. N. Xia, J. A. Rogers, K. E. Paul, and G. M. Whitesides, "Unconventional methods for fabricating and patterning nanostructures," *Chemical Reviews,* vol. 99, pp. 1823-1848, Jul 1999.

[8] A. N. Broers, W. W. Molzen, J. J. Cuomo, and N. D. Wittels, "Electron-beam fabrication of 80-Å metal structures," *Applied Physics Letters,* vol. 29, pp. 596-598, 1976.

[9] R. L. Kubena, J. W. Ward, F. P. Stratton, R. J. Joyce, and G. M. Atkinson, "A low magnification focused ion beam system with 8 nm spot size," *Journal of Vacuum Science & Technology B: Microelectronics and Nanometer Structures,* vol. 9, pp. 3079-3083, 1991.

[10] F. Watt, A. A. Bettiol, J. A. Van Kan, E. J. Teo, and M. B. H. Breese, "Ion beam lithography and nanofabrication: A review," *International Journal of Nanoscience,* vol. 4, pp. 269-286, 2005.

[11] Y. K. Kim, A. J. Danner, J. J. Raftery, and K. D. Choquette, "Focused Ion Beam Nanopatterning for Optoelectronic Device Fabrication," *Selected Topics in Quantum Electronics, IEEE Journal of,* vol. 11, pp. 1292-1298, 2005.

[12] J. A. Rogers, K. E. Paul, R. J. Jackman, and G. M. Whitesides, "Using an elastomeric phase mask for sub-100 nm photolithography in the optical near field," *Applied Physics Letters,* vol. 70, pp. 2658-2660, 1997.

[13] Y. Xia and G. M. Whitesides, "Soft Lithography," *Angewandte Chemie International Edition,* vol. 37, pp. 550-575, 1998.

[14] S. J. Clarson and J. A. Semlyen, *Siloxane Polymers*: Prentice Hall, 1993.

[15] J. C. McDonald, D. C. Duffy, J. R. Anderson, D. T. Chiu, H. Wu, O. J. A. Schueller, and G. M. Whitesides, "Fabrication of microfluidic systems in poly(dimethylsiloxane)," *ELECTROPHORESIS,* vol. 21, pp. 27-40, 2000.

[16] Y. Zhang, C.-W. Lo, J. A. Taylor, and S. Yang, "Replica Molding of High-Aspect-Ratio Polymeric Nanopillar Arrays with High Fidelity," *Langmuir,* vol. 22, pp. 8595-8601, 2006/09/01 2006.

[17] J. Gu, X. Xiao, B. Takulapalli, M. Morrison, P. Zhang, and F. Zenhausern, "A new approach to fabricating high density nanoarrays by nanocontact printing," *Journal of Vacuum Science & Technology B: Microelectronics and Nanometer Structures,* vol. 26, pp. 1860-1865, 2008.

[18] W. F. Michael Köhler, *Nanotechnology: An Introduction to Nanostructuring Techniques*: John Wiley & Sons, 2005.

[19] Z. Li, Y. Gu, L. Wang, H. Ge, W. Wu, Q. Xia, C. Yuan, Y. Chen, B. Cui, and R. S. Williams, "Hybrid Nanoimprint−Soft Lithography with Sub-15 nm Resolution," *Nano Letters,* vol. 9, pp. 2306-2310, 2009/06/10 2009.

[20] R. S. Becker, J. A. Golovchenko, and B. S. Swartzentruber, "Atomic-scale surface modifications using a tunnelling microscope," *Nature,* vol. 325, pp. 419-421, 1987.

[21] A. T. S. Wee, *Selected Topics in Nanoscience and Nanotechnology*: World Scientific, 2009.

[22] H. T. Soh, K. W. Guarini, and C. F. Quate, *Scanning Probe Lithography*: Kluwer Academic Publishers, 2001.

[23] L. J. Guo, "Nanoimprint Lithography: Methods and Material Requirements," *Advanced Materials,* vol. 19, pp. 495-513, 2007.

[24] Y. D. Hongbo Lan, Hongzhong Liu, *Nanoimprint Lithography: Principles, Processes & Materials* Nova Science Publishers Inc, 2011.

[25] S. Y. Chou, P. R. Krauss, and P. J. Renstrom, "Imprint Lithography with 25-Nanometer Resolution," *Science,* vol. 272, pp. 85-87, April 5, 1996 1996.

[26] M. A. Wood, "Colloidal lithography and current fabrication techniques producing in-plane nanotopography for biological applications," *Journal of The Royal Society Interface,* vol. 4, pp. 1-17, February 22, 2007 2007.

[27] J. P. Wright, O. Worsfold, C. Whitehouse, and M. Himmelhaus, "Ultraflat Ternary Nanopatterns Fabricated Using Colloidal Lithography," *Advanced Materials,* vol. 18, pp. 421-426, 2006.

[28] X. Zhang, L. Zhang, M. Gao, W. Zhou, and S. Xie, "High-Resolution Nanosphere Lithography (NSL) to Fabricate Highly-Ordered ZnO Nanorod Arrays," *Journal of Nanoscience and Nanotechnology,* vol. 10, pp. 7432-7435, Nov 2010.

[29] H. W. Deckman and J. H. Dunsmuir, "Natural lithography," *Applied Physics Letters,* vol. 41, pp. 377-379, 1982.

[30] X. Wei, "Recent Developments in the Fabrication of Ordered Nanostructure Arrays Based on Nanosphere Lithography," *Recent Patents on Nanotechnology,* vol. 4, pp. 194-204, 2010.

[31] X. Chen, X. Wei, and K. Jiang, "Fabrication of large-area nickel nanobump arrays," *Microelectronic Engineering,* vol. 86, pp. 871-873, 2009.

[32] Y. Xia, B. Gates, Y. Yin, and Y. Lu, "Monodispersed Colloidal Spheres: Old Materials with New Applications," *Advanced Materials,* vol. 12, pp. 693-713, 2000.

[33] L. Huaqing, J. Low, K. S. Brown, and W. Nianqiang, "Large-Area Well-Ordered Nanodot Array Pattern Fabricated With Self-Assembled Nanosphere Template," *Sensors Journal, IEEE,* vol. 8, pp. 880-884, 2008.

[34] S. H. Park, D. Qin, and Y. Xia, "Crystallization of Mesoscale Particles over Large Areas," *Advanced Materials,* vol. 10, pp. 1028-1032, 1998.

[35] M. Kondo, K. Shinozaki, L. Bergstroem, and N. Mizutani, "Preparation of Colloidal Monolayers of Alkoxylated Silica Particles at the Air-Liquid Interface," *Langmuir,* vol. 11, pp. 394-397, 1995/02/01 1995.

[36] M. Retsch, Z. Zhou, S. Rivera, M. Kappl, X. S. Zhao, U. Jonas, and Q. Li, "Macromol. Chem. Phys. 3–4/2009," *Macromolecular Chemistry and Physics,* vol. 210, pp. n/a-n/a, 2009.

[37] W. Wang and B. Gu, "Self-Assembly of Two- and Three-Dimensional Particle Arrays by Manipulating the Hydrophobicity of Silica Nanospheres," *The Journal of Physical Chemistry B,* vol. 109, pp. 22175-22180, 2005/12/01 2005.

[38] N. Denkov, O. Velev, P. Kralchevski, I. Ivanov, H. Yoshimura, and K. Nagayama, "Mechanism of formation of two-dimensional crystals from latex particles on substrates," *Langmuir,* vol. 8, pp. 3183-3190, 1992/12/01 1992.

[39] R. Micheletto, H. Fukuda, and M. Ohtsu, "A Simple Method for the Production of a Two-Dimensional, Ordered Array of Small Latex Particles," *Langmuir,* vol. 11, pp. 3333-3336, 1995/09/01 1995.

[40] M. H. Kim, S. H. Im, and O. O. Park, "Rapid Fabrication of Two- and Three-Dimensional Colloidal Crystal Films via Confined Convective Assembly," *Advanced Functional Materials,* vol. 15, pp. 1329-1335, 2005.

[41] D. Wang and H. Möhwald, "Rapid Fabrication of Binary Colloidal Crystals by Stepwise Spin-Coating," *Advanced Materials,* vol. 16, pp. 244-247, 2004.

[42] P. Jiang and M. J. McFarland, "Large-Scale Fabrication of Wafer-Size Colloidal Crystals, Macroporous Polymers and Nanocomposites by Spin-Coating," *Journal of the American Chemical Society,* vol. 126, pp. 13778-13786, 2004/10/01 2004.

[43] Y. Xia, Y. Yin, Y. Lu, and J. McLellan, "Template-Assisted Self-Assembly of Spherical Colloids into Complex and Controllable Structures," *Advanced Functional Materials,* vol. 13, pp. 907-918, 2003.

[44] M. Trau, D. A. Saville, and I. A. Aksay, "Field-Induced Layering of Colloidal Crystals," *Science,* vol. 272, pp. 706-709, May 3, 1996 1996.

[45] R. C. Hayward, D. A. Saville, and I. A. Aksay, "Electrophoretic assembly of colloidal crystals with optically tunable micropatterns," *Nature,* vol. 404, pp. 56-59, 2000.

[46] S. O. Lumsdon, E. W. Kaler, and O. D. Velev, "Two-Dimensional Crystallization of Microspheres by a Coplanar AC Electric Field," *Langmuir,* vol. 20, pp. 2108-2116, 2004/03/01 2004.

[47] C. Won Mook and O. O. Park, "The fabrication of micropatterns of a 2D colloidal assembly by electrophoretic deposition," *Nanotechnology,* vol. 17, p. 325, 2006.

[48] P. A. Kralchevsky and K. Nagayama, "Capillary forces between colloidal particles," *Langmuir,* vol. 10, pp. 23-36, 1994/01/01 1994.

[49] V. N. Paunov, P. A. Kralchevsky, N. D. Denkov, and K. Nagayama, "Lateral Capillary Forces between Floating Submillimeter Particles," *Journal of Colloid and Interface Science,* vol. 157, pp. 100-112, 1993.

[50] P. A. Kralchevsky and K. Nagayama, "Capillary interactions between particles bound to interfaces, liquid films and biomembranes," *Advances in Colloid and Interface Science,* vol. 85, pp. 145-192, 2000.

[51] C. L. Haynes and R. P. Van Duyne, "Nanosphere Lithography: A Versatile Nanofabrication Tool for Studies of Size-Dependent Nanoparticle Optics," *The Journal of Physical Chemistry B,* vol. 105, pp. 5599-5611, 2001/06/01 2001.

[52] A. Kosiorek, W. Kandulski, H. Glaczynska, and M. Giersig, "Fabrication of Nanoscale Rings, Dots, and Rods by Combining Shadow Nanosphere Lithography and Annealed Polystyrene Nanosphere Masks," *Small,* vol. 1, pp. 439-444, 2005.

[53] X. Zhang, E. M. Hicks, J. Zhao, G. C. Schatz, and R. P. Van Duyne, "Electrochemical Tuning of Silver Nanoparticles Fabricated by Nanosphere Lithography," *Nano Letters,* vol. 5, pp. 1503-1507, 2005/07/01 2005.

[54] C. L. Haynes, A. D. McFarland, M. T. Smith, J. C. Hulteen, and R. P. Van Duyne, "Angle-Resolved Nanosphere Lithography: Manipulation of Nanoparticle Size, Shape, and Interparticle Spacing," *The Journal of Physical Chemistry B,* vol. 106, pp. 1898-1902, 2002/02/01 2002.

[55] A. Kosiorek, W. Kandulski, P. Chudzinski, K. Kempa, and M. Giersig, "Shadow Nanosphere Lithography: Simulation and Experiment," *Nano Letters,* vol. 4, pp. 1359-1363, 2004/07/01 2004.

[56] A. V. Whitney, B. D. Myers, and R. P. Van Duyne, "Sub-100 nm Triangular Nanopores Fabricated with the Reactive Ion Etching Variant of Nanosphere Lithography and Angle-Resolved Nanosphere Lithography," *Nano Letters,* vol. 4, pp. 1507-1511, 2004/08/01 2004.

[57] N. H. Finkel, B. G. Prevo, O. D. Velev, and L. He, "Ordered Silicon Nanocavity Arrays in Surface-Assisted Desorption/Ionization Mass Spectrometry," *Analytical Chemistry,* vol. 77, pp. 1088-1095, 2005/02/01 2005.

[58] C. L. Cheung, R. J. Nikolic, C. E. Reinhardt, and T. F. Wang, "Fabrication of nanopillars by nanosphere lithography," *Nanotechnology,* vol. 17, pp. 1339-43, 2006.

[59] G. H. Jeong, J. K. Park, K. K. Lee, J. H. Jang, C. H. Lee, H. B. Kang, C. W. Yang, and S. J. Suh, "Fabrication of low-cost mold and nanoimprint lithography using polystyrene nanosphere," *Microelectronic Engineering,* vol. 87, pp. 51-55, 2010.

[60] C.-W. Kuo, J.-Y. Shiu, Y.-H. Cho, and P. Chen, "Fabrication of large-area periodic nanopillar arrays for nanoimprint lithography using polymer colloid masks," *Advanced Materials,* vol. 15, pp. 1065-1068, 2003.

[61] C. X. Cong, T. Yu, Z. H. Ni, L. Liu, Z. X. Shen, and W. Huang, "Fabrication of Graphene Nanodisk Arrays Using Nanosphere Lithography," *The Journal of Physical Chemistry C,* vol. 113, pp. 6529-6532, 2009/04/23 2009.

[62] X. Chen, X. Wei, and K. Jiang, "The fabrication of high-aspect-ratio, size-tunable nanopore arrays by modified nanosphere lithography," *Nanotechnology,* vol. 20, p. 425605, 2009.

[63] D.-G. Choi, S. G. Jang, H. K. Yu, and S.-M. Yang, "Two-Dimensional Polymer Nanopattern by Using Particle-Assisted Soft Lithography," *Chemistry of Materials,* vol. 16, pp. 3410-3413, 2004/09/01 2004.

[64] Z. M. Chen, T. Gang, X. Yan, X. Li, J. H. Zhang, Y. F. Wang, X. Chen, Z. Q. Sun, K. Zhang, B. Zhao, and B. Yang, "Ordered Silica Microspheres Unsymmetrically Coated with Ag Nanoparticles, and Ag-Nanoparticle-Doped Polymer Voids Fabricated by Microcontact Printing and Chemical Reduction," *Advanced Materials,* vol. 18, pp. 924-929, 2006.

[65] Z.-X. Lu, A. Namboodiri, and M. M. Collinson, "Self-Supporting Nanopore Membranes with Controlled Pore Size and Shape," *ACS Nano,* vol. 2, pp. 993-999, 2008/05/01 2008.

[66] H. Asoh, S. Sakamoto, and S. Ono, "Metal patterning on silicon surface by site-selective electroless deposition through colloidal crystal templating," *Journal of Colloid and Interface Science,* vol. 316, pp. 547-552, 2007.

[67] X. Chen, X. Wei, and K. Jiang, "Large-scale fabrication of ordered metallic hybrid nanostructures," *Optics Express,* vol. 16, pp. 11888-11893, Aug 4 2008.

[68] M. A. Ghanem, P. N. Bartlett, P. de Groot, and A. Zhukov, "A double templated electrodeposition method for the fabrication of arrays of metal nanodots," *Electrochemistry Communications,* vol. 6, pp. 447-453, 2004.

[69] H. J. Nam, D.-Y. Jung, G.-R. Yi, and H. Choi, "Close-Packed Hemispherical Microlens Array from Two-Dimensional Ordered Polymeric Microspheres," *Langmuir,* vol. 22, pp. 7358-7363, 2006/08/01 2006.

[70] Z. Ren, X. Li, J. Zhang, W. Li, X. Zhang, and B. Yang, "Tunable Two-Dimensional Non-Close-Packed Microwell Arrays Using Colloidal Crystals as Templates," *Langmuir,* vol. 23, pp. 8272-8276, 2007/07/01 2007.

[71] M. A. S. Chong, Y. B. Zheng, H. Gao, and L. K. Tan, "Combinational template-assisted fabrication of hierarchically ordered nanowire arrays on substrates for device applications," *Applied Physics Letters,* vol. 89, pp. 233104-3, 2006.

[72] W. Wu, D. Dey, O. G. Memis, A. Katsnelson, and H. Mohseni, "A novel lithography technique for formation of large areas of uniform nanostructures," in *Nanoengineering: Fabrication, Properties, Optics, and Devices V.* vol. 7039, E. A. Dobisz and L. A. Eldada, Eds., ed, 2008.

[73] W. Wu, A. Katsnelson, O. G. Memis, and H. Mohseni, "A deep sub-wavelength process for the formation of highly uniform arrays of nanoholes and nanopillars," *Nanotechnology,* vol. 18, Dec 5 2007.

[74] C. H. Chang, L. Tian, W. R. Hesse, H. Gao, H. J. Choi, J. G. Kim, M. Siddiqui, and G. Barbastathis, "From Two-Dimensional Colloidal Self-Assembly to Three-Dimensional Nanolithography," *Nano Letters,* vol. 11, pp. 2533-2537, 2011/06/08 2011.

[75] D.-G. Choi, S. Kim, E. Lee, and S.-M. Yang, "Particle Arrays with Patterned Pores by Nanomachining with Colloidal Masks," *Journal of the American Chemical Society,* vol. 127, pp. 1636-1637, 2005/02/01 2005.

[76] D. G. Choi, S. G. Jang, S. Kim, E. Lee, C. S. Han, and S. M. Yang, "Multifaceted and Nanobored Particle Arrays Sculpted Using Colloidal Lithography," *Advanced Functional Materials,* vol. 16, pp. 33-40, 2006.

[77] E. Hutter and J. H. Fendler, "Exploitation of Localized Surface Plasmon Resonance," *Advanced Materials,* vol. 16, pp. 1685-1706, 2004.

[78] A. J. Haes and R. P. Van Duyne, "A unified view of propagating and localized surface plasmon resonance biosensors," *Analytical and Bioanalytical Chemistry,* vol. 379, pp. 920-930, 2004.

[79] P. Mulvaney, "Surface Plasmon Spectroscopy of Nanosized Metal Particles," *Langmuir,* vol. 12, pp. 788-800, 1996/01/01 1996.

[80] C. L. Haynes, A. D. McFarland, L. Zhao, R. P. Van Duyne, G. C. Schatz, L. Gunnarsson, J. Prikulis, B. Kasemo, and M. Käll, "Nanoparticle Optics: The Importance of Radiative Dipole Coupling in Two-Dimensional Nanoparticle Arrays†," *The Journal of Physical Chemistry B,* vol. 107, pp. 7337-7342, 2003/07/01 2003.

[81] J. Aizpurua, P. Hanarp, D. S. Sutherland, M. Käll, G. W. Bryant, and F. J. García de Abajo, "Optical Properties of Gold Nanorings," *Physical Review Letters,* vol. 90, p. 057401, 2003.

[82] P. Hanarp, M. Käll, and D. S. Sutherland, "Optical Properties of Short Range Ordered Arrays of Nanometer Gold Disks Prepared by Colloidal Lithography," *The Journal of Physical Chemistry B,* vol. 107, pp. 5768-5772, 2003/06/01 2003.

[83] A. J. Haes, L. Chang, W. L. Klein, and R. P. Van Duyne, "Detection of a Biomarker for Alzheimer's Disease from Synthetic and Clinical Samples Using a Nanoscale Optical Biosensor," *Journal of the American Chemical Society,* vol. 127, pp. 2264-2271, 2005/02/01 2005.

[84] X.-J. Huang, J.-H. Lee, J.-W. Lee, J.-B. Yoon, and Y.-K. Choi, "A One-Step Route to a Perfectly Ordered Wafer-Scale Microbowl Array for Size-Dependent Superhydrophobicity," *Small,* vol. 4, pp. 211-216, 2008.

[85] T. Sun, L. Feng, X. Gao, and L. Jiang, "Bioinspired Surfaces with Special Wettability," *Accounts of Chemical Research,* vol. 38, pp. 644-652, 2005/08/01 2005.

[86] Y.-R. Lin, H.-P. Wang, C.-A. Lin, and J.-H. He, "Surface profile-controlled close-packed Si nanorod arrays for self-cleaning antireflection coatings," *Journal of Applied Physics,* vol. 106, pp. 114310-4, 2009.

[87] W.-L. Min, B. Jiang, and P. Jiang, "Bioinspired Self-Cleaning Antireflection Coatings," *Advanced Materials,* vol. 20, pp. 3914-3918, 2008.

[88] Y. Li, J. Zhang, S. Zhu, H. Dong, Z. Wang, Z. Sun, J. Guo, and B. Yang, "Bioinspired silicon hollow-tip arrays for high performance broadband anti-reflective and water-repellent coatings," *Journal of Materials Chemistry,* vol. 19, pp. 1806-1810, 2009.

[89] J. D. Joannopoulos, P. R. Villeneuve, and S. Fan, "Photonic crystals: putting a new twist on light," *Nature,* vol. 386, pp. 143-149, 1997.

[90] D. Cassagne, C. Jouanin, and D. Bertho, "Hexagonal photonic-band-gap structures," *Physical Review B,* vol. 53, pp. 7134-7142, 1996.

[91] E. Yablonovitch, "Inhibited Spontaneous Emission in Solid-State Physics and Electronics," *Physical Review Letters,* vol. 58, pp. 2059-2062, 1987.

[92] K. Kempa, B. Kimball, J. Rybczynski, Z. P. Huang, P. F. Wu, D. Steeves, M. Sennett, M. Giersig, D. V. G. L. N. Rao, D. L. Carnahan, D. Z. Wang, J. Y. Lao, W. Z. Li, and Z. F. Ren, "Photonic Crystals Based on Periodic Arrays of Aligned Carbon Nanotubes," *Nano Letters,* vol. 3, pp. 13-18, 2003/01/01 2002.

[93] R. W. Baker, *Membrane technology and applications*: J. Wiley, 2004.

[94] S. M. Weekes, F. Y. Ogrin, and W. A. Murray, "Fabrication of Large-Area Ferromagnetic Arrays Using Etched Nanosphere Lithography," *Langmuir,* vol. 20, pp. 11208-11212, 2004/12/01 2004.

[95] K. Shah, W. C. Shin, and R. S. Besser, "Novel microfabrication approaches for directly patterning PEM fuel cell membranes," *Journal of Power Sources,* vol. 123, pp. 172-181, 2003.

[96] Z. G. Chen, A. Taflove, and V. Backman, "Photonic nanojet enhancement of backscattering of light by nanoparticles: a potential novel visible-light ultramicroscopy technique," *Optics Express,* vol. 12, pp. 1214-1220, Apr 5 2004.

[97] CST-MICROWAVE-STUDIO, "Workflow and Solver Overview," ed: Computer Simulation Technology AG 2010.

[98] Polysciences. Polybead Polystyrene Microspheres: Technical Data Sheet [Online].

[99] Sigma. Polystyrene Latex Beads: Product Information [Online].

[100] X. Ma, J. Q. Lu, R. S. Brock, K. M. Jacobs, P. Yang, and X.-H. Hu, "Determination of complex refractive index of polystyrene microspheres from 370 to 1610 nm," *Physics in Medicine and Biology,* vol. 48, pp. 4165-4172, 2003.

[101] R. E. H. Miles, S. Rudić, A. J. Orr-Ewing, and J. P. Reid, "Influence of Uncertainties in the Diameter and Refractive Index of Calibration Polystyrene Beads on the Retrieval of Aerosol Optical Properties Using Cavity Ring Down Spectroscopy," *The Journal of Physical Chemistry A,* vol. 114, pp. 7077-7084, 2010/07/08 2010.

[102] AZ-Electronic-Materials. AZ Photoresist Safety Data Sheet [Online].

[103] MicroChemicals. Optical Parameters of Photoresists [Online].

[104] CST-MICROWAVE-STUDIO, "Advanced Topics," ed: Computer Simulation Technology AG 2003.

[105] J. Park, J. Joo, S. G. Kwon, Y. Jang, and T. Hyeon, "Synthesis of monodisperse spherical nanocrystals," *Angewandte Chemie International Edition,* vol. 46, pp. 4630-4660, 2007.

[106] T. Sugimoto, "Preparation of monodispersed colloidal particles," *Advances in Colloid and Interface Science,* vol. 28, pp. 65-108, 1987.

[107] Thermo-Scientific. Material Safety Data Sheet (Polymer Microsphere Suspension MSDS) [Online].

[108] MicroChemicals. AZ Photoresists - Introduction to our Product Range [Online].

[109] M. L. Long and J. Newman, "IMAGE REVERSAL TECHNIQUES WITH STANDARD POSITIVE PHOTORESIST," *Proceedings of the Society of Photo-Optical Instrumentation Engineers,* vol. 469, pp. 189-193, 1984 1984.

[110] M. Bolsen, "AZ® 5200," *New Jersey, Hoechst, Sommerville,* 1988.

[111] Clariant-GmbH. AZ 5214 E-Image Reversal Photoresist-Datasheet [Online].

[112] T. Okubo, K. Kimura, and H. Kimura, "Dissipative structures formed in the course of drying the colloidal crystals of monodispersed polystyrene spheres on a cover glass," *Colloid & Polymer Science,* vol. 280, pp. 1001-1008, 2002.

[113] D. P. Brown, T. L. Kraus, E. Christensen, and J. DeLong, "TWO-LAYER NANOSPHERE LITHOGRAPHY."

[114] J. C. Lötters, W. Olthuis, P. H. Veltink, and P. Bergveld, "The mechanical properties of the rubber elastic polymer polydimethylsiloxane for sensor applications," *Journal of Micromechanics and Microengineering,* vol. 7, p. 145, 1997.

[115] K. R. Williams and R. S. Muller, "Etch rates for micromachining processing," *Microelectromechanical Systems, Journal of,* vol. 5, pp. 256-269, 1996.

[116] B. Hinds. CMMED Wet Cleaning Bench Operating Procedure [Online].

[117] J. C. Riboh, A. J. Haes, A. D. McFarland, C. Ranjit Yonzon, and R. P. Van Duyne, "A Nanoscale Optical Biosensor: Real-Time Immunoassay in Physiological Buffer Enabled by Improved Nanoparticle Adhesion," *The Journal of Physical Chemistry B,* vol. 107, pp. 1772-1780, 2003/02/01 2003.

[118] A. Mohammadkhani, M. Malboubi, C. Anthony, and K. Jiang, "Surface property characterization of ordered nanostructure using SEM stereoscopic technique," in *Nanotechnology (MNE), 36th International Micro & Nano Engineering Conference, Poster, P-NANO-09*, Genoa, 2010.

[119] A. Mohammadkhani, H. Ostadi, and K. Jiang, "Morphological charactrarization of sub-micron PDMS bowl structures," in *Nanotechnology (IEEE-NANO), 12th IEEE Conference, Oral, WeA2T5.3*, Birmingham, 2012.

[120] D. Samak, A. Fischer, and D. Rittel, "3D Reconstruction and Visualization of Microstructure Surfaces from 2D Images," *CIRP Annals - Manufacturing Technology,* vol. 56, pp. 149-152, 2007.

[121] N. Yao, *Focused Ion Beam Systems: Basics and Applications*: Cambridge University Press, 2007.

[122] MeX-TM-software, ed, pp. By Alicona Imaging GmbH, Graz, Austria.

[123] D. S. Kim, B.-K. Lee, J. Yeo, M. J. Choi, W. Yang, and T. H. Kwon, "Fabrication of PDMS micro/nano hybrid surface for increasing hydrophobicity," *Microelectronic Engineering,* vol. 86, pp. 1375-1378, 2009.

[124] H. Hillborg, J. F. Ankner, U. W. Gedde, G. D. Smith, H. K. Yasuda, and K. Wikström, "Crosslinked polydimethylsiloxane exposed to oxygen plasma studied by neutron reflectometry and other surface specific techniques," *Polymer,* vol. 41, pp. 6851-6863, 2000.

[125] S. H. Tan, N.-T. Nguyen, Y. C. Chua, and T. G. Kang, "Oxygen plasma treatment for reducing hydrophobicity of a sealed polydimethylsiloxane microchannel," *Biomicrofluidics,* vol. 4, pp. 032204-8, 2010.

[126] C. J. Wohl, M. A. Belcher, S. Ghose, and J. W. Connell, "Modification of the Surface Properties of Polyimide Films using POSS Deposition and Oxygen Plasma Exposure," 2008.

[127] J. McGeough, M. Leu, K. Rajurkar, A. De Silva, and Q. Liu, "Electroforming process and application to micro/macro manufacturing," *CIRP Annals-Manufacturing Technology,* vol. 50, pp. 499-514, 2001.

[128] O. I. Pavlova, *Electrodeposition of Metals: A Historical Survey. (Istoriya Tekhniki Elektroosazhdeniya Metallov)*: Israel Program for Scientific Translations [available from the U.S. Department of Commerce, Clearinghouse for Federal Scientific and Technical Information, Springfield, Va.], 1968.

[129] W. Ehrfeld, M. Abraham, U. Ehrfeld, M. Lacher, and H. Lehr, "Materials for LIGA products," in *Micro Electro Mechanical Systems, 1994, MEMS '94, Proceedings, IEEE Workshop on*, 1994, pp. 86-90.

[130] J. W. Dini and J. Dini, *Electrodeposition: the materials science of coatings and substrates*: Noyes Publications Park Ridge, NJ, 1993.

[131] M. Schlesinger and M. Paunovic, *Modern Electroplating*: Wiley, 2011.

[132] RECOMMENDED LITHOGRAPHY PROCEDURE FOR AZ5214 RESIST [Online].

[133] MicroChemicals. Electroplating with Photoresist Masks [Online].

[134] M. A. Malik, M. A. Hashim, F. Nabi, S. A. AL-Thabaiti, and Z. Khan, "Anti-corrosion ability of surfactants: a review," *Int. J. Electrochem. Sci,* vol. 6, pp. 1927-1948, 2011.

[135] X. Wei, P. D. Prewett, and K. Jiang, "Electrochemical co-deposition of Nickel-Alumina Nanocomposite for Microsystem Applications," in *Nanotechnology, 2007. IEEE-NANO 2007. 7th IEEE Conference on*, 2007, pp. 34-38.